DEUTSCHES ELEKTRONEN-SYNCHROTRON

DESY 93-181
December 1993

The Geometric Schwinger Model on the Lattice

H. Dilger

Deutsches Elektronen-Synchrotron DESY, Hamburg

ISSN 0418-9833

NOTKESTRASSE 85 - 22603 HAMBURG

To be sure that your preprints are promptly included in the
HIGH ENERGY PHYSICS INDEX,
send them to (if possible by air mail):

DESY **Bibliothek** **Notkestraße 85** **22603 Hamburg** **Germany**	**DESY-IfH** **Bibliothek** **Platanenallee 6** **15738 Zeuthen** **Germany**

DESY 93-181
December 1993

ISSN 0418-9833

The Geometric Schwinger Model on the Lattice

Hermann Dilger

Deutsches Elektronen-Synchrotron DESY,
Notkestr. 85, 22603 Hamburg, FR Germany

Abstract

The geometric Schwinger model has an interesting non-perturbative structure related to topological index theorems. This is analyzed on the euclidean lattice with staggered fermions. Using the hybrid Monte Carlo simulation we calculate the exponential decay of the field strength correlation and the screening of the heavy quark potential including finite volume effects. For both cases the transition from strong to weak coupling behaviour is studied. These calculations are complemented by an unquenched strong coupling expansion. Furthermore, we characterize fermion bilinears by their lattice symmetry properties. The Monte Carlo results on their correlation functions can then be discussed under the aspects of the anomalous $U(1)_A$ symmetry breaking. The toron part of the effective action is measured too.

Contents

Introduction

The study of non-perturbative effects in gauge theories including fermions is a main task of lattice field theory. Such effects are the screening of the colour charge in QCD [1], the $U(1)$-puzzle in QCD [2] and the anomalous breaking of axial symmetries in QCD and in the theory of electroweak interactions [3]. The last two points are connected with the topology of the gauge field and related index theorems. An explicit control over these topological quantities in a finite volume might seem desirable before one lets the volume tend to infinity.

The analysis of these features on the lattice is still at its beginning. One of the arising problems is the computational effort for the fermion matrix inversion in Monte Carlo (MC) simulations on large lattices. Therefore it is useful to control finite volume effects explicitly. In particular, this is an important point in the investigation of charge screening, where both, finite volume effects and screening, result in a lowering of the potential at large distances. As well, the evaluation of the disconnected contributions in correlation functions of meson fields suffers from the great computational effort needed. These contributions are essential in the treatment of the $U(1)$-puzzle in QCD. Finally the fermionic zero modes, which appear in the background of topologically non-trivial gauge fields, are difficult to handle.

Another problem, which is far from being solved, is the formulation of chiral gauge theories on the lattice. This difficulty is related to the fermion doubling problem [4]. It appears to be impossible to put chiral fermions on the lattice [5]. As a consequence the lattice avoids the coupling of a gauge field to an anomalous axial current. It is unclear whether there is a physical meaning of this technical 'anomaly cancellation' on the lattice, and whether there is any relation to the physical 'anomaly cancellation' by quarks and leptons. In the understanding of this problem it may be considered a first step to analyze how the lattice reproduces the anomaly in a vectorlike theory.

The 'Geometric Schwinger Model' (GSM) is the Schwinger model [6],[7] with Dirac-Kähler fermions [8], i.e. in two dimensions with two fermion flavours. It shows a lot of the features mentioned above, but it can be treated exactly. S.I. Azakov and H. Joos calculated this model on the two-dimensional torus $\mathcal{T}_2$ [AJ], explicitly including the finite volume effects. One obtains a confining heavy quark potential in the quenched theory, which is screened in the case of dynamical fermions. Secondly there is a flavour triplet of massless particles and a singlet particle, which acquires a mass by disconnected contributions in meson correlation functions. This is similar to the $U(1)$-puzzle in QCD. Finally the axial $U(1)$-symmetry is broken by an anomaly. This is related to zero mode contributions in topologically non-trivial sectors of the gauge field.

The aim of our investigation is the reproduction of these features on the euclidean lattice with a hybrid Monte Carlo (HMC) simulation [9] and an unquenched strong coupling expansion. The model is particularly suited for a comparison of lattice and continuum results.

The first advantage is a well-defined procedure to put the theory on the lattice without spectrum doubling. One obtains staggered fermions [10] as lattice restriction of the Dirac-Kähler fermions [11]. Furthermore, the torus in the continuum corresponds to periodic boundary conditions on the lattice. At last, we can compare with exact continuum calculations in this case. We expect results on two questions:

1. How does the lattice reproduce the continuum results and what are the lattice effects?
2. How well do the MC simulation and the unquenched strong coupling expansion apply to the calculation of the features in question?

For that we investigate two kinds of observables. On the one hand we calculate the correlation function (called correlation in the following) of the field strength, leading to the gauge field mass, and the correlations of Polyakov loops, leading to the heavy quark potential. The analysis of these gauge field observables for different values of the $\tilde{\beta}$-parameter (i.e. $1/e^2$ in lattice units) shall give a survey of the lattice effects and distinguish between strong coupling and scaling region. Finite volume corrections are treated explicitly. The corresponding expectation values are evaluated by Monte Carlo simulations and with the unquenched strong coupling expansion for massless staggered fermions. The latter bases on the dimer gas representation of the strong coupling limit of a $U(N)$ lattice gauge theory with staggered fermions [12],[13].

On the other hand we calculate expectation values of correlations of lattice fermion bilinears, corresponding to the correlations of currents and (pseudo)scalars in the continuum. These are calculated in [AJ]. For that we use MC simulations with values of $\tilde{\beta}$ in the scaling region. In order to reproduce the anomalous symmetry breaking and the related mass generation for the isoscalar current, we must include disconnected contributions and contributions from topologically non-trivial sectors.

Moreover, it is important to know what are the correct lattice restrictions of the continuum bilinears. This question is treated by the analysis of the irreducible representations of the symmetry groups in the continuum and on the lattice. The effect of the anomalous symmetry breaking is included. One obtains a scheme of anomalous symmetry restoration, which should appear for $\tilde{\beta}$-values close enough to the continuum limit.

Our MC simulations are performed on a quite small lattice $L_1 \times L_2 = 6 \times 16$. This has the advantage of comparable small computational effort for quite high statistics and small error bars. It is a reasonable choice, because we can compare with exact finite volume results in the continuum. Nevertheless, the analysis of a few of the considered expectation values suffers from the small volume. These effects might be a shortcoming for models with a more complicated structure and without exact continuum results to compare with.

The paper is organized as follows: The first chapter presents the model under investigation, i.e. the GSM in the continuum and its lattice restriction. It also contains the analysis of the symmetry groups and the corresponding irreducible representations in the continuum and on the lattice. In the second chapter we discuss some special problems in our MC simulation with the HMC algorithm, arising from the special topological structure of the model. A second section describes the unquenched strong coupling expansion for gauge field observables. Then the following two chapters present the results on gauge field observables and fermion observables. The results on the heavy quark potential are already published in [14]. A summary of our results is given in the conclusion.

Chapter 1

The Model

1.1 The geometric Schwinger model in the continuum

The geometric Schwinger model on the torus was treated by H. Joos [15], S.I. Azakov and H. Joos [AJ] in the continuum. This section is aimed to present some results, which will be important for the lattice investigations.

1.1.1 Coupled Dirac-Kähler fermions

First we shall describe the concept of a geometric gauge field theory in two dimensions. For the description of this concept in more than 2 dimensions we refer to [11].

The geometric Schwinger model is based on the Dirac-Kähler equation (DK equation) [8]. It acts on the space of inhomogenous differential forms. In two dimensions these forms are written as

$$\Phi = \phi(x,\emptyset) + \phi(x,1)dx^1 + \phi(x,2)dx^2 + \phi(x,12)dx^1 \wedge dx^2 = \sum_H \phi(x,H)dx^H \ . \tag{1.1}$$

$H = \emptyset, 1, 2, 12$ is called a multi-index. On this space the free DK equation reads

$$(d - \delta + m)\,\Phi \ = \ 0 \ , \tag{1.2}$$

with the external derivative $d = dx^\mu \wedge \partial_\mu$ and the coderivative $\delta = -\epsilon^\mu \neg \partial_\mu$. We deal only with the case $m = 0$, i.e. the massless Schwinger model. The DK operator $(d - \delta)$ can be written in a form, which will prove to be useful in the following. For that we use the Clifford product for constant forms, which extends the wedge product by

$$dx^\mu \vee dx^\nu = dx^\mu \wedge dx^\nu + \delta^{\mu\nu} \ . \tag{1.3}$$

This leads to the anticommutation relations

$$\{dx^\mu, dx^\nu\}_\vee = dx^\mu \vee dx^\nu + dx^\nu \vee dx^\mu = 2\delta^{\mu\nu} \ . \tag{1.4}$$

For general constant forms the Clifford product is given by

$$dx^H \vee dx^K = \rho(H,K)dx^{H \triangle K} \ , \quad H \triangle K = (H \cup K) \setminus (H \cap K) \ , \tag{1.5}$$

with

$$\rho(H,K) = (-1)^n \ , \ n = \sharp\{(\mu_h,\mu_k) \mid \mu_h \in H, \mu_k \in K, \mu_h > \mu_k\} \ . \tag{1.6}$$

The sign factor fulfills the useful relation

$$\rho(H_1 \triangle H_2, K_1 \triangle K_2) = \rho(H_1,K_1)\rho(H_1,K_2)\rho(H_2,K_1)\rho(H_2,K_2) \ . \tag{1.7}$$

With these definitions the massless DK equation now reads

$$dx^\mu \vee \partial_\mu \Phi = 0 \ . \tag{1.8}$$

There is a close relation of the Dirac-Kähler operator and the Dirac operator $\gamma^\mu\partial_\mu$. First note that we have

$$(d-\delta)^2 = \partial^\mu\partial_\mu \ , \tag{1.9}$$

i.e. the DK operator is a root of the Laplacian in the space of inhomogenous differential forms. If we write the DK operator in the form of eq. (1.8) $(d-\delta) = dx^\mu \vee \partial_\mu$, this is proved easily with the anticommutation relations eq. (1.4). In fact, the DK operator is equivalent to the Dirac operator acting on 2 independent flavours of Dirac fermions (in 4 dimensions we would have 4 flavours). This arises naturally from the invariance of the DK operator under Clifford right multiplication, due to the associativity of the Clifford product

$$dx^\mu \vee \partial_\mu(\Phi \vee dx^H) = (dx^\mu \vee \partial_\mu\Phi) \vee dx^H \ . \tag{1.10}$$

The symmetry operations $\vee\epsilon dx^H, \epsilon = \pm 1$, form a group which is isomorphic to the Dirac group generated by the two-dimensional γ-matrices. Considered as transformation of the component functions in eq. (1.1) they act as

$$\epsilon\, d^K\, \phi(x,H) \ = \ \epsilon\, \rho(H,K)\, \phi(x, H \triangle K) \ . \tag{1.11}$$

Under these transformations the space of constant forms dx^H decomposes in twice the two-dimensional true irreducible representation given by the γ-matrices itselfs. Because of its invariance the DK operator has to be diagonal in the irreducible subspaces. In order to make this decomposition explicit we define the basis Z_{ab} matching the above symmetry

$$Z_{ab} = \frac{1}{2}\sum_H \gamma_{ab}^{H\,*}\, dx^H \ . \tag{1.12}$$

It transforms as

$$Z_{ab} \vee dx^H = Z_{ab'}\, \gamma_{bb'}^H \ . \tag{1.13}$$

We rewrite the general differential form as

$$\Phi = \sum_H \phi(x,H) dx^H = \sum_{ab} \psi_a^b(x) Z_{ab} \ . \tag{1.14}$$

Using the relations of orthogonality and completeness

$$\sum_H \gamma_{ab}^H\, \gamma_{a'b'}^{H\,*} \ = \ 2\,\delta_{aa'}\,\delta_{bb'} \ , \tag{1.15}$$

$$\sum_{ab} \gamma_{ab}^K\ \gamma_{ab}^{H\,*} \ = \ 2\,\delta^{K,H} \ , \tag{1.16}$$

we get

$$\psi_a^b(x) \ = \ \sum_H \gamma_{ab}^H\, \phi(x,H) \ , \tag{1.17}$$

$$\phi(x,H) \ = \ \frac{1}{2}\sum_{ab} \gamma_{ab}^{H\,*}\ \psi_a^b(x) \ . \tag{1.18}$$

Now the action of the DK operator on Φ can be expressed as an operation on the Dirac component functions $\psi_a^b(x)$ in the sense of eq. (1.14)

$$(d-\delta)\psi_a^b(x) \ = \ \gamma_{aa'}^\mu\, \partial_\mu \psi_{a'}^b(x) \ . \tag{1.19}$$

This proves the equivalence of the DK equation to the Dirac equation with an internal flavour (also called isospin in the following) labelled by the index b in the above equation.

Next we couple a $U(1)$-gauge field to the DK fermions by introducing the usual covariant derivative for the DK operator. The coupled DK equation reads

$$(d-\delta)_A\Phi \ = \ dx^\mu \vee (\partial_\mu - ieA_\mu)\Phi \ = \ 0 \ . \tag{1.20}$$

On the two-dimensional torus $\mathcal{T}_2$ some care is needed with the periodicity conditions for the gauge field A, which has to be considered as a connection 1-form in a $U(1)$-bundle with base space $\mathcal{T}_2$. These topological questions will be discussed in the next subsection, here we present the result only. It turns out that a general gauge field is described by

$$A^{(k)} = A^0 + C^{(k)} \ , \ \ C^{(k)} = \frac{-2\pi k}{eL_1L_2} x^2 dx^1 \ , \ k \in \mathbf{Z} \ , \tag{1.21}$$

where A^0 is smooth on $\mathcal{T}_2$, L_μ is the length of the torus in μ-direction. Using the Hodge decomposition theorem [16] the smooth part A^0 can be written as

$$A^0 \ = \ da - \delta b + t \ , \tag{1.22}$$

where $da = \partial_\mu a(x) dx^\mu$ is a pure gauge, $\delta b = -\epsilon_\mu{}^\nu \partial_\nu b(x) dx^\mu$ is the coderivative of the 2-form $b = b(x)dx^1 \wedge dx^2$, $t = t_\mu dx^\mu$, t_μ constant, is the so-called toron field. $C^{(k)}$ is a representative of the Chern class with topological quantum number k.

It is well-known that with this decomposition the coupled Dirac equation in two dimensions $\gamma^\mu(\partial_\mu - ieA_\mu)\psi = 0$ has the local solution

$$\psi(x) = e^{iet_\mu x^\mu} e^{ie\alpha(x)} \psi^0(x) \ , \tag{1.23}$$

where $\alpha(x) = a(x) + i\gamma^5 b(x)$ and $\psi^0(x)$ is a free solution. With eqs. (1.14), (1.19) this translates to a solution of the DK equation. Note that locally the $C^{(k)}$-part of the field cannot be distinguished from the δb-part. However, the question of global solutions is related to the 'topological sectors' given by $C^{(k)}$.

Finally, for the field quantization in the euclidean formalism, we set up the action leading to the coupled DK equation, together with the two-dimensional Maxwell equations for the gauge field. For that we define the 2-form $(\Phi,\Phi')_0$ by

$$(\Phi,\Phi')_0 = \sum_H \phi(x,H)\phi'(x,H) dx^{12} = \sum_{ab} \psi_a^b(x)\psi'^b_a(x) dx^{12} \ . \tag{1.24}$$

With the 2-form of the field strength $F = dA$ the action of the geometric Schwinger model then reads

$$S[A,\bar\Phi,\Phi] = S_g[A] + S_f[A,\bar\Phi,\Phi] = \frac{1}{2}\int_{\mathcal{T}_2}(F,F)_0 + \int_{\mathcal{T}_2}(\bar\Phi,(d-\delta)_A\Phi)_0 \ . \tag{1.25}$$

1.1.2 Topological properties

In this subsection we discuss the special features arising from the formulation of the geometric Schwinger model on the torus $\mathcal{T}_2$. It turns out that this model provides a quite simple example for a general topological structure, the Chern classification of principal bundles and related index theorems for covariant differential operators [16],[17].

First we give a more explicit discussion of the decomposition of the gauge field A in a smooth part A^0 and a part of constant field strength $C^{(k)}$, $k \in \mathbf{Z}$ in eq. (1.21). As mentioned above we consider A to be a connection 1-form in a $U(1)$-bundle with base space $\mathcal{T}_2$ [17]. In our case this means it must be periodic on $\mathcal{T}_2$ modulo gauge transformations

$$A_\mu(x + L_\nu) \;=\; A_\mu(x) - \frac{i}{e}\Lambda_\nu(x)^{-1}\partial_\mu\Lambda_\nu(x)\;,\; \Lambda_\nu(x) \in U(1)\;, \tag{1.26}$$

where the $\Lambda_\nu(x)$ obey a cocycle condition. The general form of a $U(1)$ gauge field A on $\mathcal{T}_2$ in eq. (1.21) follows from these requirements. However, it also comes out, if one considers the gauge invariant physical quantities derived from A: First A defines a unique phase transformation $U_\mathcal{C}$ for any closed path $\mathcal{C}$ on $\mathcal{T}_2$

$$U_\mathcal{C} = \exp(ie\int_\mathcal{C} A)\;, \tag{1.27}$$

which is a gauge invariant quantity. Secondly, as a physical quantity the 2-form of the field strength $F = dA$ must be smooth on $\mathcal{T}_2$. We write

$$F = F^0 + c^{(k)}dx^{12}\;,\; \text{with}\; \int_{\mathcal{T}_2} F^0 = 0\;. \tag{1.28}$$

Hence $F^0 = dA^0$, where A^0 is smooth on the whole torus[1]. It appears that $c^{(k)}$ is quantized (as implied by the index k). In order to show this we define $C^{(k)}$ with $dC^{(k)} = c^{(k)}dx^{12}$ in the temporal gauge

$$C^{(k)} = C_1^{(k)}(x)\,dx^1 = -c^{(k)}x_2\,dx^1\;. \tag{1.29}$$

Now the requirement that, following eq. (1.27), $C^{(k)}$ defines a unique phase transformation $U_\mathcal{C}$ for a closed loop $\mathcal{C}$ winding round $\mathcal{T}_2$ in 1-direction, yields

$$e\int_0^{L_1} dx^1 C_1^{(k)}(x) = e\int_0^{L_1} dx^1 C_1^{(k)}(x + e_2L_2) \pmod{2\pi}\;, \tag{1.30}$$

leading to $eL_1L_2c^{(k)} = 2\pi k$, $k \in \mathbf{Z}$. Therefore $C^{(k)}$ is given by

$$C^{(k)} = \frac{-2\pi k}{eL_1L_2}\,x_2\,dx^1 \tag{1.31}$$

in temporal gauge. Note that $A = C^{(1)}$ provides the solution of the free two-dimensional Maxwell equations with the lowest non-trivial quantum number $k = 1$. Therefore we call it an instanton in analogy to 4-dimensional non-Abelian gauge theories [18].

[1] In two dimensions A^0 can be easily derived from F^0, e.g. with $A^2(x) =$ constant in x_2-direction — provided $\int_{\mathcal{T}_2} F^0 = 0$.

From a more general point of view the quantization of the constant part of the field strength F is a special case of the Chern classification of gauge fields, these Chern classes are also called topological sectors here. The corresponding Chern index is

$$k = \frac{e}{2\pi}\int_{\mathcal{T}_2} dA = \frac{e}{2\pi}\int_{\mathcal{T}_2} F(x)\,dx^{12}\;,\; k \in \mathbf{Z}\;, \tag{1.32}$$

it is also called topological charge in this context.

There is an interesting relation between the global solutions of the DK equation and the topological charge. The Atiyah-Singer index theorem for DK fermions [16] states

$$n_l - n_r = 2k\;, \tag{1.33}$$

where, in terms of the Dirac representation given with eqs. (1.17), (1.18), $n_l(n_r)$ is the number of left-handed (right-handed) solutions of the DKE in a background field with Chern index k. In [15] these global solutions were calculated explicitly. Indeed there are $2k$ left-handed (right-handed) solutions for $k > 0 (k < 0)$, but no solutions of the opposite chirality, respectively. These solutions are called topological zero modes. For $k = 0$ the number of zero modes depends on the toron part of the gauge field, see below. Let us quote the explicit form of the topological zero modes Φ_l, $l = 1, \ldots, 2k$ in the simplest case $k = 1$. We have

$$\Phi_{1/2} = e^{ie(a(x)+ib(x))}\,e^{\frac{\pi k}{2\tau}(z^2-|z|^2)}\,\Theta_3(z|i\tau)\,\omega_{1/2}\;,\;\; \omega_1 = dx^1 + idx^2,\; \omega_2 = 1 - idx^{12}\;. \tag{1.34}$$

Here the toron field t is set to zero, its influence is described in eq. (1.36). $\Theta_3(z|i\tau)$ is a Jacobi Θ-function. For the definition of these Θ-functions we refer to [19].

Another important feature of gauge fields defined on the torus is the non-vanishing of the constant part, the toron $t = t_\mu dx^\mu$ (see eq. (1.22)). The values of t_μ must be defined modulo $2\pi/eL_\mu$, i.e. in the interval $[0, 2\pi/eL_\mu)$. Otherwise they would not be invariant under large gauge transformations $A \to A - A^l$, $A^l = 2\pi k_\mu dx^\mu/eL_\mu$, $k_\mu \in \mathbf{Z}$. In fact, we can write

$$A^l_\mu = \frac{i}{e}\Lambda^l(x)^{-1}\partial_\mu\Lambda^l(x)\;,\;\; \Lambda^l(x) = \exp\left(i\frac{2\pi k_\mu x^\mu}{L_\mu}\right)\;. \tag{1.35}$$

Note that $k_\mu \in \mathbf{Z}$ guarantees that $\Lambda_l(x) \in U(1)$ is smooth on $\mathcal{T}_2$.

The torons are related to the question of boundary conditions in the following sense. Consider the DK equation in the background field A with antiperiodic boundary conditions for the fermion field Φ. It is equivalent to the DK equation in the background field $A' = A + T_\epsilon$ and periodic boundary conditions in the limit $\epsilon \to 0$, with $T_\epsilon{}^\mu(x) = \frac{1}{\epsilon}\pi/e$ for $x \in [L_\mu - \epsilon, L_\mu]$, $T_\epsilon{}^\mu(x) = 0$ elsewhere. T_ϵ can be gauged to t, with $t_\mu = \pi/(eL_\mu)$ for every $\epsilon > 0$. Thus the change of periodic boundary conditions to antiperiodic boundary conditions is equivalent to a change of A by a toron part $A \to A + t$, $t = \pi/(eL_\mu)\,dx^\mu$.

In the following always periodic boundary conditions are chosen. Then, for $t = 0$ there is a global solution in the topologically trivial sector ($C^{(k)} = 0$), given by the local solution eq. (1.23) which is smooth on the whole torus in this case. These solutions are called harmonic. A difference to the topological zero modes mentioned above is that they exist only for gauge field configurations which have measure zero in the configuration space. Furthermore, the number of right-handed and left-handed solutions are equal here, as required by the index theorem eq. (1.33).

At last let us turn to the role of the toron field in the topologically non-trivial sectors. Consider a topological zero mode of the DK operator $\Phi = \sum_H \phi(x,H) dx^H$ in the background field $A^{(k)}$ with Chern index k, $k \neq 0$. It is shown in [15] that the solution $\Phi_t = \sum_H \phi_t(x,H) dx^H$ in the background $A^{(k)} + t$ is obtained from Φ by

$$\phi_t(x,H) = e^{i\frac{g}{2} t_\mu x^\mu} \phi(x + \Delta_t, H) \ , \ \Delta_t^1 = \frac{eL_1L_2}{2\pi k} t^2 \ , \ \Delta_t^2 = \frac{eL_1L_2}{2\pi k} t^1 \ . \tag{1.36}$$

That means, up to an additional gauge factor, the toron field shifts the topological zero modes round the torus. The same is valid for any eigenmode of the DK operator with topologically non-trivial background field.

1.1.3 Fermion integration

For the determination of quantum-mechanical expectation values of observables Ω in dynamical gauge fields we set up the path integral formula

$$< \Omega >= \frac{1}{Z} \int \mathcal{D}[A] \mathcal{D}[\bar{\Phi}, \Phi] \, \Omega[A, \bar{\Phi}, \Phi] \, e^{-S[A,\bar{\Phi},\Phi]} \ . \tag{1.37}$$

As usual, the configuration integral $\mathcal{D}[A]$ has to be taken only over gauge invariant degrees of freedom. These are given by eqs. (1.21), (1.22) with $b(x)$, $t_\mu \in [0, 2\pi/L_\mu)$, and the index k defining $C^{(k)}$. One proceeds now with the integration of the fermionic degrees of freedom. For that one has to be careful with the $2k$ zero modes appearing in the topological sectors $k \neq 0$, see the index theorem eq. (1.33). With the general formula for the fermion integration in the presence of zero modes $\chi_i(x)$, $i = 1, \ldots, 2k$ we obtain [20]

$$\begin{aligned}
& < \phi(x_1)\bar{\phi}(\bar{x}_1) \ldots \phi(x_n)\bar{\phi}(\bar{x}_n) > \\
= \ & \frac{1}{Z} \sum_{k=-[n/2]}^{[n/2]} \int \mathcal{D}[A^{(k)}] \, e^{-S_g[A^{(k)}]} \det{}'[D_{A^{(k)}}] \, \frac{1}{(n-2k)!} \\
\times \ & \sum_\pi \mathrm{sign}(\pi) \sum_{\bar{\pi}} \mathrm{sign}(\bar{\pi}) \ \chi_1(x_{\pi(1)}) \, \bar{\chi}_1(\bar{x}_{\bar{\pi}(1)}) \cdots \chi_{2k}(x_{\pi(2k)}) \, \bar{\chi}_{2k}(\bar{x}_{\bar{\pi}(2k)}) \\
\times \ & \mathcal{G}'(x_{\pi(2k+1)}, \bar{x}_{\bar{\pi}(2k+1)}; A^{(k)}) \ldots \mathcal{G}'(x_{\pi(n)}, \bar{x}_{\bar{\pi}(n)}; A^{(k)}) \ .
\end{aligned} \tag{1.38}$$

Here $\det'[D_{A^{(k)}}]$, $\mathcal{G}'(x, \bar{x}; A^{(k)})$ are the determinant of the DK operator and the propagator in the background field $A^{(k)}$, restricted to the subspace orthogonal to the $2k$ zero modes. For simplicity of notation we suppressed the multi-indices H in the component functions of the DK fermions $\phi(x,H)$. Of course, these indices must be treated as the arguments x. The inclusion of gauge field observables $\Omega[A]$ is obvious. If the observable has no fermionic part, the above equation reduces to its $(k=0)$-part, i.e.

$$< \Omega[A] > = \frac{1}{Z} \int \mathcal{D}[A^0] \, e^{-S_g[A^0]} \det[D_{A^0}] \, \Omega[A^0] \ . \tag{1.39}$$

For correlations of fermion bilinears, which will be investigated on the lattice later on, we have $n = 2$ in eq. (1.38). So, in general the topological sectors with $k = 0, \pm 1$ will contribute. We

obtain with the notation of eq. (1.38)

$$< \phi(x_1)\bar{\phi}(\bar{x}_1)\phi(x_2)\bar{\phi}(\bar{x}_2) >= I_4{}^0 + I_4{}^{-1} + I_4{}^1 \ , \tag{1.40}$$

$$\begin{aligned}
I_4{}^0 \ &= \ \frac{1}{Z} \int \mathcal{D}[A^0] \, e^{-S_g[A^0]} \det[D_{A^0}] \, [\mathcal{G}(x_1, \bar{x}_1; A^0)\mathcal{G}(x_2, \bar{x}_2; A^0) \\
&- \ \mathcal{G}(x_1, \bar{x}_2; A^0)\mathcal{G}(x_2, \bar{x}_1; A^0)] \ ,
\end{aligned} \tag{1.41}$$

$$\begin{aligned}
I_4^{\pm 1} \ &= \ \frac{1}{Z} \int \mathcal{D}[A^{(\pm 1)}] \, e^{-S_g[A^{(\pm 1)}]} \det{}'[D_{A^{(\pm 1)}}] \\
&\times \ [\chi_1(x_1)\bar{\chi}_1(\bar{x}_1)\chi_2(x_2)\bar{\chi}_2(\bar{x}_2) - \chi_1(x_2)\bar{\chi}_1(\bar{x}_1)\chi_2(x_1)\bar{\chi}_2(\bar{x}_2) \\
&- \ \chi_1(x_1)\bar{\chi}_1(\bar{x}_2)\chi_2(x_2)\bar{\chi}_2(\bar{x}_1) + \chi_1(x_2)\bar{\chi}_1(\bar{x}_2)\chi_2(x_1)\bar{\chi}_2(\bar{x}_1)] \ .
\end{aligned} \tag{1.42}$$

Again $\chi_1(x), \chi_2(x)$ are an orthonormal basis of the zero mode subspace in the background of $A^{(1)}$or $A^{(-1)}$ respectively, see eq. (1.34). For a more explicit form of eqs. (1.40)–(1.42) see chapter 4.

We will now present the form of the effective action Γ_{eff}, which is one of the main results in [AJ]. In principle Γ_{eff} is defined by

$$\det{}'[D_{A^{(k)}}] = e^{\frac{1}{2}\Gamma_{eff}[A^{(k)}]} \ , \tag{1.43}$$

but this expression needs regularization. In [AJ] this is done with the Pauli-Villars scheme. The result is the following

$$\begin{aligned}
\Gamma_{eff}[A^{(k)}] \ &= \ \frac{2e^2}{\pi} \int_{T_2} dx b(x) \Box b(x) \ + \ \Gamma_{reg}(M_n) \\
&+ \ \delta_{0,k} \{ 4 \ln |\Theta_1(t_+ | i\tau)|^2 - \frac{2e^2\tau}{\pi} (L_1 t_2)^2 + c(\tau) \} \\
&+ \ (1 - \delta_{0,k}) \{ 2 \ln \det \mathcal{N}_{A^{(k)}} - 2 \ln \det \mathcal{N}_{C^{(k)}} - 2|k| \ln(2|k|/L_1L_2) \}
\end{aligned} \tag{1.44}$$

with $\tau = L_2/L_1$, $t_+ = \frac{eL_2}{2\pi}(t_2 + it_1)$ and the matrix $\mathcal{N}_{A^{(k)}}$ of the zero modes Φ_i in the background field $A^{(k)}$, defined by $(\mathcal{N}_{A^{(k)}})_{i,j} = \int (\Phi_i, \Phi_j)_0$, $i,j = 1, \ldots, 2k$. $\Theta_1(z|i\tau)$ is a Jacobi Θ-function, see [19].

Let us comment the several parts of Γ_{eff}: First the term $\Gamma_{reg}(M_n)$, depending on the regulator masses M_n in the Pauli-Villars scheme, gives an A-independent factor to the regularized fermion determinant and thus drops out, if we normalize the expectation values with Z in eqs. (1.38), (1.39). We will neglect this term in the following.

Second the term $\Gamma_m[b] = \frac{2e^2}{\pi} \int_{T_2} dx b(x) \Box b(x)$ — together with the gauge field term S_g of eq. (1.25) — governs the expectation values of toron-independent gauge field observables in eq. (1.39). Such observables are e.g. Wilson loops or correlation functions of two opposite Polyakov loops, which we use for the definition of the potential later. With $F = dA = \Box b(x) dx^{12}$ the expectation values for these observables Ω are determined by

$$< \Omega >= \frac{\int \mathcal{D}[A^0] \Omega[A] e^{-S'[b]}}{\int \mathcal{D}[A^0] e^{-S'[b]}} \ , \ S'[b] = \frac{1}{2} \int_{T_2} dx \, \Box b(x) (\Box - m^2) b(x) \ , \tag{1.45}$$

with $m^2 = 2e^2/\pi$. This implies that the gauge field degrees of freedom given by $b(x)$ are described by free particles with mass m. It will appear again in the sections concerning the static potential and the correlation of the field strength in the continuum and on the lattice. We want to remark that the difference to the standard (1-flavour) Schwinger model at this point is the factor 2 in the result for m^2, which is due to the two flavours in the geometric Schwinger model.

The part $\Gamma_{tor}(t)$ of Γ_{eff} depending on the torons only (the second line in eq. (1.44)) exists only in the trivial sector. Here it leads to a toron partition

$$P(t) = e^{\frac{1}{2}\Gamma_{tor}(t)} = |\Theta_1(t_+|i\tau)|^4 \; e^{-\frac{e^2\tau}{\pi}(L_1 t_2)^2} \; e^{c(\tau)} \; , \tag{1.46}$$

since the determinant $\det[D_{A^0}]$ separates in $P(t)$ times a toron-independent part. For the contributions to expectation values from the trivial sector $k = 0$ it factors out by the normalization with the partition function Z, if the observables Ω do not depend on t (see eq. (1.45)). For the expectation values of current- and scalar-correlations this is not necessarily so, and the explicit form of $\Gamma_{tor}(t)$ becomes crucial. From the properties of $\Theta_1(z|i\tau)$ (see [19]) the following properties of the toron distribution $P(t)$ can be deduced:

1. $P(t) = 0$, for $t^1 = t^2 = 0$, the multiplicity of this zero is of the order 4. The divergences of the fermion propagators in the topologically trivial sector with zero toron field in eq. (1.41) are compensated by the zero in $P(t)$.

2. $P(t)$ is periodic with respect to the large gauge transformations defined in eq. (1.35), i.e. substitutions $t^\mu \to t^\mu + 2\pi/(eL^\mu)$.

3. $P(t)$ is invariant under the 'reflections' $t^\mu \to 2\pi/(eL^\mu) - t^\mu$.

At last $\Gamma_{zm}(b, C^{(k)})$ (the third line in eq. (1.44)) comes into play for the contributions from the non-trivial sectors $k \neq 0$. As mentioned together with eq. (1.40), this can be the case for correlations of fermion bilinears, where we get contributions from the sectors $k = 0, \pm 1$. However, the non-vanishing of the topologically non-trivial sectors depends also on the quantum number of the bilinear in question with respect to the $U(2)_L \otimes U(2)_R$ symmetry transformations of the internal isospin. We will turn back to this point in chapter 4 dealing with fermion observables.

1.2 The geometric Schwinger model on the lattice

The lattice investigation of a geometric field theory has the advantage that there is a well-defined procedure to put the theory on the lattice without spectrum doubling. It arises naturally from the geometric interpretation of differential forms and the differentiation and codifferentiation in the continuum. This procedure translates forms in the continuum into 'cochains' on the lattice and is connected to the well-known mapping of DeRham complexes on simplicial complexes [21]. The resulting lattice fermions can be mapped onto staggered fermions, also called Kogut-Susskind fermions [10]. In fact, in the continuum limit the latter are known to describe two flavours of Dirac fermions in two dimensions. This corresponds to the equivalence of DK fermions and a pair of Dirac fermions in the continuum, as described in the previous section. However, the geometric picture of the lattice restriction can serve as a guideline for the 'correct' definition of lattice quantities in the sense of the direct translation of forms in the continuum into cochains on the lattice.

In this section we want to describe the lattice restriction of coupled DK fermions and the mapping onto staggered fermions on the one hand. Then we turn to the lattice definition of topological quantities known from the continuum. We will then give first results on the behaviour of these quantities on the lattice.

1.2.1 Dirac-Kähler fermions on the lattice

The lattice restriction of DK fermions is motivated by the fact that a general differential form Φ_{cont} in the continuum may be considered as a linear mapping of every integration area $\mathcal{B}$ on a value c in $\mathbf{C}$ by $c = \int_{\mathcal{B}} \Phi_{cont}$. The lattice restriction of the forms is then given by a restriction of these integration areas to combinations, called chains $\mathcal{C}$, of general lattice cells $[y, H]$ (i.e. points, links and plaquettes), spanned by the lattice unit vectors $b_\mu, \mu \in H$ of length b at the points $y \in \Lambda_b$. The lattice analogues to the forms are then cochains Φ, i.e. linear mappings of chains into $\mathbf{C}$. They may be written as

$$\Phi = \sum_{y,H} \phi_{y,H} \, d^{y,H} \; , \; with \; d^{y,H}([y', H']) = \delta_{yy'} \, \delta_{HH'} \; . \tag{1.47}$$

Here we use the notation Φ for the lattice fields, i.e. the cochains, and denote continuum quantities with the subscript *cont*. The correspondence between cochains Φ and forms Φ_{cont} is set up by

$$\Phi(\mathcal{C}) = \Phi_{\hat{cont}}(\mathcal{C}) \equiv \int_{\mathcal{C}} \Phi_{cont} \; , \tag{1.48}$$

i.e. we obtain a cochain from a differential form in the continuum by the average over the corresponding lattice cells. Because of Stokes theorem this implies for the lattice analogues of the differentiation and codifferentiation d, δ [11]

$$d \to \breve{\Delta}, \text{ with } \breve{\Delta}\Phi(\mathcal{C}) = \Phi(\Delta\mathcal{C}) \; , \quad \delta \to \breve{\nabla}, \text{ with } \breve{\nabla}\Phi(\mathcal{C}) = \Phi(\nabla\mathcal{C}) \; , \tag{1.49}$$

where Δ and ∇ are the boundary and coboundary operator applied to lattice cells. We want to illustrate this correspondence in the case $d \to \Delta$. If Φ is given by Φ_{cont} as in eq. (1.48), we require

$$\breve{\Delta}\Phi(\mathcal{C}) = d\Phi_{cont}(\mathcal{C}) \; , \tag{1.50}$$

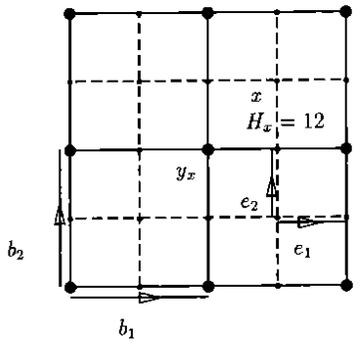

Figure 1.1: Embedding of the fine lattice Λ_{fine} in the coarse lattice Λ_{coarse}.

and thus with Stokes theorem

$$\breve{\triangle}\Phi(\mathcal{C}) = \int_{\mathcal{C}} d\Phi_{cont} = \int_{\triangle\mathcal{C}} \Phi_{cont} = \Phi(\triangle\mathcal{C}) \ . \tag{1.51}$$

The lattice operators defined in eq. (1.49) can be written as operations on the cochain component functions $\phi(x,H)$. We obtain

$$\breve{\triangle}\phi_{y,H} = \rho(\mu,H) \sum_{\mu\in H} \partial^+_\mu \phi_{y,H\setminus\mu} \ , \tag{1.52}$$

$$\breve{\nabla}\phi_{y,H} = \rho(\mu,H) \sum_{\mu\notin H} -\partial^-_\mu \phi_{y,H\cup\mu} \ , \tag{1.53}$$

where the ρ-factors are defined in eq. (1.6) and $\partial^+_\mu, \partial^-_\mu$ are the forward and backward difference operators, respectively. With these definitions the free action for the lattice fermion field, i.e. the cochain component functions reads

$$S_f^{free} = \sum_{y,H} \left\{ \bar{\phi}_{y,H} \ (\breve{\triangle} - \breve{\nabla}) \phi_{y,H} \right\} \ . \tag{1.54}$$

Again we took the massless case, but the inclusion of a mass term is obvious.

The following identifications show the equivalence to staggered fermions: We start with the embedding of our lattice Λ_b, which we call now Λ_{coarse} in a fine lattice Λ_{fine} spanned by unit vectors $e_\mu = \frac{1}{2} b_\mu$, see Figure 1.1. Every point x on Λ_{fine} has a unique representation as

$$x = y_x + e_{H_x} \ , \ \ y_x \in \Lambda_{coarse} \ , \ \ e_{H_x} = \sum_{\mu\in H_x} e_\mu \ . \tag{1.55}$$

This defines y_x and the multi-index H_x giving the position of $x \in \Lambda_{fine}$ with respect to the coarse lattice Λ_{coarse}. Now we can identify the 4-component functions $\phi_{y,H}$ on Λ_{coarse} with 1-component functions χ_x on Λ_{fine} by

$$\chi_x = \phi_{y_x,H_x} \ , \ \ \phi_{y,H} = \chi_{y+e_H} \ . \tag{1.56}$$

The free action in eq. (1.54) then becomes

$$S_f^{free} = \frac{1}{2a} \sum_{x,\mu} \rho_{\mu,x} \left[\bar{\chi}_x \chi_{x+e_\mu} - \bar{\chi}_{x+e_\mu} \chi_x \right] \ . \tag{1.57}$$

For simplicity of notation we have written $\rho_{\mu,x}$ for the sign factors $\rho(\mu, H_x)$. The factor $1/(2a)$, where $a = b/2$ is the lattice constant of the fine lattice, comes from the $1/b$ in the difference operators used in eqs. (1.52), (1.53). Note that with eq. (1.48) $\phi_{y,H}$ is derived from the component function of a continuum form $\phi_{cont}(y', H)$ by the average over $y' \in [y, H]$. In this sense it may seem natural to consider it as a function at the center $x = y + e_H$ of the cell $[y, H]$ rather than at y.

The coupling of the lattice fermion field is obtained by the substitution of the difference operators $\partial^\pm_\mu$ by the corresponding gauge covariant expressions. However, it is a priori not clear, whether this should be done for the differences on the coarse lattice in eqs. (1.52), (1.53) with gauge fields on the links of Λ_{coarse}, or with gauge fields on the links of Λ_{fine} leading to the coupled staggered fermion action corresponding to eq. (1.57)

$$S_f = \frac{1}{2a} \sum_{x,\mu} \rho_{\mu,x} \left[\bar{\chi}_x U_{[x,\mu]} \chi_{x+e_\mu} - \bar{\chi}_{x+e_\mu} U^\dagger_{[x,\mu]} \chi_x \right] \ . \tag{1.58}$$

Both methods formally lead to the coupled DK equation in the continuum limit, but for finite lattice constant the coupled staggered fermion action eq. (1.58) has the advantage to preserve the full symmetry of the free case. This has positive consequences in perturbative calculations [22].

In the lattice Schwinger model the link variables $U_{[x,\mu]}$ are taken from $U(1)$, and we write U^* instead of $U^\dagger$. For the lattice restriction of the action describing the free gauge field we take the 'compact' version introduced by K. Wilson, which also uses $U(1)$-link variables

$$S_g = \frac{\bar{\beta}}{2} \sum_x (2 - P_x - P_x^{-1}) \ , \ \ P_x = U_{[x,1]} U_{[x+e_1,2]} U^*_{[x+e_2,1]} U^*_{[x,2]} \ . \tag{1.59}$$

With $\bar{\beta} = 1/(e^2 a^2)$ it leads to the free gauge field action eq. (1.25) in the continuum limit. For the implications of the 'non-compact' version $S_g^0 = (\bar{\beta}/2) \sum_x (A^1_x + A^2_{x+e_1} - A^1_{x+e_2} - A^2_x)^2$, $A^\mu_x \in \mathbf{R}$, see section 3.2 on Polyakov loop correlations.

We are now ready to set up expectation values of observables $\Omega[U, \bar{\chi}, \chi]$ on the lattice with the path integration formula

$$< \Omega >= \int \mathcal{D}[U] \mathcal{D}[\bar{\chi}, \chi] \, \Omega[U, \bar{\chi}, \chi] \, e^{-S_g[U]} \, e^{-S_f[U,\bar{\chi},\chi]} \ , \tag{1.60}$$

where S_f is the staggered fermion action taken from eq. (1.58). The whole action $S_g + S_f$ is gauge invariant with respect to gauge transformations on the points x of the fine lattice Λ_{fine}. Since this is the lattice we are working with in the following, we simply write Λ instead. Coarse lattice quantities are given a subscript.

Again, we perform the integration over the fermionic degrees of freedom with the well-known Grassmann integration formula. For that we write the fermion action S_f in eq. (1.58) as

$$S_f = \sum_{x,y} \bar{\chi}_x \, M[U]_{xy} \, \chi_y \ , \ \ M[U]_{xy} = \frac{1}{2a} \rho_{\mu,x} \left[U_{[x,\mu]} \delta_{x+e_\mu,y} - U^*_{[y,\mu]} \delta_{x-e_\mu,y} \right] . \tag{1.61}$$

Then we obtain for gauge field observables $\Omega[U]$

$$< \Omega > = \frac{1}{Z} \int \mathcal{D}[U] e^{-S_g[U]} \det(M[U]) \Omega[U] , \quad (1.62)$$
$$\text{with} \quad Z = \int \mathcal{D}[U] e^{-S_g[U]} \det(M[U]) .$$

For fermion observables one obtains expressions in the inverse fermion matrix $M[U]$ defined in eq. (1.61). Let us quote the case of 4-fermi expectation values which we need later on

$$< \bar{\chi}_{x'} \chi_x \bar{\chi}_{y'} \chi_y > = \frac{1}{Z} \int \mathcal{D}[U] e^{-S_g[U]} \det(M[U]) \quad (1.63)$$
$$\times \left[(M[U])^{-1}_{xx'} (M[U])^{-1}_{yy'} - (M[U])^{-1}_{xy'} (M[U])^{-1}_{yx'} \right] .$$

However, this expression assumes the absence of zero modes in the fermion matrix. Comparing with the continuum properties (see subsection 1.1.2) we have to deal with two questions.

First we must be careful with the lattice analogues to the topological zero modes in the continuum, which might be exact zero modes on the lattice too [23]. Even if not, we expect them to be approximately zero. So in eq. (1.63) there will be large values of $(M[U])^{-1}_{xy}$ combined with small values of $\det(M[U])$. Therefore a separate treatment in MC simulations may be necessary, see the next subsection on instantons on the lattice.

Second we expect approximate zero modes corresponding to the harmonic zero modes in the continuum. In fact, in the free case it can be seen easily that there are exact harmonic zero modes on the lattice too. In the continuum the corresponding divergences, appearing for zero toron field $t = 0$, are compensated in a well-defined way by the toron partition $P(t)$, i.e the fermion determinant. This poses the question whether the lattice fermion determinant has the same properties, see the subsection on torons on the lattice.

Finally, let us turn to the expected dependence of expectation values on the $\bar{\beta}$-parameter in eq. (1.59). On the lattice we calculate expectation values of dimensionless observables $\bar{\Omega}$, i.e. observables expressed in units of the lattice constant a by

$$\bar{\Omega} = \Omega a^{-d} , \quad (1.64)$$

where Ω is a physical observable of dimension $[m^d]$ in the formal continuum limit $a \to 0$. If we determine the a-dependence of the lattice parameters accordingly, we expect scaling behaviour for each expectation value in the continuum limit according to eq. (1.64), where the quantities in physical units Ω remain finite (if finite in the continuum). The only parameter in the lattice Schwinger model is $\bar{\beta} = 1/(e^2 a^2)$ in eq. (1.59), here e is the lattice coupling in physical units. For $a \to 0$ the lattice coupling tends to the (bare) coupling of the continuum theory, which is finite, because the Schwinger model needs no renormalization procedure. So the continuum limit is achieved by

$$\bar{\beta}, \bar{L}_1, \bar{L}_2 \to \infty , \quad \text{with} \quad \bar{\beta}/(\bar{L}_1 \bar{L}_2) , \ \bar{L}_1/\bar{L}_2 \text{ constant} . \quad (1.65)$$

If the volume effects are under control we consider merely large $\bar{\beta}$ as the continuum limit or scaling case. For gauge field observables it will turn out in chapter 3 that $\bar{\beta} = 10$ is very close to perfect scaling behaviour, for $\bar{\beta} = 3$ finite a effects come into play and for $\bar{\beta} = 1, 0.3$ the system comes to the region where it is described by the first orders of a strong coupling expansion.

1.2.2 Instantons on the lattice

For the treatment of the Schwinger model on the lattice we must control the remnants of the topological properties in the continuum, mentioned in section 1.1.2. In articles of J. Smit, J.C. Vink [23],[24] a lattice definition of the topological charge is discussed and the spectrum of the coupled Dirac operator for staggered fermions is investigated, see also [25]. In this section we will describe some of these results and present our measurements of the suppression of non-trivial topological sectors on the lattice due to approximate zero modes. These appear as remnant of the index theorem in the continuum eq. (1.33).

The lattice definition of the topological charge Q_{top} is given in terms of the lattice field strength $F_x \equiv F^{12}_x$, which is given by

$$e^{iF_x} = P_x , \ F_x \in [-\pi, \pi) , \quad \text{with } P_x = U_{[x,1]} U_{[x+e_1,2]} U^*_{[x+e_2,1]} U^*_{[x,2]} \quad (1.66)$$

In the continuum limit $a \to 0$ this yields $F_x \to e a^2 F^{cont}(x)$, i.e. F_x is given in lattice units and the coupling e is absorbed. Then in analogy to the Chern index k in the continuum eq. (1.32), Q_{top} is given by

$$Q_{top} = \frac{1}{2\pi} \sum_x F_x , \quad Q_{top} \in \mathbf{Z} . \quad (1.67)$$

In order to see that indeed Q_{top} has its values in $\mathbf{Z}$ let us define $A^\mu_x \in [-\pi, \pi)$ as the phase of $U_{[x,\mu]}$[2]. Then it is obvious that

$$\tilde{F}_x = A^1_x + A^2_{x+e_1} - A^1_{x+e_2} - A^2_x , \quad F_x - \tilde{F}_x = 2\pi n_x , \quad n_x \in \mathbf{Z} . \quad (1.68)$$

If $n_x \neq 0$ we call this a vortex of order n_x. Now, since on a periodic lattice $\sum_x \tilde{F}_x = 0$, we have

$$Q_{top} = \frac{1}{2\pi} \sum_x F_x = \frac{1}{2\pi} \sum_x (\tilde{F}_x + 2\pi n_x) = \sum_x n_x . \quad (1.69)$$

This proves that $Q_{top} \in \mathbf{Z}$.

Even without fermions, i.e. in pure QED_2, the topological charge on the lattice is an interesting feature, because the configurations in the various sectors given by Q_{top} are separated by a potential barrier of height $2\bar{\beta}$. This stems from the fact that a smooth deformation of the link variables $U_{[x,\mu]}$ leading from one minimum to the minimum in the neighbouring topological sector must change at least one vortex $n_x \to n_x \pm 1$. Therefore it must pass a point where $F_x = \pi$ for at least one $x \in \Lambda$. So pure QED_2 provides a toy model for the check of the tunneling behaviour of MC algorithms [26]. We also simulated pure QED_2 as a first check of the MC algorithm we use. For that we measured Polyakov loop correlations at large distances, which get important contributions from the non-trivial sectors (see section 2.1.2).

Back to the geometric Schwinger model on the lattice, i.e. including staggered fermions, the situation changes completely. Remember that in the continuum the topologically non-trivial sectors do not contribute to the expectation values of gauge field observables (see eq. (1.39)), because the fermion determinant vanishes due to the topological zero modes. As described in [23] the spectrum of the coupled Dirac operator on the lattice shows exact zero modes

[2] In fact, it is not important to fix A^μ_x in the mentioned interval, but it must be explicitly defined without (mod 2π)-identifications. For example we could also use the definition given for the determination of lattice torons, see subsection 1.2.3.

only in the special case $F_x = constant = 2\pi k/\bar{V}, |k| = 1, 2$, $\bar{V}$ is the volume in lattice units. Their number and chirality corresponds to the continuum situation, determined by the index theorem eq. (1.33). For weekly fluctuating lattice field strength these zero modes become approximate zero modes (AZMs) only. So, configurations with non-trivial topological charge $Q_{top} \neq 0$ are suppressed, but not totally forbidden. When we get further away from the continuum with a lower $\bar{\beta}$ and more strongly fluctuating F_x this suppression gets weaker, or in other words AZMs corresponding to the topological charge can no longer be made out.

For gauge field observables the contributions of configurations with $Q_{top} \neq 0$ is to be considered as a lattice effect, vanishing with $\bar{\beta} \to \infty$. However, for certain fermion observables there are $k \neq 0$-contributions in the continuum, see eq. (1.38). Corresponding to this we expect contributions for the lattice analogues coming from high values of the propagators M^{-1}_{xy} in eq. (1.63). These contributions should not vanish as $\bar{\beta}$ becomes large. Roughly speaking, the fluctuation of the lattice field strength F_x at finite $\bar{\beta}$ is a sort of regularization of the naive expectation value formula for fermion observables eq. (1.63). This should assure the correct limiting procedure required by the existence of topological zero modes in the continuum.

For the evaluation of such contributions from non-trivial topological sectors in MC simulations we applied the following procedure: We performed separate measurements in systems, which are restricted to the various topological sectors. Then an extra simulation with fluctuating Q_{top} must estimate the weight of the sectors with topological charge k

$$q_k = \frac{1}{Z} \int \mathcal{D}[U] \, \det(m[U]) \, e^{-S_g[U]} \, \delta_{k,Q_{top}[U]} \, , \tag{1.70}$$

which is now a crucial quantity.

Since we expect contributions from the sectors $Q_{top} = 0, \pm 1$ to correlations of fermion bilinears from the continuum formula eq. (1.38), we estimated $q_1 = q_{-1}$ by MC simulations for the cases needed later on. The identity of q_k and q_{-k} comes from the charge conjugation symmetry eq. (1.105). In the case of very small q_1, i.e. for $\bar{\beta} = 10$ we used the trick to modify the gauge field action by

$$S'_g[U] = S_g[U] - c(\delta_{1,Q_{top}[U]} + \delta_{-1,Q_{top}[U]}) \, , \tag{1.71}$$

and measured

$$\begin{aligned} q'_1(c) &= \frac{\int \mathcal{D}[U] \, \det(m[U]) \, e^{-S'_g[U]} \, \delta_{1,Q_{top}[U]}}{\sum_k \int \mathcal{D}[U] \, \det(m[U]) \, e^{-S'_g[U]} \, \delta_{k,Q_{top}[U]}} \\ &= \frac{C q_1}{1 + 2q_1(C-1)} \, , \quad \text{with } C = e^{\bar{\beta}c} \, . \end{aligned} \tag{1.72}$$

Vice versa we have

$$q_1 = \frac{q'_1(c)}{C + 2(1-C)q'_1(c)} \, . \tag{1.73}$$

If we take $c = 0.5$, $q'_1(c)$ is far larger than q_1 and therefore can be estimated to a higher accuracy with a fixed number of configurations. The results for q_1 are presented in Table 1.1. For the statistics of these measurements we refer to subsection 2.1.3.

At last let us comment on the existence of exact zero modes. Any contribution of gauge field configurations with such modes is suppressed in a MC algorithm, since this algorithm

$\bar{\beta}$:	10	3	1	0.3
q_1 :	0.00203 ± 0.00010	0.090 ± 0.003	0.218 ± 0.002	0.172 ± 0.002

Table 1.1: The probability q_1 of configurations with topological charge $Q_{top} = 1$ on a 6×16-lattice for different $\bar{\beta}$.

won't produce any configuration with an exact zero mode, disregarding whether it leads to contributions to expectation values (in a similar way as in the continuum). As pointed out above exact zero modes exist only for configurations with constant field strength and therefore in a part of measure zero in configuration space. On the other hand the integrand, $\det(M[U])$ times the propagators giving the correlations of fermion bilinears, should remain finite, as we conclude from the continuum situation. Thus we expect no systematic error related to exact zero modes for the MC simulation in our case. However, it is a priori not clear, whether the Conjugate Gradient matrix inversion algorithm we used manages to produce reasonable results with not too much expense. This question is treated in subsection 2.1.1.

1.2.3 Torons on the lattice

First we discuss the definition of torons on the lattice in the topologically trivial sector, which is given by $\sum F_x = 0$, F_x is the field strength on the lattice, see eq. (1.66). We use the compact version of the gauge field action, i.e. we have to find an expression for the torons in terms of the link variables $U_{[x,\mu]} \in U(1)$. As a first trial we may choose

$$e^{iA^\mu_x} = U_{[x,\mu]} \, , \quad \text{with } A^\mu_x \in [-\pi, \pi) \, , \quad t^\mu_{naive} = \frac{1}{\bar{V}} \sum_x A^\mu_x \, . \tag{1.74}$$

As for the field strength F_x in eq. (1.66) we define all lattice fields in lattice units and with an absorbed coupling e with respect to the corresponding continuum quantities. The choice of A^μ_x in the above interval is then meant to guarantee the interpretation of A^μ_x as $A^\mu_x = eaA^\mu_{cont}(x)$ in the limit $a \to 0$. However, this definition of the toron field makes no sense because it isn't gauge invariant, even if the configuration $[U]$ is a pure gauge. We may cure this problem by choosing a smooth gauge, e.g. temporal gauge (see below) before evaluating eq. (1.74). However, this is not satisfactory, because for the corresponding continuum quantity no such procedure is required.

Instead we proceed by the restriction of the phases of a complete set of gauge invariant link combinations, i.e. the field strength F_x and the phases of two Polyakov loops p^1, p^2 to the standard interval $[-\pi, \pi)$. Then we determine A^μ_x in an arbitrary gauge, while strictly obeying the lattice version of $F = dA$, given by Stokes' theorem. This leaves no (mod 2π)-ambiguities. In temporal gauge, i.e. with constant gauge fields in time direction and for one fixed time value in space direction, this leads to the following steps:

Determination of the gauge invariant observables F_x, p^1, p^2 in the standard interval by

$$e^{iF_x} = U^1_x U^2_{x+e_1} (U^1_x)^{-1} (U^2_{x+e_2})^{-1} \, , \; F_x \in [-\pi, \pi) \, , \tag{1.75}$$

$$e^{ip^1} = \prod_{x_1} U^1_{(x_1,0)}\,, \qquad p^1 \in [-\pi,\pi)\,, \tag{1.76}$$

$$e^{ip^2} = \prod_{x_2} U^2_{(0,x_2)}\,, \qquad p^2 \in [-\pi,\pi)\,, \tag{1.77}$$

where we have written $U_{[x,\mu]}$ as $U^\mu_{(x_1,x_2)}$.

Gauge fixing (temporal gauge)

$$A^2_x = \begin{cases} p^2/L^2 & \text{for } x_1 = 0\,, \\ (p^2 + \sum_{x_1'=0}^{x_1-1} \sum_{x_2'} F_{x'})/L^2 & \text{for } x_1 \neq 0\,. \end{cases} \tag{1.78}$$

$$A^1_x = p^1/L^1 \quad \text{for } x_2 = 0\,. \tag{1.79}$$

Matching of the remaining A^μ_x so as to fulfill the conditions

$$F_x = A^1_x + A^2_{x+e_1} - A^2_x - A^1_{x+e_2}\,. \tag{1.80}$$

Evaluation of t^μ by

$$t^\mu = \frac{1}{V} \sum_x A^\mu_x \pmod{2\pi/L^\mu}\,. \tag{1.81}$$

We want to make the following remarks. The determination of the A^μ_x in eqs. (1.78), (1.80) is performed according to the rule that all lattice variables are to be thought of as integrals over the corresponding continuum quantities. So the defining equation of the field strength $F(x) = dA(x)$ combined with Stokes theorem forbids shifts by 2π which would arise by the definition of A^μ_x in the standard interval. A 2π-shift of p^1, p^2 in eqs. (1.76), (1.77) corresponds to a large gauge transformation: $A^\mu_x \to A^\mu_x + 2\pi k^\mu/L^\mu$ and thus $t^\mu \to t^\mu + 2\pi k^\mu/L^\mu$. So the projection of this variables to the standard interval is not necessary but part of the gauge fixing. As soon as p^1, p^2 are fixed, the sums of phases A^μ_x along all Polyakov lines on the lattice are given by matching A^μ_x and F_x according to Stokes theorem. This already determines t^μ. So the determination of the torons doesn't depend on the special gauge chosen with eqs. (1.78), (1.79). In that sense, the reason of the non-gauge invariance of the first naive proposal t^μ_{naive} in eq. (1.74) is not the possibly wild fluctuating gauge but the violation of the above connection of F and A, as postulated in eq. (1.80).

The alternate definition of the toron field is to choose a smooth gauge as above and then to evaluate t^μ_{naive} as in eq. (1.74). In the continuum limit, i.e. for sufficiently small $F_x \sim a^2$ this makes no difference to the definition t^μ given above, but for intermediate couplings the latter should be closer to the continuum results, since here the lattice is treated correctly in the sense of an effective theory. Both definitions of lattice torons are compared in Figure 1.3.

We analyzed the toron partition $P(t)$ on a 6×16-lattice with MC simulation for $\bar\beta = 10$ and $\bar\beta = 3$ ($\bar\beta = 10$ will turn out to be a value close to the continuum, see chapter 3). For both values of $\bar\beta$ we evaluated 10,000 equilibrated configurations producing a block diagram of the lattice toron partition. We compared also with the partition $P(t_{naive})$ of the alternate toron definition where A^μ_x is brought to the standard interval in temporal gauge (see eq. (1.74)). For better statistics in the block diagrams Figure 1.2 (full line) and Figure 1.3 the t_2-dependence is integrated out.

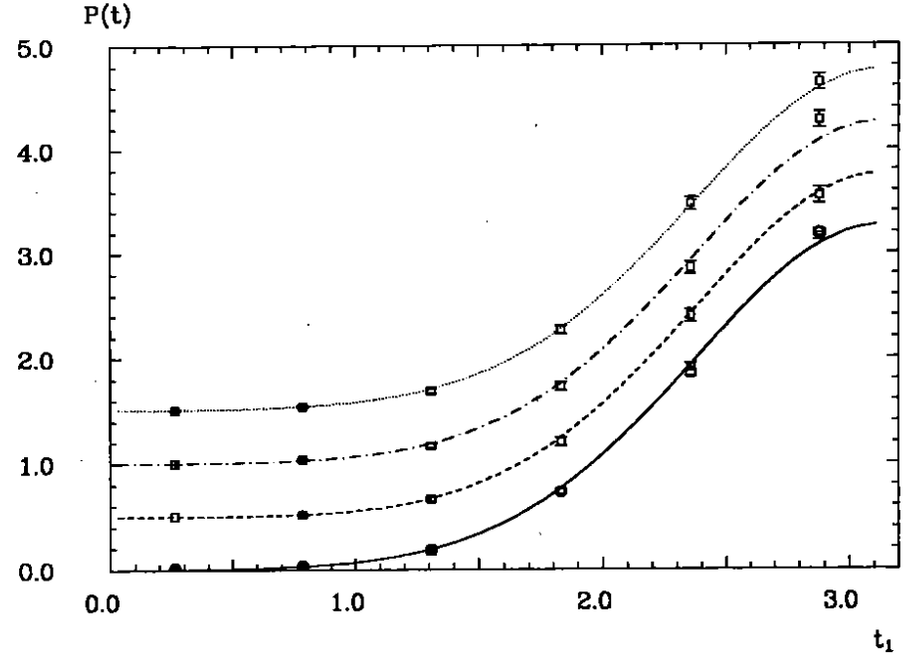

Figure 1.2: Continuum toron partition and MC results for the lattice toron partition with $\bar\beta = 10$ (squares). For the continuum curves and corresponding MC data t_2 is integrated over the intervals $[0, \frac{\pi}{L_2}]$ (full line), $[0, \frac{\pi}{3L_2}]$ (dashed line), $[\frac{\pi}{3L_2}, \frac{2\pi}{3L_2}]$ (dashed-dotted line), $[\frac{2\pi}{3L_2}, \frac{\pi}{L_2}]$ (dotted line). The curves are shifted by 0.5 in y-direction successively in the above order. For the first one the circles are MC data at $\bar\beta = 3.0$.

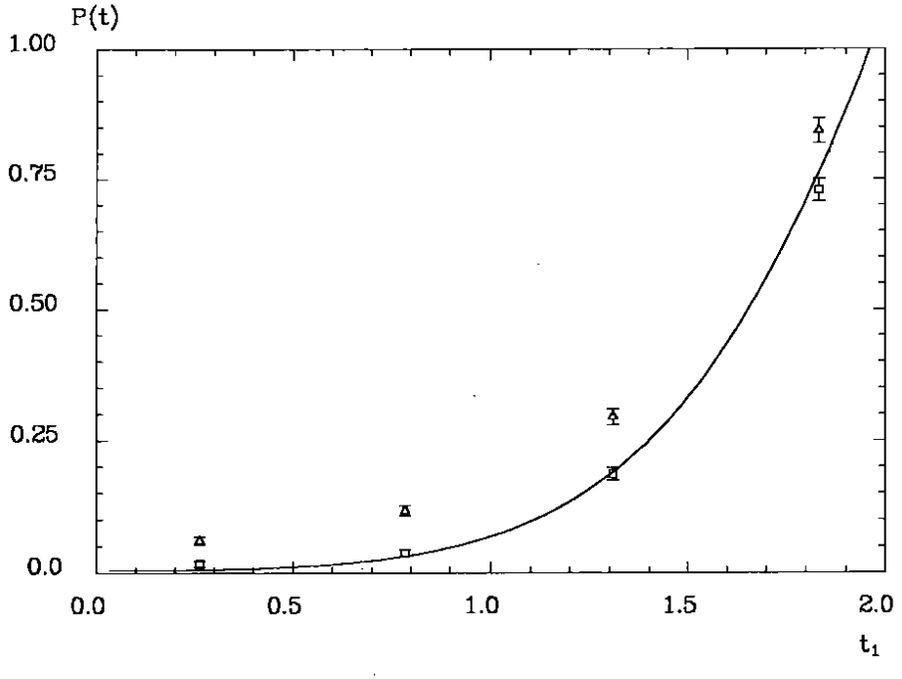

Figure 1.3: Lattice toron partitions $P(t)$ (squares) and $P(t_{\rm naive})$ (triangles) for $\bar{\beta} = 3$.

Furthermore we used the reflection symmetry of the continuum toron partition $P_{cont}(t)$, see eq. (1.46), i.e. we identified t^μ and $2\pi/L^\mu - t^\mu$. This symmetry could also be seen on the lattice. The remaining t_1-range $[0, \pi/L_1]$ is subdivided in six equal intervals and the probability that t_1 is found in one of these is plotted as function at the center of the interval. The effect of this average over the intervals is smaller than the error bars.

In Figure 1.2 we also plotted the t_1-dependence of $P_{cont}(t)$ integrated over $t_2 \in [0, \frac{\pi}{3L_2}]$, $[\frac{\pi}{3L_2}, \frac{2\pi}{3L_2}]$ and $[\frac{2\pi}{3L_2}, \frac{\pi}{L_2}]$. This is compared with the values of the block diagram for the lattice toron with the corresponding t_2-intervals. The t_1-intervals are chosen as above. The normalization for the three curves for splited t_2 are the same, the curve for the integrated t_2 is normalized such that it is the average of these. On a 6×16-lattice a t_2-dependence only within 3 percent is expected from the continuum calculation with $\tau = L^2/L^1 = 8/3$. This behaviour is reproduced by the toron partition on the lattice, as can be seen in Figure 1.2. As a check we measured $P(t)$ on a 4×4-lattice too. There $P(t)$ becomes symmetric for $t_1 \leftrightarrow t_2$, as expected.

For $\bar{\beta} = 10$ no difference between t^μ and t^μ_{naive} could be seen within the error bars. Figure 1.2 shows the block diagram for $P(t)$ described above. It fits the continuum curves. For $\bar{\beta} = 3$ the results for $P(t)$ show a striking similarity to the $\bar{\beta} = 10$-case. So they also agree with the continuum curve within the error bars, see Figure 1.2. This means a very small influence of lattice effects on this partition. In that sense the MC results confirm that the definition of

lattice torons with eqs. (1.75), (1.81) is the correct one and reproduces the toron properties in the continuum also for finite lattice spacings a. In contrary, for $\bar{\beta} = 3$ and small t_1 it can be seen that $P(t_{naive})$ is farer away from the continuum result as expected, see Figure 1.3.

As a check for the hybrid Monte Carlo algorithm used to generate the lattice configurations, the result for the lattice toron partition shows a good reliability of this algorithm, also in the presence of the torons, i.e. non-local quantities coupled to fermions. Moreover, the Conjugate Gradient inversion of the fermion matrix works well even in this case where the toron partition is connected to the suppression of certain toron values by the existence of approximate zero modes of the Dirac operator.

Finally let us turn to the definition of the lattice torons in non-trivial topological sectors. For $k \neq 0$ the definition of t^μ by eq. (1.80) must fail, because there we have $\sum F_x \neq 0$. Again, we proceed analogous to the continuum definition of the toron field in eq. (1.21). There a gauge field $A^{(k)}_\mu(x)$ with topological charge k is decomposed into a topologically trivial gauge field and a field $C^{(k)}_\mu(x)$ of constant field strength by

$$A^{(k)}_\mu(x) = A^0_\mu(x) + C^{(k)}_\mu(x) \ , \quad C^{(k)}_1(x) = \frac{-2\pi k}{eL^1L^2}\, x_2 \ , \quad C^{(k)}_2(x) = 0 \ . \tag{1.82}$$

The toron part of $A^{(k)}_\mu(x)$ is then defined to be the toron part of $A^0_\mu(x)$ given with eq. (1.22). The field $C^{(k)}$ in temporal gauge is not totally fixed by its field strength. The two other requirements for its definition can be chosen to be

$$\int dx^1 C^{(k)}_1(x_1, 0) = 0 \ , \quad \int dx^2 C^{(k)}_2(0, x_2) = 0 \ . \tag{1.83}$$

The lattice analogue to this toron definition for non-zero topological charge can be seen to be a procedure like in the topologically trivial sector, but with the replacement of F_x by $F_x - \sum F_x/\bar{V}$ in eqs. (1.78), (1.80). The fixing of p^1 and p^2 in eqs. (1.76), (1.77) then corresponds to the additional conditions for the subtracted field $C^{(k)}$ in eq. (1.83).

1.3 Symmetry properties

The investigation of the symmetry properties of a lattice model and the relation of the corresponding quantum numbers to continuum quantum numbers is a useful guideline for the definition of lattice observables. This section presents some results on the relation of continuum and lattice quantum numbers in the geometric Schwinger model. These results are based on earlier work on the representation theory in geometric field theories of H. Joos, M. Schäfer [27] and W. Neudenberger [28], see also [29],[30]. In particular, we focus on the consequences of the anomaly in the axial $U(1)$-symmetry for the lattice formulation. A more detailed description of the representation theory of the full symmetry in the Schwinger model in the continuum and on the lattice shall be given in a future publication [31].

1.3.1 Continuum symmetry

The symmetry of the action in the geometric Schwinger model is given by the two-dimensional euclidean group, combined with the flavour transformations we described already in subsection 1.1.1. Without a mass term in the action, the left-handed and right-handed part of the fermion fields can be transformed independently, leading to a $U(2)_R \otimes U(2)_L$ flavour symmetry. The natural form of the DK fermions for these transformations is provided by the Dirac basis, since this basis results from the diagonalization of the flavour transformations, see eqs. (1.12)–(1.14). There are spinorial rotations generated by

$$S\,\psi^b_a(x) \;=\; (x_1\partial_2 - x_2\partial_1)\psi^b_a(x) \;+\; \frac{1}{2}(\gamma^1\gamma^2)_{aa'}\psi^b_{a'}(x) \tag{1.84}$$

and the space reflection (we identify the 1-direction with space)

$$\Pi\,\psi^b_a(x_1,x_2) \;=\; \gamma^2_{aa'}\psi^b_{a'}(-x_1,x_2)\;. \tag{1.85}$$

These rotations and reflections form the spinorial euclidean group $\mathcal{SP} \cong O(2)$ [3]. The transformation rules for the gauge field are obvious. The chiral flavour transformations are generated by the right Clifford product $\vee dx^K$ (see eq. (1.13)) for the right-handed or left-handed part of the DK fermions, denoted by $\psi^b_{R(L)} = \frac{1}{2}(1 \pm \gamma^5)\psi^b$ in the Dirac basis. One obtains

$$d^K\,\psi^b_{R(L)}(x) \;=\; \psi^{b'}_{R(L)}(x)\,\gamma^K_{b'b}\;. \tag{1.86}$$

We denote the group of chiral flavour transformations by $\mathcal{F}$. Since the reflection does not commute with the axial flavour transformations, and the center elements (-1) in $\mathcal{F}$ and $\mathcal{SP}$ are the same transformation, the symmetry group for the geometric Schwinger model is

$$\mathcal{G} = [\,\mathcal{F} \propto (\mathcal{T} \propto \mathcal{SP})\,]\,/\,Z_2\;. \tag{1.87}$$

Here $\propto$ denotes a semidirect product, where the normal divisor is written on the left, $\mathcal{T}$ is the group of translations. In addition there is the charge conjugation symmetry defined as usual.

[3] The spinorial character of the rotations in eq. (1.84) leading to $\exp(i2\pi S) = -1$ can be absorbed by the equivalence $\exp(i\alpha S) \rightarrow \exp(i\alpha/2)$ and thus $\{\exp(i\alpha S)\} \cong SO(2)$.

Another possibility to write the symmetry group $\mathcal{G}$ results, if we take the geometric rotations generated by S^G

$$S^G\,\psi^b_a(x) \;= S\,\psi^b_a(x) \;-\; \frac{1}{2}\psi^{b'}_a(x)(\gamma^1\gamma^2)_{b'b}\;, \tag{1.88}$$

i.e. combinations of spinorial rotations with corresponding vectorial flavour transformations. We also define a geometric reflection as combination $\Pi^G = \Pi \circ d^2$, thus

$$\Pi^G\,\psi^b_a(x_1,x_2) \;=\; \gamma^2_{aa'}\,\psi^{b'}_{a'}(-x_1,x_2)\,\gamma^2_{b'b}\;. \tag{1.89}$$

The group of these geometric transformations can also be mapped on $O(2)$ [4] and is denoted by $\mathcal{GR}$. The difference to $\mathcal{SP}$ lies in the combination with the flavour transformations: the geometric rotations and reflections in general do not commute with the vectorial flavour transformations. Since the DK fermions are transformed as tensors under geometric rotations and reflections, these are more naturally restricted to the lattice symmetry [11].

We restrict the following description of the irreducible representations (irreps) of $\mathcal{G}$ to the point group

$$\overline{\mathcal{G}} \;=\; \mathcal{G}/\mathcal{T} \;=\; (\mathcal{F} \propto \mathcal{SP})\,/\,Z_2 \;\cong\; [\,U(2)_R \times U(2)_L\,] \propto O(2)\;. \tag{1.90}$$

In terms of the representation theory of the complete symmetry group $\mathcal{G}$ this means we give only the representations with zero euclidean momentum. This will be sufficient for our purpose, namely the choice of lattice bilinears corresponding to currents, scalars and pseudoscalars with the different flavour quantum numbers in the continuum.

The irreps of $\overline{\mathcal{G}}$ can be constructed by the Wigner-Mackey procedure [32]. Its application in geometric field theories is described in [27]. Here we only want to mention that within this procedure the irreps of a group $\mathcal{G}$ with normal divisor $\mathcal{N}$ are first characterized by an orbit under the action of $\mathcal{G}$ in the space of irreps of $\mathcal{N}$, denoted by one representative irrep. Secondly they are characterized by an irrep of the fixpoint group $\mathcal{S}_{fix}$ (little group). $\mathcal{S}_{fix}$ is that subgroup of $\mathcal{G}/\mathcal{N}$ which leaves the chosen representative irrep of $\mathcal{N}$ invariant.

So in our case the irreps of $\overline{\mathcal{G}}$ are first characterized by an orbit of irreps of $\mathcal{F}$ under $\overline{\mathcal{G}}$. Since we have

$$U(2) \cong (\,SU(2) \otimes U(1)\,)\,/\,Z_2\;, \tag{1.91}$$

these irreps are given by a set of indices $(I_R, Q_R; I_L, Q_L)$, where $I_R, I_L = 1/2, 1, \ldots$ give the isospin with respect to the right- and left-handed $SU(2)$-transformations, $Q_R, Q_L \in \mathbf{Z}$ give the charge with respect to the right- or left-handed phase transformations $\in U(1)$. Because of the factor Z_2, odd (even) charge has to be combined with half-integer (integer) isospin. If $I_R \neq I_L$ or $Q_R \neq Q_L$, these irreps form (non-trivial) orbits under the action of the reflection $\in \mathcal{SP}$ interchanging left- and right-handed indices.

Secondly, the irreps of $\overline{\mathcal{G}}$ are characterized by the irreps of the fixpoint group $\subset \mathcal{SP}$, which is the group of rotations $\cong SO(2)$ in the case of non-trivial orbits under the reflection. This leads to an index $l \in \mathbf{Z}$. If left- and right-handed indices are equal $\mathcal{SP} \cong O(2)$ itself is the fixpoint group and we get indices $l > 0$ (non-trivial action of the rotations, $\mathcal{SP}$ is represented

[4] The fact that geometric and spinorial rotations and reflections can be mapped on each other is a special feature in two dimensions.

in a 2-dimensional irrep) or $l = 0^+, 0^-$ (trivial action of the rotations, $\mathcal{SP}$ is represented 1-dimensional). In the latter case $\pm$ is the parity index. Again, because of the factor Z_2 in eq. (1.90), odd (even) $Q_V = Q_R + Q_L$ has to be combined with odd (even) l.

Summing up we get a set of quantum numbers ξ characterizing the irreps of $\overline{\mathcal{G}}$

$$\xi \;=\; (I_R, Q_R; I_L, Q_L; l)\;, \tag{1.92}$$

where I_R, Q_R and I_L, Q_L are the right-handed and left-handed isospin and charge, l gives the representation of the rotations. In the case of equal right-handed and left-handed quantum numbers and for trivial action of the rotations the parity is also determined ($l = 0^+, 0^-$).

Now we want to relate the general fermion bilinears to these irreducible representations. The point group $\overline{\mathcal{G}}$ acts locally on the 16 components $\bar{\psi}^b_a(x)\psi^{b'}_{a'}(x)$. We define the 2×2-matrices τ^i, acting on the flavour index b, by the Pauli spin matrices for $i = 1,2,3$ and by $\tau^0 = \mathbf{1}_2$. Then we form the isoscalar current

$$j^0_\mu(x) = \bar{\psi}^b_a(x)\,\gamma^\mu_{aa'}\tau^0_{bb'}\,\psi^{b'}_{a'}(x)\;, \tag{1.93}$$

which transforms under the 2-dimensional irrep $\mathbf{2} : \xi = (0,0;0,0;2)$. The 6 components of the isovector current

$$j^i_\mu(x) = \bar{\psi}^b_a(x)\,\gamma^\mu_{aa'}\tau^i_{bb'}\,\psi^{b'}_{a'}(x)\;,\; i = 1,2,3\;, \tag{1.94}$$

transform under the irrep $\mathbf{6} : \xi = (1,0;0,0;2)$. The interchange of I_R and I_L yields the same irrep, because both isospin combinations belong to the same orbit in $\overline{\mathcal{F}}$ under the reflection. Finally there are the scalars and pseudoscalars for the different isospins

$$s^i(x) = \bar{\psi}^b_a(x)\,\tau^i_{bb'}\,\psi^{b'}_a(x)\;,\;\; s^i_5(x) = \bar{\psi}^b_a(x)\,\gamma^5_{aa'}\tau^i_{bb'}\,\psi^{b'}_{a'}(x)\;,\; i = 0,1,2,3\;. \tag{1.95}$$

They transform under the 8-dimensional irrep $\mathbf{8} : \xi = (1/2,1;1/2,-1;0)$. Note that in two dimensions the axial and vector currents are related by duality

$$j^A_\mu(x) \;=\; \bar{\psi}(x)\,\gamma^\mu\gamma^5\,\psi(x) \;=\; i\,\epsilon_{\mu\nu}j^V_\nu(x)\;, \tag{1.96}$$

because $\gamma^\mu\gamma^5 = i\epsilon^{\mu\nu}\gamma^\nu$ in this case. For an overview of the transformation behaviour of the fermion bilinears see Table 1.2.

As it is well-known, after quantization the classical symmetry of isoscalar axial transformations $U(1)_A$ is broken by an anomaly. Therefore we consider the restriction of the point group $\overline{\mathcal{G}}$ to

$$\overline{\mathcal{G}}_a \;=\; (\,SU(2)_R \otimes SU(2)_L \otimes U(1)_V\,) \propto O(2)\;. \tag{1.97}$$

The irreducible representations of $\overline{\mathcal{G}}$ will in general decompose into smaller irreducible representations of the restricted group $\overline{\mathcal{G}}_a$. The irreps of $\overline{\mathcal{G}}_a$ are characterized by

$$\xi_a \;=\; (I_R, I_L, Q_V; l)\;, \tag{1.98}$$

similar to the irreps of $\mathcal{G}$, with the difference that we have only the quantum number $Q_V = Q_R + Q_L$ instead of Q_R, Q_L separately. This can change the cases in which the reflections are fixpoint operations. Thus the irreps of the full group $\overline{\mathcal{G}}$ can decompose. For the irreps we are interested in, we get the following splitting rules

$$(\mathbf{2})|_{\overline{\mathcal{G}}} \to (\mathbf{2})|_{\overline{\mathcal{G}}_a}\;,\;\; (\mathbf{6})|_{\overline{\mathcal{G}}} \to (\mathbf{6})|_{\overline{\mathcal{G}}_a}\;,\;\; (\mathbf{8})|_{\overline{\mathcal{G}}} \to (\mathbf{4}^+ \oplus \mathbf{4}^-)\big|_{\overline{\mathcal{G}}_a}\;, \tag{1.99}$$

where $\mathbf{4}^\pm$ are the 4-dimensional irreps of $\overline{\mathcal{G}}_a$ given by $\xi_a = (1/2,1/2,0;0^\pm)$. Table 1.2 shows the explicit realization of this decomposition in the space of fermion bilinears.

1.3.2 Lattice symmetry

The lattice approximation of the DK fermions and gauge fields described in subsection 1.2.1 leads to a restriction of the continuum symmetry to the lattice symmetry group $\mathcal{G}_L$. $\mathcal{G}_L$ is a subgroup of the continuum symmetry group $\mathcal{G}$ but with a more complicated structure, see [29]-[33]. We only want to give a brief description of the lattice symmetry transformations here. First there are translations on the coarse lattice Γ_{coarse}, see eq. (1.55)

$$T^\mu\,\chi_x \;=\; \chi_{x-2e_\mu}\;. \tag{1.100}$$

The existence of translations only on the coarse lattice can be understood from the meaning of the lattice fields χ_x as cochains on Γ_{coarse}, see subsection 1.2.1. Next we have the geometric rotations, restricted to discreet rotations by multiples of 90°. These are generated by

$$\omega^G\,\chi_x \;=\; \rho^\omega_x\,\chi_{\omega^{-1}x}\;,\;\; \text{with } \omega^{-1}\,(x_1,x_2) \;=\; (-x_2,x_1)\;. \tag{1.101}$$

The sign factor ρ^ω_x is (-1) for $H_x = 2$, 1 else. The geometric space reflection gets the form

$$\Pi^G\,\chi_x \;=\; (-1)^{x_1}\,\chi_{\Pi x}\;,\;\; \text{with } \Pi(x_1,x_2) \;=\; (-x_1,x_2)\;. \tag{1.102}$$

The generators of the vector flavour transformations (see eq. (1.11)) on the lattice get tied up with translations on the fine lattice

$$d^K\,\chi_x = \rho(H_x,K)\,\chi_{x+e_K}\;,\; e_K = \sum_{\mu\in K} e_\mu\;. \tag{1.103}$$

Therefore they do not give rise to a continuous symmetry except for the mere phase transformations $\in U(1)_V$. On the other hand there is a continuous lattice remnant of the $U(2)_A$, which we denote by $\mathcal{A} = \{A^3(\alpha)\}$,

$$A^3(\alpha)\,\chi_x = e^{i\epsilon_x\alpha}\,\chi_x\;,\; A^3(\alpha)\,\bar{\chi}_x = e^{i\epsilon_x\alpha}\,\bar{\chi}_x\;,\;\; \epsilon_x = (-1)^{x_1+x_2}\;. \tag{1.104}$$

In the continuum this corresponds to the opposite rotation of ψ_R and ψ_L by $\exp(i\alpha\tau^3)$ in the flavour indices b, see eq. (1.117). Finally we have a lattice charge conjugation C, given by

$$\begin{aligned} C\,\chi_x \;&=\; \epsilon_x\bar{\chi}_x\;,\;\; C\,\bar{\chi}_x \;=\; -\epsilon_x\chi_x\;,\\ CU_{[x,\mu]} \;&=\; U^*_{[x,\mu]}\;,\;\; \epsilon_x \;=\; (-1)^{x_1+x_2}\;. \end{aligned} \tag{1.105}$$

The latter will not be considered as a member of the lattice symmetry group $\mathcal{G}_L$.

Since they are related to translations on the fine lattice, the lattice flavour transformations d^K in eq. (1.103) can only be reduced out in momentum space. We set up the modified Fourier transformation with

$$\bar{\psi}^b_a(p) = \frac{1}{N}\sum_x e^{-ipx}\,\gamma^{H_x\,*}_{ab}\,\bar{\chi}_x\;,\;\; \psi^b_a(p) = \frac{1}{N}\sum_x e^{ipx}\,\gamma^{H_x}_{ab}\,\chi_x\;, \tag{1.106}$$

$$\bar{\chi}_x = \frac{1}{N}\sum_{p,a,b} e^{ipx}\,\gamma^{H_x}_{ab}\,\bar{\psi}^b_a(p)\;,\;\; \chi_x = \frac{1}{N}\sum_{p,a,b} e^{-ipx}\,\gamma^{H_x\,*}_{ab}\,\psi^b_a(p)\;. \tag{1.107}$$

$N^2 = L_1 L_2/2$ makes this a orthonormal transformation. The momenta p run over the Brillouin zone of the coarse lattice $p_\mu = 2\pi n_\mu / L_\mu \in [-\pi/2, \pi/2)$, since the translations are also given on the coarse lattice. Then the flavour transformations obtain the form

$$d^K \, \psi_a^b(p) = e^{-i(p,e_K)} \, \psi_a^{b'}(p) \, \gamma_{b'b}^K \, . \tag{1.108}$$

Again we consider the lattice point group $\overline{\mathcal{G}}_L = \mathcal{G}_L / \mathcal{T}_L$ and its irreducible representations, $\mathcal{T}_L$ are the coarse lattice translations in eq. (1.100). We have

$$\overline{\mathcal{G}}_L \;=\; [\, U(1)_V \otimes \mathcal{A} \propto (\overline{\mathcal{F}}_L \propto \mathcal{GR}_L) \,] \;/\; Z_2 \; , \tag{1.109}$$

where $\mathcal{GR}_L \cong D_4$ is generated by ω^G, Π^G and $\overline{\mathcal{F}}_L = \{\pm d^K\}$, with $(d^K)^2 = 1$, because the translations are divided out. The division by Z_2 appears, because the (-1) in $U(1)_V$ and in $\overline{\mathcal{F}}_L$ are the same transformation. Note that the transformations $A^3(\alpha) \in \mathcal{A}$ commute with the geometric reflection Π^G, but we have

$$d^\mu \; A^3(\alpha) \; (d^\mu)^{-1} \;=\; A^3(-\alpha) \; . \tag{1.110}$$

In the discussion of the irreps of $\overline{\mathcal{G}}_L$ we will not explicitly include the $U(1)_V$-part (see eq. (1.109)), because all fermion bilinears on the lattice and in the continuum transform trivial under the $U(1)_V$-transformations. Moreover, these transformations are no subject to the lattice restriction. Again the Wigner-Mackey procedure can be used to classify the irreps of $\overline{\mathcal{G}}_L$. These irreps can be mesonic or fermionic depending on the representation of the center $\{\pm 1\}$ of $\overline{\mathcal{F}}_L$. We do not consider the fermionic irreps with the true representation of this center, since they require an odd fermion number due to the factor Z_2 in eq. (1.109).

Next to that, the set of quantum numbers η defining the irreps of $\overline{\mathcal{G}}_L$ depends on whether the axial transformations $A^3(\alpha)$ are represented trivial or non-trivial. For $A^3(\alpha) \to 1$ the irreps are further determined by an orbit in the space of irreps of the lattice flavour transformations $\overline{\mathcal{F}}_L = \{\pm d^K\}$. Modulo its center, $\overline{\mathcal{F}}_L$ is isomorphic to $Z_2 \otimes Z_2$ and the mesonic irreps are characterized by the mapping

$$(d^1, d^2) \to (\sigma^1, \sigma^2) \; , \quad \sigma^\mu \equiv e^{i\pi L_\mu} = \pm 1 \; , \quad L_\mu = 0, 1 \; . \tag{1.111}$$

The irreps (L_1, L_2) form a non-trivial orbit under the geometric rotation ω^G for $(L_1, L_2) = (0,1), (1,0)$. In this case the remaining fixpoint group, generated by $(\omega^G)^2$, Π^G, is isomorphic to $Z_2 \otimes Z_2$ and the remaining quantum numbers are determined by $(\omega^G)^2$, $\Pi^G \to \pm 1$. In the other cases $\mathcal{GR}_L \cong D_4$ is the remaining fixpoint group. Its irreps are the 2-dimensional χ^0 and 1-dimensional irreps, determined by $\omega^G, \Pi^G \to \pm 1$.

If $A^3(\alpha)$ is represented non-trivial, the irreps m of $\mathcal{A}$

$$A^3(\alpha) \to e^{im\alpha} \; , \quad m \in \mathbf{Z} \quad (m \neq 0) \tag{1.112}$$

form orbits $\{m, -m\}$ under the transformations d^μ according to eq. (1.110). So in this case the irreps of $\overline{\mathcal{G}}_L$ are given by $|m|$ and the irreps of the fixpoint group $\{1, d^{12}\} \otimes D_4$, thus by $d^{12} \to \pm 1$ and the irreps of D_4 sketched above.

Summing up we obtain three different sets of lattice quantum numbers η depending on the representation of $A^3(\alpha) \to e^{im\alpha}$ and $d^{12} \to s^{12} = \pm 1$:

$$\begin{aligned} \eta &= (|m|, \overline{K}, \chi) \; , \quad \text{for } m = 0, \; s^{12} = 1 \; , \\ \eta &= (|m|, \overline{K}, s^{\omega^2}, s^\Pi) \; , \quad \text{for } m = 0, \; s^{12} = -1 \; , \\ \eta &= (|m|, s^{12}, \chi) \; , \quad \text{for } m \neq 0 \; . \end{aligned} \tag{1.113}$$

Here s^{ω^2} and s^Π are the sign factors representing $(\omega^G)^2$ and Π^G respectively. $\overline{K}$ denotes a representative of the flavour orbit and χ defines the representation of the lattice rotations and reflections $\in \mathcal{GR}_L$.

For an overview over the quantum numbers of certain lattice irreps and their realization in the space of 'minimal' lattice bilinears see Table 1.2. The representation of $d^{12}, \omega^G, (\omega^G)^2$ and Π^G is denoted by a mere $+$ or $-$, if they are represented diagonal by a sign factor.

1.3.3 The relation of continuum and lattice representations

It is well-known that one obtains restrictions on the quantum numbers of a lattice observable Ω designed to approximate a continuum observable Ω_{cont} with the following procedure: If we restrict the continuum symmetry group $\mathcal{G}$ to the lattice group $\mathcal{G}_L$ the space of an irreducible representation of $\mathcal{G}$ decomposes into irreducible subspaces of $\mathcal{G}_L$. The lattice approximation of an observable, transforming under an irreducible continuum representation $U_\mathcal{G}^\xi$, should be described by lattice observables, transforming under those irreducible lattice representations $U_{\mathcal{G}_L}^\eta$ which appear in the restriction of $U_\mathcal{G}^\xi$ to $\mathcal{G}_L$. The intertwining numbers $I(\xi, \eta)$ state how often a lattice irrep $U_{\mathcal{G}_L}^\eta$ is contained in the restriction of an continuum irrep to the lattice symmetry group $U_\mathcal{G}^\xi|_{\mathcal{G}_L}$

$$U_\mathcal{G}^\xi\big|_{\mathcal{G}_L} \;=\; \bigoplus_\eta I(\xi, \eta) \, U_{\mathcal{G}_L}^\eta \; . \tag{1.114}$$

So $I(\xi, \eta) \neq 0$ is a necessary condition for the interpretation of a lattice observable with lattice quantum number(s) η as approximation of a continuum observable with continuum quantum number(s) ξ.

The splitting of the relevant continuum irreps into lattice irreps can be read off from Table 1.2. The irreducible continuum representation **2** remains irreducible, the **6** decomposes in 3 lattice doubletts, the **8** decomposes in 4 lattice doubletts. It appears that all continuum irreps belonging to fermion bilinears decompose in different lattice irreps. Conversely this means that in this special case we can relate a continuum quantum number ξ to the lattice quantum numbers η in a unique way.

On the other hand we expect that there are observables in the different irreducible subspaces of $U_\mathcal{G}^\xi|_{\mathcal{G}_L}$ which show the same behaviour in the continuum limit. We call this symmetry restoration. In our case, if M_x and M_x' (with lattice quantum numbers η, η') are bilinears belonging to the same continuum quantum number ξ by the above intertwining procedure, we expect the same decay masses for the corresponding correlations in the continuum limit, i.e. $m_\eta = m_{\eta'}$. If symmetry restoration takes place only in the framework of the anomalous broken continuum point group $\overline{\mathcal{G}}_a$, see eq. (1.97), while the full symmetry is not restored, we conclude that the lattice indeed reproduces the anomaly in the continuum limit.

Let us see what is the difference between full and anomalous symmetry restoration. Since we have

$$\overline{\mathcal{G}}_L \;\subset\; \overline{\mathcal{G}}_a \;\subset\; \overline{\mathcal{G}} \; , \tag{1.115}$$

the decomposition of the irreps of $\overline{\mathcal{G}}$ to irreps of $\overline{\mathcal{G}}_a$ due to the anomaly is compatible with the decomposition to irreps of $\overline{\mathcal{G}}_L$ due to the lattice restriction: The irreducible representation spaces with respect to $\overline{\mathcal{G}}$ labelled by ξ decompose in irreducible subspaces ξ_a with respect to the representation of $\overline{\mathcal{G}}_a$, see eqs. (1.98), (1.99). The further restriction of $\overline{\mathcal{G}}_a$ to $\overline{\mathcal{G}}_L$ then leads

to those irreducible subspaces η with respect to $\overline{\mathcal{G}}_L$ which we obtain by the restriction of $\overline{\mathcal{G}}$ to $\overline{\mathcal{G}}_L$ in one step. Thus, if m_η are the decay masses of correlations of lattice bilinears with quantum numbers η, anomalous symmetry restoration is indicated by the following relation in the continuum limit

$$\begin{aligned} m_\eta &\rightarrow m_{\eta'} \ , \ \text{for } \xi_a(\eta) = \xi_a(\eta') \ , \ \text{thus } \xi(\eta) = \xi(\eta') \ , \\ m_\eta &\neq m_{\eta'} \ , \ \text{for } \xi_a(\eta) \neq \xi_a(\eta') \ , \ \text{but } \ \xi(\eta) = \xi(\eta') \ . \end{aligned} \tag{1.116}$$

Here $\xi(\eta)$ ($\xi_a(\eta)$) are the quantum numbers with respect to the (anomalous broken) continuum symmetry. As mentioned above, they are determined by η in the case of irreps belonging to fermion bilinears. If the lattice is in the scaling region, eq. (1.116) should hold approximately, results are given in chapter 4.

Table 1.2 presents the stepwise decomposition of the irreducible spaces of $\overline{\mathcal{G}}$ in irreducible subspaces with respect to the action of $\overline{\mathcal{G}}_a$ and $\overline{\mathcal{G}}_L$. The decomposition structure can be read off from the explicit local realization of these irreps in the space of fermion bilinears, see eqs. (1.93)–(1.95). For that one has to consider the geometric reflection Π^G the geometric rotation ω^G by $\pi/2$, see eqs. (1.88), (1.89)[5], and the following flavour transformations, here taken to be vectorial (V^i) and axial (A^i) instead of left-handed and right-handed, $i = 0,1,2,3$

$$\begin{aligned} V^i(\alpha)\,\psi^b_a &= \exp\left(i\alpha\,\psi^{b'}_a \tau^i_{b'b}\right) \ , \ V^i(\alpha)\,\bar\psi^b_a = \exp\left(-i\alpha\,\tau^i_{bb'}\bar\psi^{b'}_a\right) \ , \\ A^i(\alpha)\,\psi^b_a &= \exp\left(i\alpha\,\gamma^5_{aa'}\,\psi^{b'}_{a'}\tau^i_{b'b}\right) \ , \ A^i(\alpha)\,\bar\psi^b_a = \exp\left(i\alpha\,\tau^i_{bb'}\,\bar\psi^{b'}_{a'}\gamma^5_{a'a}\right) \ . \end{aligned} \tag{1.117}$$

The τ^i-matrices, $i = 0,1,2,3$ are defined in eqs. (1.93)–(1.95)[6]. For $\overline{\mathcal{G}}_a$ the axial isoscalar transformation must be omitted and for $\overline{\mathcal{G}}_L$ only the axial transformation $A^3(\alpha)$ remains continuous. The discreet lattice remnants of the flavour transformations $\overline{\mathcal{F}}_L = \{d^K\}$ are represented 1-dimensional as mentioned in eq. (1.111).

Now we can choose lattice bilinears in the various irreducible spaces with respect to $\overline{\mathcal{G}}_L$. For that we use the identification of the lattice symmetry operations in eqs. (1.101)–(1.104) with the corresponding versions in the continuum symmetry, restricted to $\overline{\mathcal{G}}_L$. In Table 1.2 we give the minimal lattice bilinears transforming under those irreps of $\overline{\mathcal{G}}_L$ which are obtained in the above decomposition of the continuum irreps **2, 6, 8**. Here minimal lattice bilinears means that we take the minimal number of links between $\bar\chi$ and χ. These fields must be covariant under coarse lattice translations. We use the following definitions

$$M^0_L(x) = \frac{1}{2} e^{i\pi(L,x)}\ \bar\chi_x\,\chi_x \ , \tag{1.118}$$

$$M^{\mu\,+}_L(x) = \frac{1}{2} e^{i\pi(L',x)}\ \left[\bar\chi_x\,U_{[x,\mu]}\,\chi_{x+e_\mu} + \bar\chi_{x+e_\mu}\,U^*_{[x,\mu]}\,\chi_x\right] \ , \tag{1.119}$$

$$M^{\mu\,-}_L(x) = \frac{i}{2} e^{i\pi(L',x)}\ \left[\bar\chi_x\,U_{[x,\mu]}\,\chi_{x+e_\mu} - \bar\chi_{x+e_\mu}\,U^*_{[x,\mu]}\,\chi_x\right] \ , \tag{1.120}$$

$$M^{12}_L(x) = \frac{1}{8} e^{i\pi(L',x)} \sum_{(\mu,\nu)} \bar\chi_x\,U_{[x,\mu]}\,U_{[x+e_\mu,\nu]}\,\chi_{x+e_\mu+e_\nu} \ . \tag{1.121}$$

[5]The lattice versions of these geometric transformations are given in eqs. (1.101), (1.102).

[6]Here it is important to define the τ-matrices corresponding to the γ-matrices in the definition of the Dirac basis eqs. (1.12), (1.14), i.e. $\tau^3 \hat{=} \gamma^5$. This explains why the transformations $A^3(\alpha)$ can have a distinctive role in the lattice restriction of the symmetry.

Here $L = (L_1, L_2)$, $L_\mu = 0,1$ is understood in the sense of eq. (1.111), i.e. $\exp(i\pi(L,x)) = (\sigma^1)^{x_1}(\sigma^2)^{x_2}$, $\sigma^\mu = \exp(i\pi L_\mu) = \pm 1$. For $M^{2\pm}_L(x), M^{12}_L(x)$, L' is given by $(L'_1, L'_2) = (1 - L_1, L_2)$, for $M^{1\pm}_L(x)$ $L' = L$. Furthermore, for the field $M^{12}(x)$ the double indices (μ,ν) run over $(\pm1,\pm2),(\pm2,\pm1)$, and we have defined $U_{x,-\mu} = U^*_{x-e_\mu,\mu}$. The definitions of the continuum bilinears $j^i_\mu(x), s^i(x), s^i_5(x)$ are given in eqs. (1.93)–(1.95).

Since the lattice flavour transformations d^K are related to translations (see eq. (1.103)) and the lattice point group $\overline{\mathcal{G}}_L = \mathcal{G}_L/\mathcal{T}$ is no subgroup of $\mathcal{G}_L$, we have to define the operation of $\overline{\mathcal{G}}_L$ on lattice fields modulo translations. In this sense L gives the quantum number of the above lattice bilinears $M^a_L(x)$ with respect to the lattice flavour transformations d^K, considered as elements of the point group. Modulo translations they act according to eq. (1.111).

We have summarized our results in Table 1.2. It contains a complete group theoretical analysis of the fermion bilinears in the continuum, including the effects of anomalous symmetry breaking. The relation to lattice bilinears is defined in terms of the point groups on the lattice and in the continuum. These results are the basis for the analysis of our lattice simulations of fermion observables in chapter 4. There the correlations of local fields $M^0_L(x)$ and of 1-link fields $M^1_L(x)$ are calculated and conclusions on anomalous symmetry restoration are drawn.

cont. bilin.	$\xi(\overline{\mathcal{G}})$	$\xi_a(\overline{\mathcal{G}}_a)$	lattice quantum numbers η $\lvert m\rvert$	(L_1,L_2)	d^{12}	$(\omega^G)^2$	ω^G	Π^G	lattice bilin.
j_1^0	$(0,0;0,$	$(0,0,$	0	$(0,0)$	$(+)$	$\chi^0(D_4)$		$(-)$	$M^{1+}_{(0,0)}$
j_2^0	$0;2)$	$0;2)$						$(+)$	$M^{2+}_{(0,0)}$
j_1^3	$(1,0;0,$	$(1,0,$	0	$(1,1)$	$(+)$	$\chi^0(D_4)$		$(+)$	$M^{2-}_{(1,1)}$
j_2^3	$0;2)$	$0;2)$						$(-)$	$M^{1-}_{(1,1)}$
j_1^1			1	$((0,1))$	$-$	$(+)$	$+$	$+$	$M^{0}_{(0,1)}$
j_2^2				$((1,0))$					$M^{0}_{(1,0)}$
j_2^1			1	$((0,1))$	$-$	$(+)$	$+$	$-$	$M^{12}_{(0,1)}$
j_1^2				$((1,0))$					$M^{12}_{(1,0)}$
s^0	$(\frac{1}{2},1;\frac{1}{2},$	$(\frac{1}{2},\frac{1}{2},$	1	$((0,0))$	$+$	$(+)$	$+$	$+$	$M^{0}_{(0,0)}$
s_5^3	$-1;0)$	$0;0^+)$		$((1,1))$					$M^{0}_{(1,1)}$
s_5^1			0	$(0,1)$	$(-)$	$-$		$+$	$M^{2-}_{(0,1)}$
s_5^2				$((1,0))$				$(-)$	$M^{1-}_{(1,0)}$
s_5^0		$(\frac{1}{2},\frac{1}{2},$	1	$((0,0))$	$+$	$(+)$	$+$	$-$	$M^{12}_{(0,0)}$
s^3		$0;0^-)$		$((1,1))$					$M^{12}_{(1,1)}$
s^1			0	$(0,1)$	$(-)$	$-$		$-$	$M^{1+}_{(0,1)}$
s^2				$((1,0))$				$(+)$	$M^{2+}_{(1,0)}$

Table 1.2: Intertwining of the irreps of $\overline{\mathcal{G}}$, $\overline{\mathcal{G}}_a$, $\overline{\mathcal{G}}_L$ and realization of these irreps in the space of continuum and lattice bilinears. The lattice quantum numbers are given in brackets if they do not characterize the lattice irrep. They are only given for the second basis member of the irreducible subspace if they differ with respect to the first member.

Chapter 2

Tools

2.1 Hybrid Monte Carlo

For the Monte Carlo results presented in this thesis we used the hybrid Monte Carlo (HMC) algorithm with pseudofermions [9]. With that method we generated equilibrated gauge field configurations for different $\tilde{\beta}$-parameters on a 16×6-lattice. It is well-known [34] that for staggered fermions there is an easy way to cure the doubling which arises for pseudofermions. Let us briefly describe this algorithm. We substitute the fermion determinant by

$$\det(M[U]) = \int \mathcal{D}[\Phi_e^\dagger, \Phi_e]\, e^{-S_P[\Phi_e^\dagger, \Phi_e, U]}\ ,\ S_P = \Phi_e^\dagger (M[U]^\dagger M[U])^{-1} \Phi_e\ . \tag{2.1}$$

The pseudo fermion field Φ is bosonic and complex, so the integration of these degrees of freedom would lead to $|\det(M[U])|^2$. However, for staggered fermions it is possible to take Φ only on the even points on the lattice (which we indicated by Φ_e), and thus to remove the unwanted square [34].

Because the pseudofermions are bosonic fields the corresponding integrals can be evaluated by MC methods. So the algorithm has to generate configurations of gauge fields U and pseudofermions Φ_e, governed by the action S_P in eq. (2.1) and the gauge field action S_g in eq. (1.59). This is achieved by updating Φ_e and U in turns while the other degrees of freedom are held fix respectively. For the pseudofermion update an exact heatbath [35] is used (because of the inverse fermion matrix in the pseudofermion action). The update of the gauge field U is a Metropolis step, where the proposal is produced by the molecular dynamics (MD) method. Roughly speaking this method has the advantage to propose comparatively uncorrelated configurations without a breakdown of the acceptance rate in the Metropolis decision. For a detailed description of this algorithm we refer to the literature [9],[36].

In the following subsections we want to discuss its behaviour in the context of the topological properties of the lattice Schwinger model with staggered fermions. In particular there are two problems. First the MD steps and the Metropolis decision require an inversion of the fermion matrix, i.e. a solution of a linear equation $(M^\dagger M)\xi = \eta$, see eq. (2.1). The influence of the approximate zero modes (AZMs) from subsection 1.2.2 must be discussed. Secondly we argued in that subsection that the algorithm has to tunnel a potential barrier if it wants to change the topological sector. It will turn out that this requires extra Metropolis steps called instanton hits [24],[37]. At last, in subsection 2.1.3 we present the statistics of the generated configurations.

$\bar{\beta}$:	10	3	1	0.3
N_{CG} $(Q_{top}=0)$:	17.9 ± 0.1	23.8 ± 0.1	38.2 ± 0.3	46.1 ± 0.3
N_{CG} $(Q_{top} \neq 0)$:	26.0 ± 0.1	28.2 ± 0.1	39.6 ± 0.2	46.7 ± 0.3

Table 2.1: The average number N_{CG} of Conjugate Gradient iterations in the topologically trivial and non-trivial sectors for different $\bar{\beta}$.

2.1.1 Inversion of the fermion matrix

As mentioned above, equations of the form

$$(M[U]^\dagger M[U])\xi = \eta \tag{2.2}$$

must be solved in the HMC algorithm. First this occurs in the MD method for the gauge field proposal. It leads to the main effort determining the expense of an uncorrelated configuration and thus the efficiency of the algorithm. Secondly, such an equation must be evaluated for the Metropolis decision which guarantees that the generated configurations are in equilibrium. Thus the matrix inversion must be sufficiently exact. In addition the evaluation of fermionic expectation values in eq. (1.63) also leads to eq. (2.2) with

$$\eta = M[U]\zeta^{(a)} \ , \ \zeta_x^{(a)} = \delta_{xa} \ . \tag{2.3}$$

For the numeric solution of eq. (2.2) we used the Conjugate Gradient (CG) algorithm without preconditioning [38]. For small lattices as ours it is known to be the simplest and best method. However, we had to check its performance, because the appearance of AZMs in the gauge field sectors with $Q_{top} \neq 0$ means bad-conditioned matrices, i.e. there are eigenvalues on very different scales. For such matrices the convergence rate of inversion algorithms is known to become small (or the algorithm won't even converge at all). The impact of (topological) AZMs on a multigrid inversion algorithm in the Schwinger model was investigated in [39].

In order to control this behaviour we measured the average number N_{CG} of CG iterations needed for the evaluation of eqs. (2.2), (2.3) up to a given accuracy ($\|r^{(n)}\|^2 < 10^{-8}$, see below) on a 6×16-lattice and for $\bar{\beta} = 10, 3, 1, 0.3$. The results are presented in Table 2.1. The influence of the AZMs in the topologically non-trivial sectors can be seen for $\bar{\beta} = 10$. However, the average iteration number N_{CG} indicates no severe problems with the convergence of the matrix inversion due to the AZMs. On the other hand, for lowering $\bar{\beta}$ the different behaviour of the CG algorithm in the different sectors vanishes, but the total number of iterations increases.

Second we checked whether the CG algorithm remains sufficiently exact for the termination condition we used. A termination condition should terminate the algorithm solving the linear equation (2.2) after the iteration n, if the error of the approximate solution $\xi^{(n)}$ is small enough, i.e. $\|\xi - \xi(n)\|^2 < \epsilon$, where ϵ is a given small number. However, one does not know the solution vector ξ. Thus the termination condition has to be formulated in terms of the residuum $r^{(n)}$ after the nth iteration

$$\|r^{(n)}\|^2 < \epsilon \ , \ \ r^{(n)} = \eta - (M[U]^\dagger M[U])\,\xi^{(n)} \ . \tag{2.4}$$

Since the residuum vector $r^{(n)}$ is $M^\dagger M$ times the error vector $(\xi - \xi^{(n)})$, in the subspaces with very small eigenvalues a small residuum means not necessarily a small error. In particular we expect this for the presence of AZMS as lattice-remnants of the index theorem.

In order to control this difficulty, we took a few configurations at $\bar{\beta} = 10$. In this background we calculated the values of fermion observables (see chapter 4), where we took different termination conditions for the CG solver of eqs. (2.2), (2.3), given by ϵ in eq. (2.4). If the dependence on ϵ could be seen to vanish compared with statistical errors for $\epsilon < \bar{\epsilon}$ we took $\bar{\epsilon}$ to give a good termination condition. With a value $\epsilon = 10^{-8}$ the largest relative deviation could be seen to be smaller than 1% for configurations from both sectors $Q_{top} = 0$ and $Q_{top} = 1$. However, the largest relative deviations appeared for very small values which get far bigger statistical errors in the simulation. So we consider $\epsilon = 10^{-8}$ to yield a sufficient accuracy of the CG algorithm.

2.1.2 Instanton hits

As mentioned already in subsection 1.2.2, the topological sectors on the lattice are separated by a potential barrier in the gauge field action S_g eq. (1.59). The fact that the MC algorithm may not manage to tunnel this barrier must not be mixed up with the suppression of the non-trivial topological sectors for $a \to 0$. For two reasons one should include the influence of these sectors. First we argued in subsection 1.2.2 that the contributions with $Q_{top} \neq 0$ to fermionic expectation values may correspond to the $k \neq 0$ contributions in the continuum coming from the fermion integration formula in the presence of zero modes eq. (1.38). Secondly, a non-vanishing probability for topologically non-trivial sectors is an important lattice effect. Therefore it is crucial if one wants to study the transition of the lattice theory from the strong coupling region to scaling behaviour. This is carried out in the chapter on gauge field observables.

Because of the suppression of the non-trivial sectors in the theory with fermions, it seems reasonable to study the tunneling behaviour of the HMC algorithm in pure QED_2, i.e. without fermions, as a first check. Even in this case it can be seen that for sufficiently large $\bar{\beta}$ ($\bar{\beta} = 3, 10$ in our simulations) we must use a trick to ensure the ergodicity of the system with respect to the topological charge. The so-called instanton hits [24],[37] propose a change in the gauge field $U \to U'$ which changes the topological charge $Q_{top} \to Q_{top} \pm 1$. Since we deal with $U(1)$-fields this may be expressed as

$$A_x^\mu \to A_x^{\mu\prime} = A_x^\mu \pm \Delta A_x^\mu \ , \ \text{ with } U_{[x,\mu]} = e^{iA_x^\mu} \ . \tag{2.5}$$

An equal probability for positive and negative sign in eq. (2.5) and a following Metropolis decision ensure the detailed balance of this updates.

The crucial point is now the acceptance rate P_A in this Metropolis decision, which will in practice decide over the applicability of the method. In other words we must provide sensible proposals so that the change of Q_{top} will not lead to unnecessary costs in the action. The best proposal will be the one which leads from the minimum in one sector to the minimum in the neighbouring sector. In pure QED_2 this is easy to achieve. With ΔFx obtained from ΔA_x^μ as in eq. (1.66) we choose ΔA_x^μ in an arbitrary gauge so that

$$\Delta F_x = \pm \frac{1}{2\pi\bar{V}} \ , \tag{2.6}$$

$\bar{V}$ is the volume in lattice units. This procedure can be shown to work well in pure QED_2 [40], in the sense that the acceptance rate P_A remains finite in the continuum limit

$$\lim_{a\to 0} P_A(\frac{\beta}{a^2}, \frac{V}{a^2}) = P_A^c(\beta, V) > 0 \ , \quad \text{for any fixed } \beta, V. \tag{2.7}$$

We checked the implementation of these instanton hits in our algorithm on a 10×10 lattice by measuring Polyakov loops, which get substantial contributions from $Q_{top} \neq 0$ (see section 3.2.1). The analytic results for large $\bar{\beta}$ in this section where easily reproduced within very small statistical errors.

The situation including dynamical fermions is more involved. We did no systematic investigation of this case. Nevertheless we want to present some ideas on the arising problems. We would like to translate the criterion for a proposed shift in the gauge field phase ΔA_x^μ jumping from the minimum of the combined action $S_g[U] + S_P[\Phi, U]$ at $Q_{top} = 0$ to the minimum at $Q_{top} = \pm 1$, the pseudofermion field Φ is fixed[1]. Starting with a pure gauge configuration U, a proposal as in eq. (2.6) minimizes the gauge field part $S_g[U']$ of the action for the new configuration U'. On the other hand a relatively smooth field strength F_x' brings the AZMs in the topologically non-trivial sectors closer to zero and thus increases the pseudofermion part $S_P[\Phi, U']$. In the simulations for $\bar{\beta} = 3, 10$ (where instanton hits were necessary) the increase of $S_P[\Phi, U']$ could be seen to have the far more important effect on the acceptance rate P_A for the instanton hits given with eq. (2.6). However, the implementation of these hits still sort of worked for our 6×16-lattice, if we guaranteed that the lattice toron (see subsection 1.2.3) was simultaneously shifted by a random number. Then the penalty for instanton hits, which are not well-adapted to the situation with dynamical fermions, are large autocorrelation times in the topological charge Q_{top}, see the next subsection on the statistics of the generated configurations.

The toron shifts are implemented as

$$\delta t_\mu = R\, 2\pi / L_\mu \ , \tag{2.8}$$

where R is a random number between 0 and 1. Note that the toron components are defined (mod $2\pi/L_\mu$) due to large gauge transformations, see eq. (1.81). The necessity of toron shifts can be understood from the situation in the continuum, see subsection 1.1.2. There the toron partition is peaked at $t_\mu = \pi/L_\mu$ for the trivial topological sector $k = 0$. We reproduced this behaviour on the lattice, see subsection 1.2.3. Now, if the pseudofermion field is fixed, the toron partition is different, but the peaks of these fixed pseudofermion partitions must approximately lie near the peak after (pseudo)fermion integration. For $k \neq 0$ the effective action Γ_{eff} after fermion integration does not depend on the toron t. Again for fixed pseudofermion field this is not true. However, we mentioned together with eq. (1.36) that a shift in the toron part of the gauge field corresponds to a shift in the eigenmodes of the DKE round the torus. Vice versa this means that for fixed fermion field and after integration over the remaining parts of the gauge field a peak of the toron partition can be situated at any t, $t_\mu \in [0, 2\pi/L_\mu)$. The situation could be seen to be the same on the lattice. In fact, the dependence of the pseudofermion action $S_P[\Phi, U]$ on the lattice toron for fixed Φ is very strong. So we must

[1] It may seem more sensible to propose a simultaneous shift of U and Φ, because the pseudofermion action S_P at $Q_{top} \neq 0$ strongly depends on the matching of Φ avoiding the AZMs in the background of U.

Lattice size:	P_A :	q_1 :
4×4	$0.144 \cdot 10^{-2} \pm 0.014 \cdot 10^{-2}$	$0.136 \cdot 10^{-2} \pm 0.014 \cdot 10^{-2}$
8×8	$0.350 \cdot 10^{-2} \pm 0.029 \cdot 10^{-2}$	0.030 ± 0.008
12×12	$0.107 \cdot 10^{-2} \pm 0.013 \cdot 10^{-2}$	0.122 ± 0.016
16×16	$0.209 \cdot 10^{-3} \pm 0.068 \cdot 10^{-3}$	0.200 ± 0.044

Table 2.2: The acceptance rate P_A for instanton hits with arbitrary toron-shift and the probability q_1 of the first topological sector for different lattice sizes and fixed $\bar{\beta} = 4$.

allow for random shifts in the lattice toron when proposing a gauge field configuration in a new topological sector[2].

In order to show the very limited applicability of the described instanton hits with constant shift in the field strength and a simultaneous toron-shift, we measured the acceptance rate P_A for these hits and, for comparison, the probability q_1 for $Q_{top} = 1$ (see eq. (1.70)). We took a fixed $\bar{\beta} = 4$ and different lattice sizes $\bar{V}$, see Table 2.2. For increasing $\bar{V}$ the acceptance rate P_A breaks down in spite of the increase in q_1, which should rise the acceptance rate for topologically non-trivial proposals too. So for larger lattices the instanton hit procedure must be improved.

2.1.3 Statistics of the generated configurations

The Monte Carlo results in this thesis are extracted from gauge field configurations on a $\bar{L}_1 \times \bar{L}_2$-lattice for $\bar{\beta}$-values $\bar{\beta} = 10, 3, 1, 0.3$. In most cases, i.e. for plaquette correlations and correlations of fermion bilinears, we took $\bar{L}_1 = 6$ and $\bar{L}_2 = 16$, for Polyakov loop correlations we read the same configurations as a 16×6-ensemble, i.e. we interchanged the x_1- with the x_2-direction. As mentioned in subsection 1.2.2, for the measurement of fermion observables at $\bar{\beta} = 3, 10$ we generated configurations in the topological sectors $Q_{top} = 0$ and $Q_{top} = 1$ separately and determined the probability of these sectors in an extra simulation.

Let us first give the parameters of the HMC algorithm used to generate these configurations. For the Molecular Dynamics method producing the proposal for a gauge field update we used the following fine tuning parameters: The artificial time ('computer time') τ, up to which the Hamiltonian equations in the Molecular Dynamics method are integrated, is always set to 1. Then the number of steps n_{MD} for this integration was tuned to get acceptance probabilities in the range $0.5 - 0.8$, yielding n_{MD} between 8 and 25. We used the same parameters in the metropolis decision and in the Molecular Dynamics. For the measurement of q_1 (see subsection 1.2.2) with $\bar{\beta} = 3, 10$ we put N_{inst} instanton hits between the updating steps for the gauge field and the pseudofermion field. Since the instanton hits worked not very well, leading to large correlations in the topological charge Q_{top}, we took $N_{inst} = 10$. Then the costs in computer time for these hits were in the same order of magnitude as the costs for the HMC

[2] Again it would be more sensible to deduce the proposed toron-shift somehow from the pseudofermion, which is fixed for the gauge field update, — with a $\pm$ for the reversibility.

Ensemble		$t_a(Q_{top})$	$t_a(q_1)$	$t_a(t_1)$	t_a^g	t_a^f	n_d	N_{tot}
$\bar{\beta}=10,$	$Q_{top}=0$	—	—	8.1	13.9	15.1	5	10,000
$\bar{\beta}=10,$	$Q_{top}\neq 0$	—	—	23.5	11.8	83.6	6	5,000
$\bar{\beta}=10,$	$Q_{top}\in \mathbf{Z}$	62.0	62.7	24.2	—	—	20	4,800
$\bar{\beta}=3,$	$Q_{top}=0$	—	—	10.2	11.7	19.5	8	10,000
$\bar{\beta}=3,$	$Q_{top}\neq 0$	—	—	19.6	9.8	69.7	5	5,000
$\bar{\beta}=3,$	$Q_{top}\in \mathbf{Z}$	16.8	18.5	11.7	—	—	8	10,000
$\bar{\beta}=1,$	$Q_{top}\in \mathbf{Z}$	≤ 3	≤ 3	≤ 3	6.0	—	3	24,000
$\bar{\beta}=0.3,$	$Q_{top}\in \mathbf{Z}$	≤ 2	≤ 2	≤ 2	4.0	—	2	30,000

Table 2.3: Number and autocorrelation times for the 6×16-configurations used for later Monte Carlo results.

steps. The costs for instanton hits are mainly coming from the metropolis decision including one CG solution of eq. (2.2).

The estimation of the statistical errors $\sigma_\infty(\Omega)$ in the expectation values of the measured observables Ω are determined by a jackknife procedure and checked by putting the data into large blocks (of about 1000 configurations). We define the autocorrelation times $t_a(\Omega)$ by

$$t_a(\Omega)=\left(\frac{\sigma_\infty}{\sigma_0}\right)^2\approx 2\,\tau_{int}(\Omega)\,, \tag{2.9}$$

where $\tau_{int}(\Omega)$ is the integrated autocorrelation time. Depending on these autocorrelation times, we took a configuration for the evaluation of expectation values after n_d generated configurations. So we obtained an ensemble of N_{tot} configurations with distance n_d. In Table 2.3 we give for all generated configurations N_{tot}, n_d, the autocorrelation times $t_a(Q_{top})$, $t_a(q_1)$ and $t_a(t_1)$, which is the toron component which shows larger autocorrelations, if $L_1<L_2$. For an overview of the autocorrelations in the remaining observables we give t_a^g, the largest autocorrelation time for gauge field observables (see chapter 3), and t_a^f, the largest autocorrelation time for fermion observables (see chapter 4), if the corresponding expectation values are measured.

For the equilibration of the system we took 7,000 configurations for $\bar{\beta}=10$ and 10,000 configurations for $\bar{\beta}=3$ and more than 20,000 configurations for $\bar{\beta}=1.0, 0.3$.

2.2 Strong coupling with staggered fermions

In this section we describe a strong coupling expansion (SCE) for massless staggered fermions in order to determine expectation values of gauge field observables in the strong coupling region, i.e. for small $\bar{\beta}$. This expansion is formulated for a fixed lattice volume $\bar{V}$ and in principle its convergence behaviour depends on $\bar{V}$. Without a parameter (as e.g. a hopping parameter), which could be chosen small enough for a cluster expansion, we couldn't show convergence in the thermodynamic limit $\bar{V}\to\infty$ along the lines given by E.Seiler [41] for the hopping parameter expansion with Wilson fermions. However, for Polyakov loop correlations we analyzed the volume dependence of expectation values numerically. It could be seen to vanish for large volumes $\bar{V}$.

In the first subsection we will give the general procedure of such an expansion, which is related to the evaluation of dense dimer gas expectation values [12],[13]. By several authors the representation of the strong coupling limit for staggered fermions as a dimer gas is evaluated with the simulation of this statistical system [42],[43]. Another way to deal with this system is given by S.Samuel [44]. He derived a method to represent dimer gas expectation values as Grassmann integrals with a free fermion action.

Following this line we will calculate the first orders in the SCE for the expectation values of plaquette correlations and Polyakov loop correlations in the second and third subsection, respectively. The results were checked by comparison with Monte Carlo simulations in the strong coupling region, see the chapter on gauge field observables. This comparison also gives control over the $\bar{\beta}$-range, in which the calculated orders of the SCE for staggered fermions provide qualitatively correct results.

2.2.1 The general procedure

The expectation values of gauge field observables $\Omega[U]$ can be written as

$$<\Omega>=\frac{Y_\Omega}{Z}\equiv\frac{<\Omega[U]\det M[U]>_g}{<\det M[U]>_g}\,. \tag{2.10}$$

Here $<\,>_g$ denotes the expectation value in pure QED_2

$$<\Omega>_g=\frac{\int\mathcal{D}[U]\,e^{-S_g[U]}\,\Omega[U]}{\int\mathcal{D}[U]\,e^{-S_g[U]}}\,. \tag{2.11}$$

The fermion matrix $M[U]$ is given in eq. (1.61). A fermion determinant is usually treated with Wilson fermions using the hopping parameter expansion [45]. For the above determinant $\det M[U]$ for massless staggered fermions such an expansion is not known yet. Instead, it was proposed to proceed with its evaluation by the Cramer rule [12], [13]

$$\det M[U]=\sum_G\omega_G[U]\,,\quad \omega_G[U]=(-1)^n\prod_{[x,\mu]\in G}sign(\mu)\,\rho_{\mu,x}\,U_{[x,\mu]}\,. \tag{2.12}$$

G is a general graph consisting of oriented links $[x,\mu]$, $\mu=\pm1,\pm2$ (where $U_{[x,-\mu]}\equiv U^*_{[x-e_\mu,\mu]}$), which touches every lattice point exactly once with the starting point and once with the ending point of a link. Therefore G consists of n oriented loops, see Figure 2.1(a), where n gives the factor $(-1)^n$ in the above equation. We call G a fermion graph.

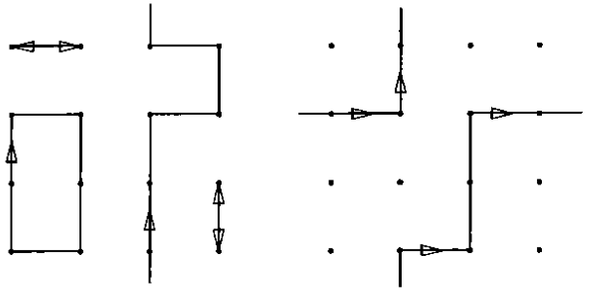

a) b)

Figure 2.1: a) A graph G on a 4×4-lattice consisting of two dimers, a Wilson loop of area $\bar{A} = 2$ and a loop of Polyakov type. b) A spiral loop on a 4×4-lattice.

It is useful to distinguish between four kinds of such loops (see Figure 2.1): The smallest loop, consisting of two opposite links, is called a dimer. It has no orientation and the weight $\omega = 1$. Second we have Wilson loops $W_{\bar{A}}[U]$ of area $\bar{A}$[3]. A third kind are loops winding once round the torus as e.g. Polyakov loops. If G shall contribute to the sum in eq. (2.12) after gauge integration, these loops must appear in pairs of opposite orientation, because otherwise they could not be screened by the loops in the gauge field action S_g or the observable $\Omega[U]$ itself[4], leading to a summand with trivial gauge factor. At last there are loops winding spirally round the torus, which obey the same restriction, see Figure 2.1(b).

In order to calculate the expectation value in eq. (2.10) we perform the gauge field integration under the sum representing the fermion determinant in eq. (2.12). This leads to

$$Y_\Omega = \sum_G < \Omega \omega_G >_g \ , \quad Z = \sum_G < \omega_G >_g \ . \tag{2.13}$$

We may separate the sign-factors in the pure gauge expectation values with the notation (compare with eq. (2.12))

$$< \Omega \omega_G >_g = \ \sigma(G) < \Omega \tilde{G} >_g \ , \quad \tilde{G}[U] \ = \prod_{[x,\mu] \in G} U_{[x,\mu]} \ . \tag{2.14}$$

Here we consider $\tilde{G}[U]$ to be a product of the link variables on the oriented links which form the graph G. In the lattice SM $\sigma(G)$ is always positive, if the loops winding round the torus appear in pairs (see e.g. [43]). As mentioned above, this is necessary for a non-vanishing contribution of G to the expectation values of combined Wilson loops [5], which are the observables we are interested in. Thus the sign $\sigma(G)$ is dropped in the following.

[3]For the definition of $\bar{A}$ on the torus, or the periodic lattice respectively, we always take the possibility to fill out the loop, which leads to the smallest area.

[4]Here a observable Ω of the Wilson type, i.e. a combination of Wilson loops or pairs of opposite Polyakov loops, is assumed. In other cases the mentioned requirement is to be applied to the graph of Ω and G.

[5]Any pair of opposite oriented loops of the Polyakov type or of the spiral type can be considered as a Wilson loop too.

We must now calculate expectation values of combined Wilson loops in pure QED_2, given by eq. (2.11). For that one proceeds with a strong coupling expansion (for the pure gauge theory), combined with a duality transformation [46]. First we restrict ourselves to single loops $W_{\bar{A}}[U]$ of area $\bar{A}$ in lattice units. The expectation value depends only on this area $\bar{A}$. For an infinitely large lattice we get immediately

$$< W_{\bar{A}} >_g = \tilde{I}_1(\bar{\beta})^{\bar{A}} \ , \qquad \tilde{I}_k(\bar{\beta}) = I_k(\bar{\beta}) / I_0(\bar{\beta}) \ . \tag{2.15}$$

$\bar{V}$ is the volume of the lattice in lattice units and the I_k denote the modified Bessel functions of order k. It is convenient to take $\gamma \equiv \tilde{I}_1(\bar{\beta})$, which is of order $\bar{\beta}$ for $\bar{\beta} \to 0$, as expansion parameter in the SCE. On a finite lattice with periodic boundary conditions eq. (2.15) must be substituted by

$$< W >_g = \frac{\sum_{k=-\infty}^{\infty} \tilde{I}_{k+1}(\bar{\beta})^{\bar{A}} \tilde{I}_k(\bar{\beta})^{\bar{V}-\bar{A}}}{\sum_{k=-\infty}^{\infty} \tilde{I}_k(\bar{\beta})^{\bar{V}}} \ . \tag{2.16}$$

It can be seen that the finite volume corrections are of high orders in $\tilde{I}_k(\bar{\beta})$ or $\bar{\beta}^k$, respectively. The suppression of these corrections is given by $\tilde{I}_1(\bar{\beta})^{\bar{V}-\bar{A}}$. So the strong coupling expansion up to a finite order $N \ll \bar{V} - \bar{A}$ implies the infinite volume approximation, given with eq. (2.15). In this case a combination of non-overlapping loops covering the area $\bar{A}$ also leads to the pure gauge expectation value given in eq. (2.15), independent of the relative orientation of the single loops.

For the general case of possibly overlapping loops in $\Omega \tilde{G}$ we have to determine the numbers $\bar{A}_k$ of lattice plaquettes surrounded by k lines of equal orientation[6]. Then we obtain

$$< \Omega \tilde{G} >_g = \prod_{k \neq 0} \tilde{I}_k(\bar{\beta})^{\bar{A}_k} \ . \tag{2.17}$$

Note that $\tilde{I}_k(\bar{\beta})$ is of order $\bar{\beta}^k$ or γ^k for $\bar{\beta} \to 0$. Keeping in mind that the lines of a fermion graph G can not cross each other, it turns out that up to the orders evaluated in the following ($N = 1$ for plaquette correlations, $N = 3$ for Polyakov loop correlations) the case of overlapping loops does not occur, thus $\bar{A}_k = 0$ for $|k| > 1$.

In principal the evaluation of the expressions in eq. (2.13) by eq. (2.17) sets up the strong coupling expansion with staggered fermions, because on a finite lattice the number of graphs G is finite. However, the sum over all fermion graphs G in eq. (2.13) is not really under control by the expansion in the parameter γ. The reason is the existence of the dimer loops which have a trivial gauge factor. So there are many graphs G leading to the same functional $\tilde{G}[U]$ in eq. (2.14) and thus to the same powers of γ after gauge integration. Although their number is finite on a finite lattice, it increases rapidly with the lattice size.

Let us first discuss the zero order of the SCE. Here we have the expectation value

$$< \Omega >^0 = Y_\Omega^0 / Z^0 \ , \qquad Z^0 = \sum_D 1, \qquad Y_\Omega^0 = \sum_{D_\Omega} 1 \ , \tag{2.18}$$

[6]For this counting we must first define a plaquette with $k = 0$. In the formula for finite volume the choice of this plaquette can be seen to be arbitrary. For a consistent treatment of the infinite volume limit arising from a strong coupling approximation this plaquette has to be chosen so as to maximize the expression in eq. (2.17).

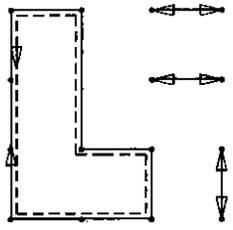

Figure 2.2: Screening of the graph of Ω (dashed line) by a fermion graph G (full line) on a 4×4 lattice.

where D is a general combination of dimers covering all lattice points but having no points in common. For D_Ω the dimers are not allowed to touch the graph of Ω either. The reason for the latter restriction is that Ω must be screened by the loops in a fermion graph G to yield a trivial gauge factor. The remaining lattice points then must be covered with dimers which have no gauge factor too, see Figure 2.2. Of course, the screening mechanism in zero order SCE is only possible if the graph of Ω is of the kind, which would be allowed in the fermion determinant too, i.e. its lines are not allowed to cross or touch.

For the further calculation we use the representation of the sums in eq. (2.18) as integrals over Grassmann variables with a free fermion action, given by S. Samuel [44]. The effect of the double periodic boundary conditions on $\mathcal{T}_2$ are treated with methods described in [47]. The result is

$$Z^0 = \frac{1}{2}(Z^{--} + Z^{-+} + Z^{+-}) \;, \quad Y^0_\Omega = \frac{1}{2}(Y^{--}_\Omega + Y^{-+}_\Omega + Y^{+-}_\Omega - Y^{++}_\Omega) \;, \tag{2.19}$$

$$Z^{\epsilon_1\epsilon_2} = \int \mathcal{D}[\bar\phi,\phi] e^{-\bar\phi Q^{\epsilon_1\epsilon_2}\phi} \;, \; Y^{\epsilon_1\epsilon_2}_\Omega = \left| \int \mathcal{D}[\bar\phi,\phi] e^{-\bar\phi Q^{\epsilon_1\epsilon_2}\phi} \prod_{x\in\Omega} \tilde\phi(x) \right| \;.$$

Here $\bar\phi$ lives on the even, ϕ on the odd sites of the lattice, and $\tilde\phi(x) = \bar\phi(x)$ $(\phi(x))$ for x even (odd). The product over all $x \in \Omega$ means over all x which are touched by the graph of the observable Ω. The fermion matrix $Q^{\epsilon_1\epsilon_2}$ which determines the free fermion action is 2 times the fermion matrix M of eq. (1.61) restricted according to the restriction of $\bar\phi, \phi$ to even (odd) points and without gauge fields, $\epsilon_1, \epsilon_2 = \pm$ denote periodic and antiperiodic boundary conditions in space and time direction, respectively. Thus we have

$$\bar\phi Q^{\epsilon_1\epsilon_2}\phi = \sum_{x:even} \sum_\mu \rho^{\epsilon_1\epsilon_2}_{\mu,x} \bar\phi_x (\phi_{x+e_\mu} - \phi_{x-e_\mu}) \;, \tag{2.20}$$

where the boundary conditions are included in $\rho^{\epsilon_1\epsilon_2}_{\mu,x}$.

If we perform again the Grassmann integrals, using the diagonalization of the free fermion action in eq. (2.20) in the sense of eq. (1.106), we get (see Appendix A)

$$Z^{\epsilon_1\epsilon_2} = \prod_{\{p\}^{\epsilon_1\epsilon_2}} (4 \sum_{\mu=1,2} \sin^2 p_\mu) \;. \tag{2.21}$$

Up to the effect of the boundary conditions, the momenta p in $\{p\}^{\epsilon_1\epsilon_2}$ are the momenta in the Brillouin zone of the coarse lattice. They are given by

$$p_\mu = \frac{2\pi}{L_\mu}(n_\mu + \alpha_{\epsilon_\mu}) \;, \; n_\mu \in [-\frac{L_\mu}{4}, \frac{L_\mu}{4}) \cap \mathbf{Z} \;, \; \alpha_+ = 0 \;, \; \alpha_- = \frac{1}{2} \;. \tag{2.22}$$

The $Y^{\epsilon_1\epsilon_2}_\Omega$ can be calculated by $Y^{\epsilon_1\epsilon_2}_\Omega = Z^{\epsilon_1\epsilon_2} y^{\epsilon_1\epsilon_2}_\Omega$, $y^{\epsilon_1\epsilon_2}_\Omega$ is the usual n-point function of the free fermion action in eq. (2.20). For that a reasonable limit has to be taken for the zero mode appearing with $\epsilon_1\epsilon_2 = ++$. It causes Z^{++} to be 0, while in general $Y^{++}_\Omega \neq 0$. This gives in principle the 0th order strong coupling expectation value of all observables $\Omega[U]$. Explicit formulas for the $Y^{\epsilon_1\epsilon_2}_\Omega$ are given in Appendix A.

Now we come to the Nth order of the strong coupling expansion. For that we identify $\tilde G[U]$ with its graph, i.e. the graph $\tilde G$ is obtained from G, if one omits all dimers (which have trivial gauge factors). The graph $\tilde G$ may be called reduced fermion graph. Furthermore we define the order $ord(\tilde G)$ of $\tilde G$ by

$$< \tilde G >_g = \gamma^{ord(\tilde G)} \tag{2.23}$$

in the infinite volume limit. So we have

$$< \Omega >^N \;=\; Y^N_\Omega / Z^N \;=\; y^N_\Omega / z^N \tag{2.24}$$

$$y^N_\Omega \;=\; Y^N_\Omega / Z^0 \;=\; x(\Omega) + \sum_{n=1}^{N} \gamma^n \sum_{\tilde G, ord(\Omega\,\tilde G)=n} x(\tilde G) \;. \tag{2.25}$$

$$z^N \;=\; Z^N / Z^0 \;=\; 1 + \sum_{n=1}^{N} \gamma^n \sum_{\tilde G, ord(\tilde G)=n} x(\tilde G) \;, \tag{2.26}$$

where

$$x(\tilde G) \;=\; Y^0_{\tilde G} \,/\, Z^0 \tag{2.27}$$

is the zero order expectation value of $\tilde G$, given by eq. (2.19). We call it dimer weight of $\tilde G$. The computational effort of the evaluation of eqs. (2.25), (2.26) is mainly given by the determination of $x(\tilde G)$.

With the normalization by Z^0 the obtained dimer weights $x(\tilde G)$ for the reduced fermion graph $\tilde G$ seem to be volume-independent for large volumes. We checked this by a numeric evaluation of eq. (2.19) for all graphs consisting of one loop with area $\bar A = 1, 2$. However, the sums over all $\tilde G$ in eqs. (2.25), (2.26) include all possibilities of loops on the whole torus and thus are strongly volume-dependent. It is an important question, whether this volume dependence vanishes for $< \Omega >^N = y^N_\Omega / Z^N$, if the volume $\bar V$ is sufficiently large. We numerically checked the volume dependence for Polyakov loop correlations to gain first hints, see subsection 2.2.3. In any case, we use the above strong coupling expansion for a fixed volume as check and complement of our Monte Carlo simulations for the investigation of the scaling to strong coupling transition of the lattice Schwinger model.

2.2.2 Evaluation for plaquette correlations

With the strong coupling expansion up to 1. order we want to calculate the lattice analogue of the field strength correlation $< F(x)F(y) >$, which is related to the mass of the gauge field.

As explained in section 3.1 we choose

$$\phi(x-y) := < \Phi_x \Phi_y > , \quad \Phi_x = P_x - P_x^{-1} , \tag{2.28}$$

where $P_x \in U(1)$ is the Wilson plaquette at point x, see eq. (1.59). Furthermore we define the zero momentum lattice correlation

$$\eta(t) = \sum_{x_1} < \Phi_{(x_1,t)} \Phi_{(0,0)} > . \tag{2.29}$$

We have written $x = (x_1, t)$, i.e. we identify the 2-direction with the euclidean time. It is shown in section 3.1 that in the scaling limit, i.e. for sufficiently large $\bar{\beta}$ we expect

$$\eta(t) = \frac{4}{\bar{\beta}} \left(-\delta_{t,0} + m \frac{\cosh(\frac{mL_2}{2} - mt)}{2\sinh(\frac{mL_2}{2})} \right) . \tag{2.30}$$

with $m = \sqrt{2/(\pi\bar{\beta})}$. Since no misunderstanding is possible here, we dropped the bars for quantities in lattice units (t,m,L_2).

We want to determine the leading terms of $\phi(x-y)$ or $\eta(t)$ in the strong coupling expansion sketched in the previous subsection. For $x-y = (0,0)$ the SCE of $\phi(x-y)$ can be seen to yield the continuum result for $\bar{\beta} \to \infty$: Define c_k to be the weight of all fermion graphs $\tilde{G}$ which surround the plaquette at $x = (0,0)$ k times, without the factor coming from the plaquette itself

$$Z = \sum_{k=-\infty}^{\infty} c_k \tilde{I}_k(\bar{\beta}) . \tag{2.31}$$

Then we get with eq. (2.17)

$$\phi(0,0) = \frac{1}{Z} \sum_{k=-\infty}^{\infty} c_k (\tilde{I}_{k-2}(\bar{\beta}) - 2\tilde{I}_k(\bar{\beta}) + \tilde{I}_{k+2}(\bar{\beta})) . \tag{2.32}$$

In the sense of asymptotic series (see eq. (3.26)) this leads to

$$\phi(0,0) = \frac{1}{Z} \sum_{k=-\infty}^{\infty} c_k \tilde{I}_k(\bar{\beta}) \left(\frac{-4}{\bar{\beta}} + \mathcal{O}(\bar{\beta}^{-2}) \right) = \frac{-4}{\bar{\beta}} + \mathcal{O}(\bar{\beta}^{-2}) . \tag{2.33}$$

This is exactly the contribution corresponding to the two-dimensional lattice δ-function in $\phi(x-y)$ in eq. (2.30). So in the following we will consider $\eta(t)$ without the contribution of the lattice δ-function. Then a comparison with MC data is reasonable only for $t \neq 0$, so $t = 0$ is not regarded here.

In order to calculate $\eta(t)$ in the SC approximation we must evaluate the sums over reduced fermion graphs $\tilde{G}$ in eqs. (2.25), (2.26). For the evaluation of the numerator of the expectation value $< \Phi_1 \Phi_2 >$ it is useful to decompose the graphs $\tilde{G}$ in two groups:

Group 1: At least one loop of $\tilde{G}$ covers both plaquettes $P_1 = P_{(x_1,t)}$ and $P_2 = P(0,0)$ coming from the observable $\Phi_{(x_1,t)}\Phi_{(0,0)}$. These graphs are the only ones which contribute to the numerator of $< \Phi_1 \Phi_2 >$.

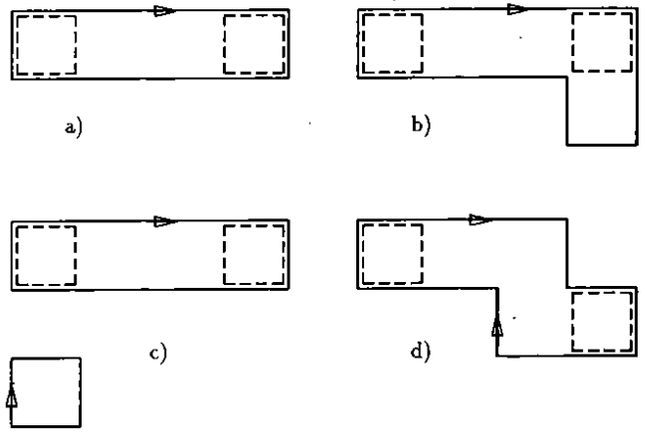

Figure 2.3: Strong coupling fermion graphs for the plaquette correlation.

Group 2: P_1 and P_2 are covered separately. Therefore to each such graph there exists exactly one other graph, in which all loops around P_1 are inverted. This graph will give the same contribution to $< P_1^{-1} P_2 >$ as the original one to $< P_1 P_2 >$. So for $< \Phi_1 \Phi_2 >$ these contributions cancel.

The contributions of the graphs of group #1 take certain powers of the SC expansion parameter γ. In the present calculation the leading and next to leading order in γ are considered.

In the definition of $\eta(t)$ eq. (2.29) only the term with $x_1 = 0$ contributes in leading order. The graphs $\tilde{H}_t$ contributing to this order consist of the smallest loop covering $P_{(0,0)}$ and $P_{(0,t)}$ with both orientations, see Figure 2.3(a). The graphs $\tilde{H}'_t$ contributing in next to leading order are zero order graphs with a bump of one plaquette (Figure 2.3(b)) or with an extra plaquette (Figure 2.3(c)), and the smallest graphs covering $P_{(0,0)}$ and $P_{(\pm 1,t)}$ (Figure 2.3(d)).

Together with the plaquettes in $\phi((0,t))$ ($\phi((\pm 1,t))$) such a reduced fermion graph $\tilde{H}_t$ ($\tilde{H}'_t$) consisting of N plaquettes gets a weight from the gauge integration $[1 - \tilde{I}_2(\bar{\beta})]^2 \gamma^{N-2}$. Although it is of order $\bar{\beta}^2$, we included the $\tilde{I}_2(\bar{\beta})$ from the case of equal orientation of the Wilson plaquette P_1 (P_2) and the covering fermion loop, because this leads to an overall factor.

For the expansion of Z up to the first order we just have the contributions of graphs which consist of one plaquette $\square_x$ at an arbitrary lattice point x. They are weighted by a factor γ. Altogether one obtains in the first order SCE (here the factor 2 counts the orientations of the loop covering P_1 and P_2 explicitly)

$$\eta(t) = 2(1 - \tilde{I}_2(\bar{\beta}))^2 \gamma^{t-1} \frac{y_t}{z} , \tag{2.34}$$

$$y_t = x(\tilde{H}_t) + \gamma \sum_{\tilde{H}'_t} x(\tilde{H}'_t) + \mathcal{O}(\gamma^2) , \tag{2.35}$$

$t:$	1	2	3	4	5	6	7
$a_0:$	-2.909	-3.695	-4.503	-5.300	-6.102	-6.901	-7.705
$a_1:$	1.668	2.552	3.214	3.998	—	—	—

Table 2.4: The SC coefficients for the plaquette correlation a_0, a_1.

$$z = 1 + 2\gamma \sum_{x'} x(\Box_{x'}) + \mathcal{O}(\gamma^2) . \tag{2.36}$$

The first order approximation $\eta^1(t)$ of $\eta(t)$ is defined by

$$\ln \eta(t) = \sum_n h_n(t)\gamma^n , \qquad \eta^1(t) = e^{h_0(t)+h_1(t)\gamma} . \tag{2.37}$$

With $C = 2(1 - \tilde{I}_2(\bar{\beta}))^2/\tilde{I}_1(\bar{\beta})$ this leads to

$$\begin{aligned} \ln \frac{\eta_t^1}{C} &= t \ln\gamma + \ln x(\tilde{H}_t) + \gamma \Big(\sum_{\tilde{H}'_t} \frac{x(\tilde{H}'_t)}{x(\tilde{H}_t)} - 2 \sum_{x'} x(\Box_{x'})\Big) \\ &= t \ln\gamma + a_0(t) + \gamma a_1(t) . \end{aligned} \tag{2.38}$$

The results for a_0 and a_1 on a 6×16-lattice are given in Table 2.4. Because of the appearing n-point functions for larger N we calculated a_0 only for $t = 1, \ldots, 7$ and a_1 only up to $t = 4$.

For the evaluation of the gauge field mass M_P, determining the decrease of the field strength correlation, $\eta(t)$ must be fitted by an exponential decay, i.e. we write

$$\eta(t) \simeq c \exp(-M_P t). \tag{2.39}$$

Note that if graphs the other way around $\mathcal{T}_2$ are taken into account this would mean a substitution of $\eta(t)$ by $\eta(t) + \eta(L_2 - t)$ and we would have to fit by $c' \cosh(M_P(L_2/2 - t))$ instead (compare with eq. (2.30)).

Because of eq. (2.39) we fittedd $a_0(t), a_1(t)$ by a straight line. The values of $a_0(t)$ and $a_1(t)$ for a 6×16-lattice showed good linear behaviour in t, see Table 2.4. So this fit gave no rise to additional errors. Altogether we found for the mass

$$M_P = -\ln(\gamma) + 0.80 - 0.8\,\gamma \tag{2.40}$$

The leading term for $\bar{\beta} \to 0$ is given by

$$\lim_{\bar{\beta}\to 0} \tilde{I}_1(\bar{\beta}) = \frac{\bar{\beta}}{2} \;\Rightarrow\; \lim_{\bar{\beta}\to 0} M_P = -\ln\bar{\beta} + \mathcal{O}(1) \tag{2.41}$$

The SCE estimates of the gauge field mass M_P are compared with MC results and the scaling behaviour in section 3.1. It appears that for $\bar{\beta} = 1$ and $\bar{\beta} = 0.3$ the MC measurements are quite well described by the first order of the SCE.

2.2.3 Evaluation for Polyakov loop correlations

Next we turn to the expectation values of Polyakov loop correlations in the SCE. This observable is defined by

$$PL(R)[U] = \prod_{x_2=1}^{L_2} U^2_{(0,x_2)} \prod_{x_2=1}^{L_2} U^{2^*}_{(R,x_2)} , \tag{2.42}$$

where $U_{[x,\mu]}$ is written as $U^{\mu}_{(x1,x2)}$. We use the Polyakov loop correlation for the definition of the heavy quark potential

$$V(R) = -\frac{1}{L_2} \ln < PL(R) > . \tag{2.43}$$

In section 3.2 we show that we expect in the scaling limit

$$V(R) = \frac{\pi m}{4} \frac{\cosh m\frac{L_1}{2}}{\sinh m\frac{L_1}{2}} \left[1 - \frac{\cosh m(\frac{L_1}{2} - R)}{\cosh m\frac{L_1}{2}}\right] , \quad m^2 = \frac{2}{\pi\bar{\beta}} . \tag{2.44}$$

Again all quantities are understood in lattice units.

Since we want to compare with MC simulations later on, we calculate this potential on a 16×6-lattice, i.e. we interchange the extensions in 1- and 2-direction for the analysis of this special observable. The reason is that the expectation value $< PL(R) >$ exponentially decreases with L_2. On the other hand L_1 must be large enough for a sensible evaluation of the R-dependence of the correlation.

In two dimensions it is possible to calculate Y^0_Ω for $\Omega = PL(R)$, i.e. two opposite Polyakov loops at distance R, as

$$Y^0_{PL(R)} = Z_{PL}(R)\; Z_{PL}(L - R) , \tag{2.45}$$

where $Z_{PL}(R)$ is the dimer gas partition function on a $R \times T$-lattice with boundary conditions simulating the presence of a Polyakov loop. In fact, as mentioned together with eq. (2.18), $Y^0_{PL(R)}$ is the number of possibilities to arrange the dimers on the lattice so that they cover all lattice points but do not touch the points on the lines of the two Polyakov loops. This number factorizes as in eq. (2.45), where $Z_{PL}(R)$ is the number of dimer configurations on a periodic $R \times L_2$-lattice, which do not touch the points at $x_1 = 0\,(R)$. The latter restriction can be expressed as a restriction for the Grassmann fields in the integrals representing the dimer partition function (compare with eq. (2.19))

$$Z_{PL}(R) = \int \mathcal{D}[\bar{\phi}, \phi] e^{-\bar{\phi} Q^+ \phi} , \tag{2.46}$$

where $\bar{\phi}, \phi$ live on the $R \times L_2$-lattice, with the restriction $\bar{\phi}(x) = 0, \phi(x) = 0$ for $x_1 = 0\,(R)$. The choice of the boundary condition in 2-direction must be antiperiodic (see [47]). This system can be represented as a system on a double lattice of size $2R \times L_2$, where those modes are set to zero, which are symmetric with respect to the geometric parity Π^1 defined in eq. (1.102). Then diagonalization yields (see Appendix A)

$$Z_{PL}(R) = \begin{cases} \displaystyle\prod_{p_1,p_2} (4 \sum_{\mu=1,2} \sin^2 p_\mu) & \text{for } R \text{ odd} \\ \displaystyle\prod_{p_2} |2 \sin p_2| \prod_{p_1} (4 \sum_{\mu=1,2} \sin^2 p_\mu) & \text{for } R \text{ even} \end{cases} , \tag{2.47}$$

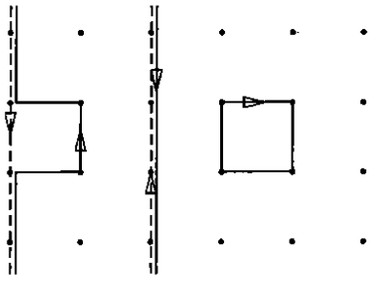

Figure 2.4: A reduced fermion graph screening two opposite Polyakov loops (dashed) up to deviations $\tilde{H}$, leading to a second order contribution. $\tilde{H}$ can be divided in $\tilde{H}_A$ (the bump) and $\tilde{H}_B$ (the extra plaquette) left and right of one of the Polyakov loops.

where p_1, p_2 take the values

$$p_1 = \begin{cases} \frac{\pi}{2R}, \frac{3\pi}{2R}, \ldots, \frac{(R-2)\pi}{2R} & \text{for } R \text{ odd} \\ \frac{\pi}{R}, \frac{2\pi}{R}, \ldots, \frac{(R/2-1)\pi}{R} & \text{for } R \text{ even} \end{cases} ,$$

$$p_2 = \frac{2\pi(n_2+1/2)}{L_2} , \; n_2 \in [-L_2/4, L_2/4) \cap \mathbf{Z} . \tag{2.48}$$

Now we come to the next to leading orders in the SC expansion. We must calculate $x(\tilde{G})$ for reduced fermion graphs $\tilde{G}$, which screen $PL(R)$ (two opposite Polyakov loops at distance R) up to deviations. These deviations lead to powers in the expansion parameter γ (see eq. (2.25)). We divide the points of $\tilde{G}$ into those lying on the graph of $PL(R)$ and the rest, which may be considered as a graph $\tilde{H}$[7], see Figure 2.4. Again $\tilde{H}$ can be divided in parts $\tilde{H}_A, \tilde{H}_B$ left and right of one of the two Polyakov loops in $PL(R)$. It is easy to see that $x(\tilde{G})$ factorizes

$$x(\tilde{G}) = x(PL(R)) \; x_{PL(R)}(\tilde{H}_A) \; x_{PL(L_1\text{-}R)}(\tilde{H}_B) . \tag{2.49}$$

Here $x(PL(R))$ is the zero order expectation value given with eqs. (2.19), (2.45) and $x_{PL(R)}(\tilde{H})$ gives the number of possible dimer configurations on the $R \times L_2$-sublattice, not touching $\tilde{H}$ and the two Polyakov loops, normalized by $Z_{PL}(R)$. The $x_{PL(R)}(\tilde{H})$ can be computed as n-point functions under the Polyakov loop boundary conditions mentioned above. For explicit formulas see Appendix A.

With the expressions for $Z, Y^0_{PL(R)}, x_{PL(R)}(\tilde{H})$ we can now enter the SCE given with eqs. (2.25), (2.26). We define the Nth order SC approximation of the potential $V(R)$ in two ways: $V^N(R)$ and $V^N_{alt}(R)$. For $V^N(R)$ the expansion of $V(R)$ terminates with the Nth

[7]With higher orders, graphs $\tilde{G}$ possibly don't cover Ω. This problem can be circumvented with a little of dimer configuration counting.

power of γ

$$V(R) = \sum_{k=0}^{\infty} v_k(R)\,\gamma^k \; , \; V^N(R) = \sum_{k=0}^{N} v_k(R)\,\gamma^k . \tag{2.50}$$

We expect this definition to be compatible with the thermodynamic limit lattice size to infinity. Numerical evaluations of the volume-dependence seem to confirm this, see below.

The alternate definition is

$$< PL(R) >= \sum_{k=0}^{\infty} w_k(R)\,\gamma^k \; , \; V^N_{alt}(R) = -\frac{1}{L_2} \ln\left(\sum_{k=0}^{N} w_k(R)\,\gamma^k\right) . \tag{2.51}$$

It can be seen that w_N is given by v_k, $k = 1, \ldots, N$, but not in a L_2-independent manner. In fact, if the expansion coefficients v_k become independent of L_2 for sufficiently large L_2, it follows from eq. (2.51) that $\lim_{L_2\to\infty} V^N_{alt}(R) = V^0_{alt}(R)$ for $\bar{\beta}, L_1$ fix. In other words the alternate definition of the SC approximation $V^N_{alt}(R)$ does not well-behave in the large L_2 limit. However, for $L_2 = 6$ it appears that the convergence is faster for V^N_{alt}, in particular V^N_{alt} decreases uniformly with $N = 0, 1, 2, 3$, whereas the corrections in V^N change their sign with each N. In this sense it yields a resummation of the expansion in eq. (2.50), which improves convergence for small L_2.

For a comparison with Monte Carlo data we have evaluated the potential V^N_{alt} for a 16×6-lattice up to order $N = 3$, see Figure 2.5 for V^N_{alt}. With the 'convergence criterion' $|V^3(R) - V^2(R)| < |V^2(R) - V^1(R)|$ for all R we found 'convergence' up to $\bar{\beta} = 0.6$. The transition to scaling, i.e. weak coupling behaviour is sketched in section 3.2.

At last, let us quote the results on the volume-dependence of $V^N(R)$ defined in eq. (2.50). We want to take this SC potential as an alternative possibility to extract the gauge field mass in the sense of eq. (2.44), i.e. as inverse screening length M_S (see also section 3.2). However, there are oscillations of the lattice potential, which make the assumption of an exponentially decreasing, oscillating contribution necessary for a sensible fit, see Figure 2.5. Therefore we made the ansatz

$$V^N(R) = c_1 \cosh\left(M_S(\frac{L_1}{2} - R)\right) \; + \; c_2\,(-1)^R \cosh\left(M_d(\frac{L_1}{2} - R)\right) \; + \; c_3 . \tag{2.52}$$

The dependence of M_S, c_1, M_d, c_2[8] on L_1 is quite small. We compared these quantities on a 16×6- and a 64×6-lattice in the SCE up to $N = 2$ for $\bar{\beta} = 0.3$. The relative deviations could be seen to be smaller than 1% for all R. In contrary, the L_2-dependence is much stronger for M_d, i.e. the oscillating contribution, though for large L_2 this effect also seems to vanish. This is shown in Table 2.5 for M_S, c_1, M_d, c_2 with $N = 2$ and $\bar{\beta} = 0.3$ for lattices with different L_2. However, the main part of the L_2-dependence of M_d appears already in zero order SC approximation. Thus we consider this dependence to be a real strong coupling effect rather than a problem of the correct definition of the SC expansion.

[8]The constant c_3 is determined by $\bar{V}^N(0) = 0$.

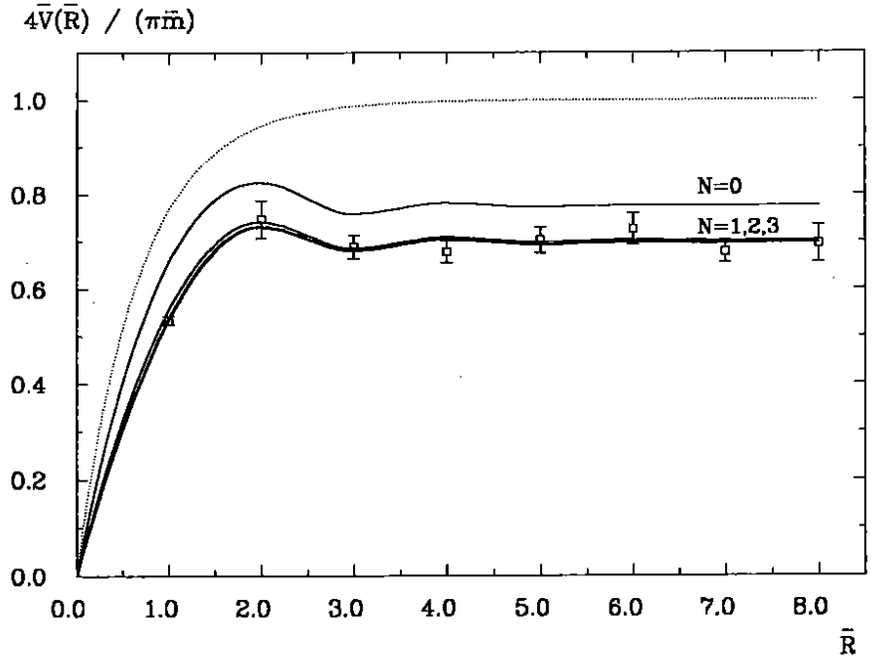

Figure 2.5: The heavy quark potential for $\tilde{\beta} = 0.3$: The full lines show the strong coupling approximations $V^N_{alt}(R)$ for $N = 0, 1, 2, 3$ (interpolated by a spline) and the points are MC results. The dotted line shows what we expect from the continuum for ideal scaling.

size:	16×6	16×12	16×24	16×48	16×96	16×192
M_S :	2.705	2.792	2.675	2.631	2.619	2.615
c_1 :	−1.068	−1.033	−1.012	−1.021	−1.031	−1.036
M_d :	0.873	0.535	0.354	0.292	0.271	0.261
c_2 :	0.263	0.221	0.187	0.184	0.186	0.187

Table 2.5: The L_2-dependence of $V^2(R)$ for $\tilde{\beta} = 0.3$.

Chapter 3

Gauge Field Observables

3.1 Plaquette correlations

In section 2.2 we discussed the formulas for a strong coupling expansion of the expectation values of certain gauge field observables. On the other hand we can calculate these expectation values with Monte Carlo methods, which are valid not only in the strong coupling region. A comparison of SCE, MC simulations and continuum results gives a survey of lattice quantities for different $\tilde{\beta}$-parameters, i.e. we can distinguish between the scaling and strong coupling region and control the behaviour at the transition. In this investigation the comparison with finite volume calculations in the continuum make it possible to work on quite small lattices. We also control the influence of topological sectors.

In this first section we deal with the correlation of the field strength. The first subsection presents the continuum results of [AJ]. Then we give the connection to the plaquette correlations on the lattice. In the third subsection the MC results are presented and we compare with strong coupling calculations and the continuum results.

3.1.1 Continuum results

As already mentioned in section 1.1.3 together with eq. (1.45), gauge field observables in the (geometric) Schwinger model are described by free massive particles. In particular, the correlation of the field strength is given with the free massive Greens function G_m by

$$f(x-y) := < F(x)F(y) > = -m^2 G_m(x-y) + \delta^{(\prime)}(x-y) \,, \tag{3.1}$$

where

$$m^2 = \frac{2e^2}{\pi} \,, \quad (-\Box + m^2) G_m(x) = \delta^{(\prime)}(x) = \delta(x) - \frac{1}{L_1 L_2} \,. \tag{3.2}$$

The prime always denotes omitted zero modes, the corresponding functions have zero average. So f(x) fulfills[1]

$$(1 - m^2 \Box^{-1}) f(x) = \delta^{(\prime)}(x) \,, \tag{3.3}$$

[1]The inverse $\Box$-operator is defined on the subspace orthogonal on the constant mode, and we set $\Box^{-1} c = 0$.

and its Fourier decomposition is

$$f(x) = \frac{1}{L_1 L_2} \sum_p{}' \frac{p^2}{p^2 + m^2} e^{-ipx} \ . \tag{3.4}$$

For the $p_1 = 0$-correlation, which will give directly the singlet mass, we write

$$h(x_2) = \int dx_1 f(x_1, x_2) = \frac{1}{L_2} \sum_{p_2}{}' \frac{p_2^2}{p_2^2 + m^2} e^{-ip_2 x_2} \ . \tag{3.5}$$

Therefore $h(t)$ is the solution of

$$(1 - m^2 \partial_t^{-2}) h(t) = \delta^{(\prime)}(t) \tag{3.6}$$

in the space of L_2-periodic functions orthogonal on the constant mode. This may be solved by putting $h(t) = -\partial_t^2 H(t)$, which defines $H(t)$ up to a constant. One obtains for $h(t)$

$$\begin{aligned} h(t) &= g_m(t) + \delta(t) \ , \\ g_m(t) &= \frac{-m}{2 \sinh \frac{mL_2}{2}} \cosh(\frac{mL_2}{2} - mt) = \frac{-m}{2} e^{-mt} + m \frac{\cosh mt}{e^{mL_2} - 1} \ . \end{aligned} \tag{3.7}$$

This is not dependent on the extension L_1, which is integrated out for $h(t)$. So for the lattice calculations it makes sense to take a small extension L_1 in space direction.

3.1.2 Plaquette correlations on the lattice

For a lattice expression which reproduces $F(x)$ in the continuum limit we choose

$$\Phi_x = P_x - P_x^{-1} = 2i \sin F_x \ , \tag{3.8}$$

$P_x = e^{iF_x}$ is the Wilson plaquette at point x, see eq. (1.59), F_x is the lattice field strength in units of the lattice constant a, where the coupling e is absorbed, see eq. (1.66). Obviously this is leading to

$$\lim_{a \to 0} \Phi_x = 2iea^2 F_{cont}(x) \ , \tag{3.9}$$

where $F_{cont}(x)$ is the field strength in the continuum. We further define

$$\phi(x - y) = < \Phi_x \Phi_y > \ , \tag{3.10}$$

and the zero momentum lattice correlation

$$\eta(t) = \sum_{x_1} < \Phi_{(x_1,t)} \Phi_{(0,0)} > \ . \tag{3.11}$$

For clearness we will now denote quantities in lattice units with a bar, e.g. $\bar{x} = x/a, \bar{m} = ma$, etc. As mentioned in section 1.2.1 together with eq. (1.65), in the continuum limit scaling is expected for $\bar{\beta} = 1/a^2 e_{cont}^2$, e_{cont} is the coupling in the continuum, see eq. (3.2). So we expect for $\bar{\beta} \to \infty$

$$\eta(\bar{t}) = -4e^2 a^4 \sum_{\bar{x}_1} f(a\bar{x}_1, a\bar{t}) = \frac{-4}{\bar{\beta}} a \int dx_1 f(x_1, t) = \frac{-4}{\bar{\beta}} a h(t) \ . \tag{3.12}$$

With eq. (3.7) we obtain the scaling result

$$\eta(\bar{t}) = \frac{4}{\bar{\beta}} \left(-\delta_{\bar{t},0} + \bar{m} \frac{\cosh(\frac{\bar{m}\bar{L}_2}{2} - \bar{m}\bar{t})}{2 \sinh(\frac{\bar{m}\bar{L}_2}{2})} \right) \ . \tag{3.13}$$

So, if we evaluate $\eta(\bar{t})$ by MC simulations or a strong coupling expansion, we expect a decay with $\bar{t}$ as in eq. (3.13) governed by a lattice mass $\overline{M}_P$ which should tend to $\bar{m}$ in the scaling limit, i.e. for large $\bar{\beta}$. In section 2.2 we described already how to calculate $\eta(\bar{t})$ up to the first order of the SCE. It turned out that the behaviour of $\eta(\bar{t})$ is well described by a decay $\sim \cosh \overline{M}_P(\overline{L}/2 - \bar{t})$. The result for $\overline{M}_P$ on a 6×16 lattice is given in eq. (2.40). For results in the scaling region we use MC simulations.

3.1.3 Monte Carlo simulations

For the numerical extraction of the mass $\overline{M}_P$ from the plaquette correlation we took the configurations on a 6×16-lattice for $\bar{\beta} = 10, 3, 1$ and 0.3 described in subsection 2.1.3. We measured $\eta(\bar{t})$ defined in eq. (3.11) and fitted by

$$\eta(\bar{t}) = c \cosh \left(\overline{M}_P (\frac{\overline{L}_2}{2} - \bar{t}) \right) \ . \tag{3.14}$$

Figure 3.1 gives a plot of the leading and next to leading order SCE for $\overline{M}_P$, the scaling line ($\overline{M}_P = \bar{m}$) and the MC estimations of $\overline{M}_P$ with eq. (3.14). The latter can be seen to agree with the scaling expectation for $\bar{\beta} = 10$ and to lie near this line for $\bar{\beta} = 3$.

For the constant c in eq. (3.14) the deviations from the continuum result in eq. (3.13) are bigger but nevertheless show a behaviour which approximates the ideal scaling case with increasing $\bar{\beta}$. For $\bar{\beta} = 10$ we find $c = 0.0120(4)$ from the MC simulation, compared with the scaled continuum value $c = 2\bar{m}/[\bar{\beta} \sinh(\bar{m}\overline{L}_2/2)] = 0.0136$. It can be seen that this deviation in c becomes much smaller when we take the correlation function of $F_x \in [-\pi, \pi)$ instead of $\Phi_x \sim \sin F_x$. However F_x is no simple expression in terms of the link variables $U_{[x,\mu]}$ and therefore is not so easy to handle in the SCE.

For $\bar{\beta} = 1$ and $\bar{\beta} = 0.3$ the measurements are well-described by the first order of the SCE. Yet the error bar for $\bar{\beta} = 0.3$ is relatively large due to the very small values of $\eta(\bar{t})$ to be measured in this case. In fact, here we could only use the η-values for $\bar{t} = 1, 2$, leading to $\overline{M}_P = \ln(\eta(2)/\eta(1))$. This situation makes measurements for smaller $\bar{\beta}$ unpracticable, in particular in the region where the scaling expectation $\overline{M}_P = \bar{m}$ becomes larger than the SC values for $\overline{M}_P$, which increase logarithmically with $\bar{m}$, see eq. (2.41).

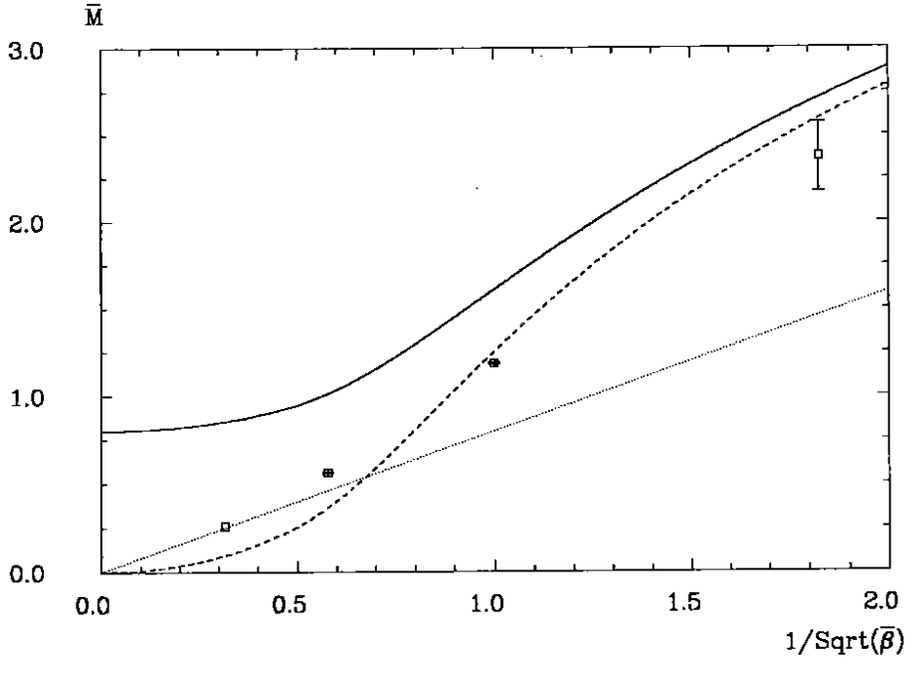

Figure 3.1: The lattice gauge field mass $\overline{M}_P$ extracted from the plaquette correlation in dependence on $\bar{\beta}^{-1/2}$. The full line gives the zero order of the SCE, the dashed line gives the first order SCE, and the dotted line shows what we expect for perfect scaling. The points are MC measurements.

3.2 The heavy quark potential

Along the lines of the previous section we now deal with the heavy quark potential extracted from the correlation of two opposite Polyakov loops. In this case the influence of dynamical fermions is the screening of the linear potential of pure QED_2. Therefore the Schwinger model may be taken as an exercise for the much more expensive investigation of the screening effect in QCD [1]. In particular it appears that it is difficult to distinguish between screening and finite size effects. This could be treated explicitly in our calculations in the Schwinger model. Since we want to see the fermion influence, we first give the results for the expectation values of Wilson loops and Polyakov loop correlations in pure QED_2, i.e. without dynamical fermions. It turns out that in this case the compact and the non-compact formulation of the lattice gauge field action lead to a different finite size behaviour, corresponding to the effect of the topological sectors in the continuum.

Again we start with the continuum results with and without fermions in the first subsection. In the second subsection we treat pure QED_2 on the lattice in the compact and non-compact formulation and the case including dynamical fermions for the heavy quark potential in the scaling limit. Finally the third section presents Monte Carlo results, which are compared with the strong coupling expansion and the scaling results. We also compare the mass M_S, extracted from the potential as inverse screening length, with the mass M_P from the plaquette correlation, and discuss the appearance of the oscillations in the strong coupling potential.

3.2.1 Continuum results

We start with the calculation of Wilson loop expectation values in pure QED_2. Following the Hodge decomposition, eq. (1.22) we write a general gauge potential in Lorentz gauge as

$$A_\mu = t_\mu + \epsilon_\mu{}^\nu \partial_\nu b(x) - \frac{c_k}{2}\epsilon_\mu{}^\nu x_\nu \ , \qquad c_k = \frac{2\pi k}{eV} \ , \tag{3.15}$$

$k \in \mathbf{Z}$ denotes the topological sector of A_μ, $V = L_1 \times L_2$ is the volume of the torus $\mathcal{T}_2$. It follows for the field strength

$$F(x) = \epsilon^{\mu\nu}\partial_\mu A_\nu = -\Box b(x) + c_k \ . \tag{3.16}$$

Using Stokes' Theorem, the expectation value of a Wilson loop $W = \partial B_A$ around the surface B_A of area A can now be given as

$$< W >_g \ = \ \frac{\sum_{k=-\infty}^{\infty} \int \mathcal{D}[b(x)] e^{-\frac{1}{2}\int_{\mathcal{T}_2} dx F(x)^2} e^{-ie\int_{B_A} dx F(x)}}{\sum_{k=-\infty}^{\infty} \int \mathcal{D}[b(x)] e^{-\frac{1}{2}\int_{\mathcal{T}_2} dx F(x)^2}} \tag{3.17}$$

$$= \ < W >_{g,C}^{(0)} \ \frac{\sum_{k=-\infty}^{\infty} e^{-\frac{1}{2}c_k^2 + iec_k A}}{\sum_{k=-\infty}^{\infty} e^{-\frac{1}{2}c_k^2}} \ . \tag{3.18}$$

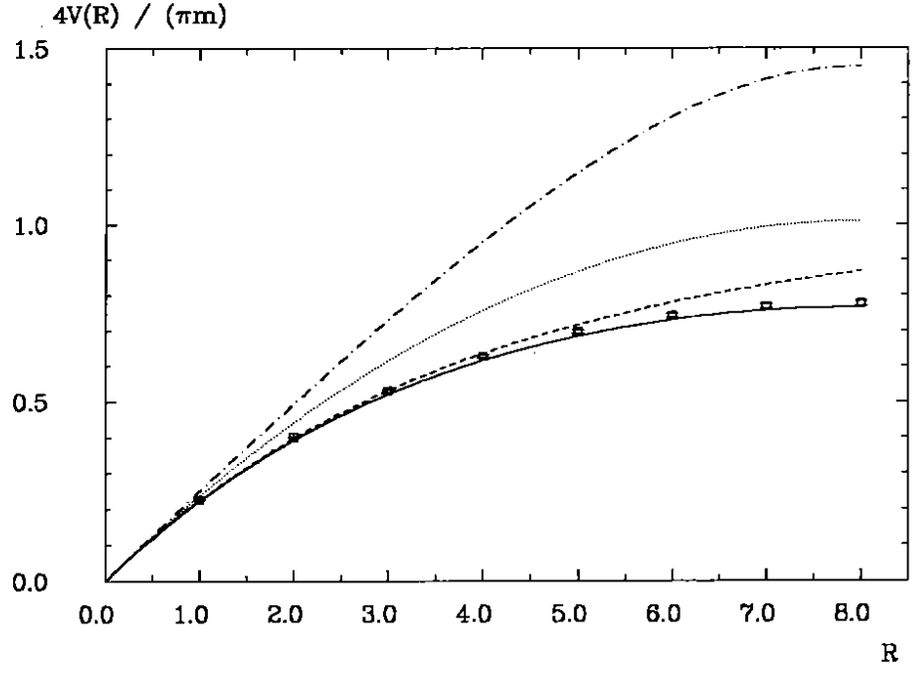

Figure 3.2: Continuum potential: unquenched (full line), unquenched with infinite volume approximation (dashed), quenched non-compact (dotted) and quenched compact (dashed-dotted). The squares show MC measurements for $\bar{\beta} = 10$.

$< W >_g^{(0)}$ is the expectation value restricted to the topologically trivial sector. It can be evaluated by Gaussian integration, where some care is needed for the treatment of the constant zero mode of $\Box$. This yields

$$< W >_g^{(0)} = \exp\left(-\frac{e^2}{2}A(1-\frac{A}{V})\right) . \tag{3.19}$$

For the inclusion of the topologically non-trivial sectors the sums in eq. (3.18) can be expressed in terms of Jacobi Θ-functions [19]. We obtain

$$< W >_g = \exp(-\frac{e^2}{2}A)\frac{\Theta_3(\frac{A}{V}\tau \mid \tau)}{\Theta_3(0 \mid \tau)} , \qquad \tau = \frac{ie^2V}{2\pi} . \tag{3.20}$$

In Figure 3.2 we give the quenched potential between two heavy fermions. For a simple comparison we took the parameters of our $\bar{\beta} = 10$ lattice simulation in units of the lattice constant, thus $L_1 = 16$, $L_2 = 6$, $1/e^2 = 10$. The potential is extracted from the expectation values in eqs. (3.19), (3.20) of an $R \times L_2$ Wilson loop, i.e. two opposite Polyakov loops $PL(R)$

at distance R

$$V(R) = \frac{-1}{T} \ln < PL(R) >_g . \tag{3.21}$$

In the geometric Schwinger model, i.e. including Dirac-Kähler fermions the correlation between two opposite Polyakov loops can be calculated similar to the procedure sketched in subsection 3.1.1 (see [AJ]). One obtains

$$V(R) = \frac{\pi m}{4\sinh m\frac{L_1}{2}}\left(\cosh m\frac{L_1}{2} - \cosh m(R-\frac{L_1}{2})\right) \tag{3.22}$$

$$= \frac{\pi m}{4}\left(1-e^{-mR}\right) - \frac{\pi m(\cosh mR - 1)}{2(e^{mL}-1)} , \quad m^2 = \frac{2e^2}{\pi} . \tag{3.23}$$

The finite volume correction is only given by L_1, i.e. $V(R)$ does not depend on L_2. In the limit $mL_1 \to \infty$ the second term in eq. (3.23) vanishes and the well-known screening potential remains, see Figure 3.2. Note that for gauge field observables there is no contribution from topologically non-trivial sectors in contrast to the situation in pure QED_2, see eq. (1.38).

3.2.2 The potential on the lattice

In pure QED_2 the expectation values of Wilson loops can be calculated by a strong coupling expansion, combined with a duality transformation [46], as sketched already in section 2.2. There we derived for Wilson loops $W_{\bar{A}}$ of area $\bar{A}$ in lattice units

$$< W_{\bar{A}} >_g = \int \mathcal{D}[U]\, W_{\bar{A}}[U] e^{-S_g[U]} = \frac{\sum_{k=-\infty}^{\infty} \tilde{I}_{k+1}(\bar{\beta})^{\bar{A}} \tilde{I}_k(\bar{\beta})^{\bar{V}-\bar{A}}}{\sum_{k=-\infty}^{\infty} \tilde{I}_k(\bar{\beta})^{\bar{V}}} , \tag{3.24}$$

where $\bar{V}$ is the volume of the lattice in lattice units, and where we have defined

$$\tilde{I}_k(\bar{\beta}) = I_k(\bar{\beta})/I_0(\bar{\beta}) , \tag{3.25}$$

the I_k denote the modified Bessel functions of order k. With the asymptotic expansion (see e.g. [48])

$$\ln \tilde{I}_k(\bar{\beta}) = \frac{-k^2}{2\bar{\beta}} + \frac{-k^2}{4\bar{\beta}^2} + \mathcal{O}(\bar{\beta}^{-3}) \tag{3.26}$$

we get in the limit $a \to 0$, i. efor $\bar{\beta} \to \infty$

$$< W >_g = \exp(-\frac{A}{2\beta}(1+\frac{a^2}{2\beta}))\frac{\Theta_3(\frac{A}{V}\tau \mid \tau)}{\Theta_3(0 \mid \tau)} + \mathcal{O}(a^4), \quad \tau = \frac{iV}{2\pi\beta}(1+\frac{a^2}{2\beta}). \tag{3.27}$$

Here we have fixed the values A,V,β in physical units, while $\bar{\beta} = \beta/a^2$ etc. The asymptotic formula eq. (3.27) is valid up to an error of order 10^{-2} for $\bar{\beta} = 10$ on a 16×6 lattice, which is the case we are interested in later on. With $\beta = 1/e^2_{cont}$, e_{cont} the coupling in the continuum, the above result agrees with the result of the continuum calculation in the limit $a \to 0$, if we include the non-trivial topological sectors, see eq. (3.20).

We want to compare this result with the non-compact formulation of the gauge field variables with a simple quadratic lattice action

$$S_g^{non-compact}[A] = \frac{\bar{\beta}}{2}\sum_x (\, A^1_x + A^2_{x+e_1} - A^1_{x+e_2} - A^2_x)^2 \;, \quad A^\mu_x \in \mathbf{R} \;. \tag{3.28}$$

In this case the Wilson loop expectation value can be calculated by Gaussian integration, yielding

$$< W >_g = \exp\left(-\frac{A}{2\bar{\beta}}(1-\frac{A}{V})\right) \;. \tag{3.29}$$

With $\bar{\beta} = 1/e^2_{cont}$ this is exactly the continuum result, which arises if we restrict the gauge field to the trivial topological sector, see eq. (3.19). In fact, it can be seen easily that the non-compact lattice formulation suppresses the topologically non-trivial gauge configurations $[A^{(k)}]$, $k \neq 0$ with $S_g^{non-compact}[A^{(k)}] \sim 1/a^2$ in the continuum limit.

If we include dynamical staggered fermions, we expect that for sufficiently large $\bar{\beta}$ the lattice potential is determined by the continuum potential eq. (3.23), as described in section 1.2.1 together with eq. (1.65). So if we take a lattice with the same size in physical units as the torus $\mathcal{T}_2$ in the continuum, we expect with $\bar{\beta} = \beta_{cont}/a^2$, $\beta_{cont} = 1/e^2_{cont}$ for the dimensionless combination $m^{-1}V(R)$ for sufficiently large $\bar{\beta}$

$$m^{-1}_{cont} V_{cont}(R)|_{\beta_{cont}} = \bar{m}^{-1}\bar{V}(\bar{R})|_{\bar{\beta}} \;, \qquad \bar{m}^2 = \frac{2}{\pi\bar{\beta}} \;. \tag{3.30}$$

Of course, R has to be chosen as $R = a\bar{R}$.

For gauge field observables, i.e. in our case the lattice potential $\bar{V}(\bar{R})$, no difference is expected between non-compact and compact lattice formulation in the scaling region, because $\det(M[U]) \simeq 0$ for topologically non-trivial sectors, see subsection 1.2.2. For the first non-trivial sector on the lattice, given with $Q_{top} = 1$, this suppression was measured, see Table 1.1. As long as finite size effects play a role in the lattice investigation it follows that the influence of dynamical fermions on the potential is bigger in the compact case, due to the suppression of these sectors by the fermion determinant, see Figure 3.2.

3.2.3 Monte Carlo simulations

The potential defined as in eq. (3.21), but including the effect of dynamical fermions, was calculated by MC simulations on a 16×6-lattice for different values of $\bar{\beta}$, see subsection 2.1.3 for the statistics of the evaluated configurations. The small extension in time direction $\overline{L}_2 = 6$ was necessary to see clear signals for $< PL(\bar{R}) >$, in particular in the strong coupling region. However, this is no shortcoming at least in the scaling region, because there we expect no dependence on $\overline{L}_2$ as in the continuum, eqs. (3.22), (3.23).

We found good agreement of our MC data with continuum results in the scaling region on the one hand and with the SCE in the strong coupling region on the other hand. For $\bar{\beta} = 10$ we compared the MC points with the continuum result in the sense of eq. (3.30). The MC data reproduce the continuum result eq. (3.23) within the very small error bars, see Figure 3.2. This means that the finite a effects are already small. In order to see this it was crucial to know the finite volume correction, because it dominates the finite a effects in this case.

$\bar{\beta}$:	0.1	0.3	0.5	0.7	1.0
$\overline{M}_P$:	3.76 ± 0.02	2.59 ± 0.06	2.02 ± 0.06	1.64 ± 0.13	1.25 ± 0.18
$\overline{M}_S$:	4.17 ± 0.36	2.60 ± 0.06	2.15 ± 0.11	1.91 ± 0.17	1.70 ± 0.24
$\overline{M}_d$:	0.97 ± 0.03	0.87 ± 0.03	0.83 ± 0.08	0.82 ± 0.15	0.84 ± 0.28

Table 3.1: The lattice gauge field mass, extracted from the plaquette correlation ($\overline{M}_P$) and as inverse screening length ($\overline{M}_S$) from the heavy quark potential, and the mass $\overline{M}_d$, which appears also in the strong coupling lattice potential, all evaluated by the strong coupling expansion for $\bar{\beta} = 0.3$ on 6×16- or 16×6-lattices, respectively.

For $\bar{\beta} = 0.3$ the MC measurements match the SCE for $\bar{V}^3_{alt}(\bar{R})$ in eq. (2.51), which converges rapidly in this region of $\bar{\beta}$, see Figure 2.5. However, the potential in the strong coupling region does not exactly show the qualitative behaviour $\sim (1 - \exp(-\overline{M}\bar{R}))$ we expect from the continuum calculation. Instead it can be described quite well by the ansatz

$$\bar{V}(\bar{R}) = c_1 \cosh\left(\overline{M}_S(\frac{\overline{L}_1}{2} - \bar{R})\right) \;+\; c_2\,(-1)^{\bar{R}} \cosh\left(\overline{M}_d(\frac{\overline{L}_1}{2} - \bar{R})\right) \;+\; c_3 \;, \tag{3.31}$$

where c_3 is determined by $\bar{V}(0) = 0$. This behaviour clearly appears if we use the SCE up to the third order but is smeared out by the errors in the MC results[2]. In Table 3.1 we give the masses $\overline{M}_S, \overline{M}_d$ of the above fit determined by the potential $\bar{V}^3_{alt}(\bar{R})$ in the third order SCE for various $\bar{\beta}$ in the strong coupling region. We assumed the errors to be half of the difference between the second and the third order estimation and obtained probabilities $\geq 80\%$ for our fits[3]. The relative difference between fit and the SC data to be fitted was < 0.001 for $\bar{\beta} \leq 0.3$ and < 0.004 for $\bar{\beta} \leq 1.0$. Thus the description of the strong coupling behaviour of the potential in terms of the two masses $\overline{M}_S, \overline{M}_d$ in eq. (3.31) is valid. However, we do not know what the meaning of the additional mass $\overline{M}_d$, describing the oscillations of the potential, could be. The MC simulations show that it appears only in the strong coupling region, for $\bar{\beta} = 10$ the MC calculation agrees with the continuum result. Note also the strong L_2-dependence of $\overline{M}_d$ sketched in Table 2.5.

In Table 3.1 we also compare the mass $\overline{M}_S$ obtained as inverse screening length by eq. (3.31) with the mass $\overline{M}_P$ appearing in the plaquette correlation, see section 3.1. It appears that these masses approximately coincide in the range of the errors, where we took half of the difference between zeroth and first order of the SC expansion as errors in the estimation of $\overline{M}_P$ in eq. (2.40). Note that considering the behaviour of the SCE for the potential we don't expect convergence of the SCE for $\bar{\beta} = 1.0$, as described in subsection 2.2.3. This may explain the difference between $\overline{M}_P$ and $\overline{M}_S$ for this $\bar{\beta}$-value.

[2]For $\bar{\beta} = 0.3$ we could qualitatively reproduce the strong coupling values for $\overline{M}_S, \overline{M}_d$ by the above fit for our MC data within relative errors of 30%, but for $\bar{\beta} = 1.0$ this was not possible, because the errors were too large and the fit did not match the data very well.

[3]For $\bar{\beta} = 0.1$ we had to enlarge the very small errors by a factor 16 to achieve these probabilities. This may be due to the difficulty to resolve a mass of the value ~ 4 in lattice units in such a fit.

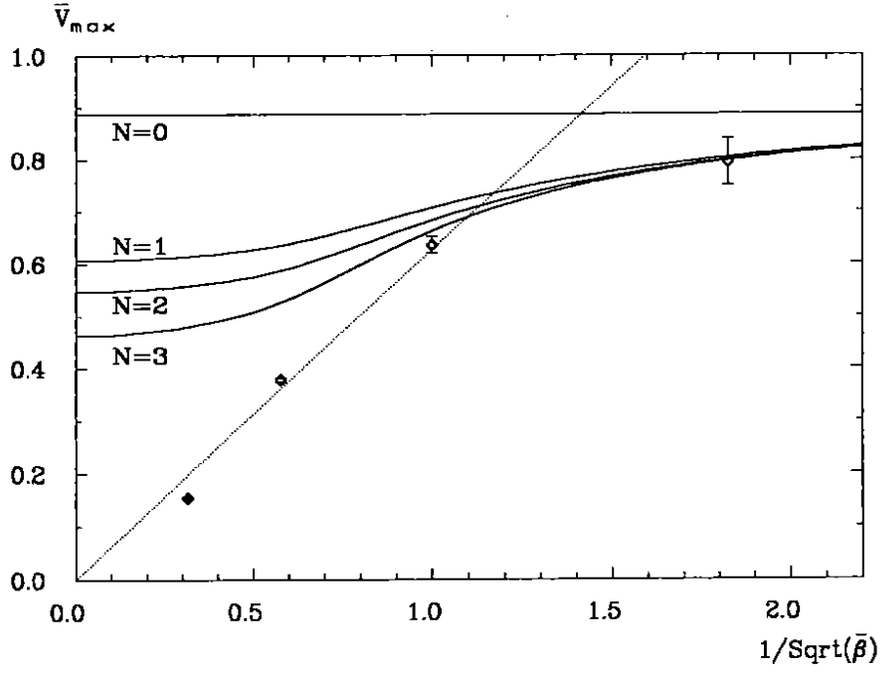

Figure 3.3: $\bar{V}_{max}$ vs. $\bar{\beta}$: MC measurements, SCE up to order N V_{alt}^N (full lines) and scaling line without finite volume corrections (dotted line). The latter explain the deviation of the $\bar{\beta} = 10$-measurement

Finally we compare the strong coupling and scaling behaviour. At strong coupling $\bar{V}(\bar{R})$ is given by the SCE, thus it is constant with $\bar{\beta}$ in leading order, or — when next to leading orders come into play — decreasing slowly as $\bar{\beta}$ increases. It appears that the first order remains important for relatively small $\bar{\beta}$. As a begins to resolve the continuum screening length $R_S = 1/m$ (usually [49] one requires $2a <$ *typical length scale*, i. e. $\bar{\beta} > 2.5$ in our case), we expect a transition to the scaling behaviour. Figure 3.3 shows this for $\bar{V}_{max} = \bar{V}(\overline{L}/2)$. As long as $\overline{L}/2 \gg \bar{R}_S$ we should find $\bar{V}_{max} \sim \bar{\beta}^{-1/2}$ in the scaling region[4]. This is confirmed by the MC data. The qualitatively same behaviour can be seen for the mass $\overline{M}_P$ in the plaquette correlation in Figure 3.1, see also Table 3.1. In both cases the MC values at $\bar{\beta} = 1.0$ are surprisingly close to the SC approximations, although the expansion parameter at $\bar{\beta} = 1.0$ is $\gamma = 0.45$ and we could not see convergence in the first four orders of the SCE of the potential at this point. On the other hand, for $\overline{M}_P$ the finite size effects are stronger, which may be explained with the bigger difference between the ideal scaling line and the strong coupling estimations at the transition region $\bar{\beta} \approx 1.0$.

[4]For $\bar{\beta} = 10$ this is not the case, but there the scaling behaviour is shown by comparison with the finite volume continuum potential, see Figure 3.2.

Chapter 4

Fermion Observables

4.1 Isovector current correlations

In this chapter we investigate the correlations between fermion bilinears, i.e. currents and (pseudo)scalars, with Monte Carlo simulations. It could be seen for gauge field observables in the last chapter that the lattice shows nearly perfect scaling behaviour for $\bar{\beta} = 10$. Furthermore, we could achieve quite small errors in the MC simulations with not too much computational effort. Whether this is the case for fermion observables is not a priori clear. In particular, the correlations under consideration are strongly dependent on topological quantities as torons and Chern classes in the continuum.

The identification of lattice fields with the currents and scalars in the continuum is achieved by a systematic investigation of the relation between lattice and continuum symmetry in section 1.3, summarized in Table 1.2. The resulting question of symmetry restoration on the lattice is treated here. Moreover, it is an important question whether the lattice can reproduce the anomalous breaking of the axial isoscalar symmetry $U(1)_A$.

In this first section we deal with the correlations of the isovector currents. The first subsection presents the continuum results of [AJ]. After some formulas for correlations of general fermion bilinears, we turn to the case of isovector currents. Here an important fact is that the isovector current correlation in a fixed background field depends only on the toron part of this field. So the lattice correlation of fermion bilinears corresponding to the continuum isovector current is calculated in a constant background field (see Appendix B). The comparison of these results with MC simulations will thus show whether the independence of the isovector current correlation from all gauge field variables but the toron holds on the lattice. This is carried out in the third subsection. Before that, we give some general formulas on correlations of lattice fermion bilinears in the second subsection, and on their evaluation within MC measurements in the third subsection.

4.1.1 Continuum results

The correlations of currents and (pseudo)scalars in the geometric Schwinger model on the torus were calculated in [AJ]. We write the general formula according to eqs. (1.40)–(1.42)

$$< \bar{\psi}(x)\Gamma\tau^k\psi(x)\ \bar{\psi}(y)\Gamma'\tau^l\psi(y) > = \ I_4{}^0 + I_4^{-1} + I_4{}^1\ , \tag{4.1}$$

where ${I_4}^k$ is the contribution of the gauge field sector with Chern index k. For convenience we use the Dirac basis ψ_a^b of eq. (1.14) for the explicit form of these fermion bilinears, Γ is a general combination of two-dimensional γ-matrices acting on the spinor index a, τ^k, $k = 0,1,2,3$, are the two-dimensional hermitian matrices acting on the flavour index b, see eqs. (1.93)–(1.95). First we turn to the term $I_4^{\pm 1}$ coming from the topological sectors $k = \pm 1$. The result of [AJ] is

$$\begin{aligned} I_4^{\pm 1} &= \frac{\eta^2(\tau)\, e^{4c^2 G(0)}\, |\Theta_1'(0|i\tau)|}{8\pi L_1^2\, |\Theta_1(z|i\tau)|}\, \frac{|\Theta_1(\frac{z}{2}|i\tau)|^4 + |\Theta_3(\frac{z}{2}|i\tau)|^4}{|\Theta_3(0|i\tau)|^4} \\ &\times\ e^{\frac{-2\pi^2}{L_1 L_2}} e^{-2\pi G_m(x-y)}\, \mathrm{Tr}\left((1 \pm \gamma_5^*)\Gamma)\right) \mathrm{Tr}\left((1 \pm \gamma_5^*)\Gamma'\right) \mathrm{Tr}\left(\tau^k \epsilon \tau^{l*} \epsilon\right) . \end{aligned} \tag{4.2}$$

We used the definitions $\tau = L_2/L_1$ (don't mix up with the flavour matrices τ^k), $\eta(\tau)$ is the Dedekind function $q^{1/12}\prod_{n=1}^{\infty}(1-q^{2n})$, $q = e^{-\pi\tau}$. In the isospin traces ϵ denotes the antisymmetric tensor, with $\epsilon_{bb'} = -\epsilon_{b'b} = \pm 1$. For the definition of the Jacobi Θ-functions see [19], the complex first argument is given by $z = \frac{1}{L_1}(x_1 - y_1 + i(x_2 - y_2))$. Finally the Greens functions $G(x)$, $G_m(x)$ are defined by

$$\Box(\Box - m^2)G(x) = \delta^{(\prime)}(x)\ , \quad (-\Box + m^2)G_m(x) = \delta^{(\prime)}(x)\ . \tag{4.3}$$

Here the zero modes are omitted, which is indicated by a prime for the δ-functions.

Because of the spin traces $\mathrm{Tr}[(1\pm\gamma_5^*)\Gamma)]$, $I_4^{\pm 1}$ vanishes if $\Gamma = \gamma^\mu$, i.e. for current correlations. It remains the $k = 0$-contribution

$$\begin{aligned} {I_4}^0 &= I_d - I_c = \frac{1}{Z}\int \mathcal{D}[A^0]\, e^{-S_0[A^0]}\, e^{\frac{1}{2}\Gamma_{eff}[A^0]} \\ &\times\ \Big\{ \mathrm{Tr}\left(\tau^k\right) \mathrm{Tr}\left(\Gamma S(x,x';A^0)|_{x=x'}\right)\ \mathrm{Tr}\left(\tau^l\right) \mathrm{Tr}\left(\Gamma' S(y,y';A^0)|_{y=y'}\right) \\ &-\ \ \mathrm{Tr}\left(\tau^k\tau^l\right) \mathrm{Tr}\left(\Gamma S(x,y;A^0)\Gamma' S(y,x;A^0)\right) \Big\}\ . \end{aligned} \tag{4.4}$$

with the fermion propagator $S(x,y;A)_{aa'} = \gamma^\mu_{aa'} s_\mu(x,y;A)$ obeying $\gamma^\mu(\partial_{x_\mu} - ieA_\mu)S(x,y;A) = -\delta(x-y)$. The disconnected term I_d (given by the second line in eq. (4.4)) vanishes for $k,l = 1,2,3$, i.e. for the correlations of isovector currents. For (pseudo)scalars these terms vanish in all cases because of the spin traces.

It follows from the form of the local solution in a background field A eq. (1.23) that $S(x,y;A)$ can be written as

$$S(x,y;A) = e^{ie\alpha(x)} S_t(x-y)\, e^{-ie\alpha^*(y)}\ , \tag{4.5}$$

with $\alpha(x) = a(x) + i\gamma^5 b(x)$, t denotes the toron part of A, see eq. (1.22), and with $S_t(x-y) = S(x,y;t)$. The Fourier representation of S_t is given by

$$S_t(x) = \frac{1}{L_1 L_2}\sum_p e^{ipx}\, \frac{i\gamma^\mu(p_\mu - \hat{t}_\mu)}{(p_1 - \hat{t}_1)^2 + (p_2 - \hat{t}_2)^2}\ . \tag{4.6}$$

Here the momentum components p_μ are given by $p_\mu = 2\pi n_\mu/L_\mu$, $n_\mu \in \mathbf{Z}$, and we defined $\hat{t}_\mu = et_\mu \in [0, 2\pi/L_\mu)$. For $t \equiv 0$, S_t is divergent due to the zero mode $n_\mu = 0$, compare with subsection 1.1.2.

Putting things together for the case of correlations of isovector currents $j_\mu^k(x) = \bar{\psi}(x)\gamma^\mu\tau^k\psi(x), k = 1,2,3$, (see eq. (1.94)), we have to consider only the connected term I_c in the $k = 0$-contribution eq. (4.4). The γ^5-matrix in $\alpha(x)$ anticommutes with the γ^μ-matrix in the current definition, the α-dependent terms cancel, and we obtain an expression in the configuration integral which depends only on the toron part t

$$< j_\mu^k(x) j_\nu^l(y) > = \frac{-2\delta_{kl}}{Z_t}\int dt\, P(t)\, \mathrm{Tr}\left(\gamma^\mu S_t(x-y)\gamma^\nu S_t(y-x)\right)\ . \tag{4.7}$$

The toron partition $P(t)$, defined in eq. (1.46), is the remnant of the regularized fermion determinant $\exp(\Gamma_{eff}/2)$, $Z_t = \int dt P(t)$ gives the normalization. In [AJ] the toron integration is performed. The divergence in S_t for $t \equiv 0$ is canceled by the zero of $P(t)$ at this point, as remarked together with eq. (1.46). The result is

$$< j_\mu^k(x) j_\nu^l(y) > = \delta_{kl}\left(\frac{-2}{\pi}\epsilon_{\mu\rho}\epsilon_{\nu\sigma}\partial_\rho\partial_\sigma\, G_0(x-y) + \frac{1}{\pi^2 L_1 L_2} R_{\mu\nu}(\tau)\right)\ . \tag{4.8}$$

Again we wrote $z = 1/L_1\,(x_1 - y_1 + i(x_2 - y_2))$. The constant $R_{\mu\nu}(\tau)$ is given in [AJ]. $G_0(x)$ is the massless Greens function on $\mathcal{T}_2$ with $-\Box G_0(x) = \delta^{(\prime)}(x)$, see eq. (4.3). Thus the correlation of the isovector current is governed by massless particles.

For the correlation of fields with a fixed momentum $q_1 \neq 0$ in space direction one obtains (with $x = (x_1, t)$)

$$m_\mu^k(t;q_1) := \int dx_1\, e^{iq_1 x_1} < j_\mu^k(x_1,t) j_\mu^k(0,0) > = \mp|q_1|\, \frac{\cosh\left[|q_1|(L_2/2 - t)\right]}{\pi \sinh\left[|q_1|L_2/2\right]}\ , \tag{4.9}$$

the sign factor is $-$ for $\mu = 1$, $+$ for $\mu = 2$. For $q_1 = 0$, $m(t;q_1)$ is constant. The decay $m(t;q_1) \sim \exp(-Et)$, with an energy $E = |q_1|$ shows the absence of a continuous multi-particle spectrum. This is a direct consequence of the isovector current correlation being determined by the free massless Greens function. It can be seen from eq. (4.8) that the isovector current j_μ^V (we dropped the isospin index k) can be written in terms of a free scalar field

$$j_\mu^V = \epsilon_{\mu\rho}\partial_\rho\, \phi^0(x)\ , \quad \text{with } \Box\phi^0(x) = 0\ . \tag{4.10}$$

This shows that $\partial_\mu j_\mu^V = 0$. The divergence of the axial current is determined with the duality relation eq. (1.96). It vanishes, because the Greens function in eq. (4.8) and the corresponding scalar field $\phi^0(x)$ is massless

$$\partial_\mu j_\mu^A = i\,\epsilon_{\mu\nu} j_\nu^V = i\,\Box\phi^0(x) = 0\ . \tag{4.11}$$

The result in eq. (4.9) will be compared with the lattice results.

4.1.2 Lattice correlations

In the following considerations all quantities are expressed in lattice units. First it follows from the form of the lattice action with staggered fermions eq. (1.58), which couples only even with odd sites of the lattice, that the lattice fermion propagator in a general background field U has the important property

$$< \chi_x \bar{\chi}_y >_U = 0\ , \quad \text{for } (x-y) \text{ even}\ . \tag{4.12}$$

This is related to the lattice remnants $A^3(\alpha)$ of the continuum axial symmetry, see eq. (1.104). For the explicit form of $< \chi_x \bar{\chi}_y >$ in a constant background field t see Appendix B.

Now we describe the correlations of local bilinears and one-link fields (bilinears including one link). For local fields $M^0(x) = \bar{\chi}_x \chi_x$, which correspond to the isovector current in the continuum for the flavour quantum number $L = (0,1), (1,0)$, see Table 1.2, we define

$$\begin{aligned} m^0(x,y;U) &= < M^0(x) M^0(y) >_U = \frac{1}{Z} \int \mathcal{D}[\bar{\chi},\chi]\, e^{-S_f[\bar{\chi},\chi,U]}\, \bar{\chi}_x \chi_x \bar{\chi}_y \chi_y \\ &= -\epsilon_{x-y} \mid < \chi_x \bar{\chi}_y >_U \mid^2 , \quad \epsilon_x = (-1)^{x_1+x_2} . \end{aligned} \tag{4.13}$$

We have used the lattice charge conjugation symmetry eq. (1.105) leading to

$$< \chi_x \bar{\chi}_y >_U = \epsilon_{x-y} \, (< \chi_y \bar{\chi}_x >_U)^* . \tag{4.14}$$

There are no disconnected contributions because of eq. (4.12), similar to the isovector current correlations in the continuum. In momentum space we set

$$m^0_L(q;U) = \sum_z e^{iqz} \sigma^L(z)\, m^0(z,0\,;U) , \quad \text{with } \sigma^L(z) \equiv \sigma^L(H_z) \equiv e^{i\pi(L,z)} , \tag{4.15}$$

with $L = (L_1, L_2)$, $L_\mu = 0,1$, corresponding to the notation in eqs. (1.118)–(1.121). In principle, in eq. (4.15) we performed a standard Fourier transformation, but with a different meaning. Since only translations on the coarse lattice Γ_{coarse} give a symmetry transformation, the momenta are defined in the Brillouin zone of Γ_{coarse}, i.e. $q_\mu = 2\pi n_\mu / L_\mu \in [-\pi/2, \pi/2)$. The remaining factors $\sigma^L(z)$ give the transformation behaviour under the restricted flavour transformations d^K, eq. (1.103). Note that $m^0_L(q;U)$ gives the correlation of the Fourier transformed covariant field in eq. (1.118)

$$M^0_L(q) = \sum_x e^{iqx} M^0_L(x) \tag{4.16}$$

after gauge field integration or in a constant background. Again L is identical with the flavour quantum number.

For the correlation of one-link fields we proceed in the same manner. However, the disconnected contributions are not necessarily zero. With the notation for the one-link bilinears

$$M^{\mu\pm}(x) = (i) \frac{1}{2} \left[\bar{\chi}_x U_{[x,\mu]}\, \chi_{x+e_\mu} \pm \bar{\chi}_{x+e_\mu} U^*_{[x,\mu]}\, \chi_x \right] , \tag{4.17}$$

corresponding to eqs. (1.119), (1.120) in section 1.3, we obtain for the connected part of its correlations

$$\begin{aligned} & m^{\mu\pm}(x,y;U) = < M^{\mu\pm}(x) M^{\mu\pm}(y) >_U^{connected} \\ = & -\frac{1}{4} \Big[P_{y+e_\mu,x+e_\mu} P_{x,y} U^*_{[x,\mu]} U_{[y,\mu]} + P_{y,x} P_{x+e_\mu,y+e_\mu} U_{[x,\mu]} U^*_{[y,\mu]} \\ \pm & \quad (P_{x+e_\mu,y} P_{y+e_\mu,x} U_{[x,\mu]} U_{[y,\mu]} + P_{y,x+e_\mu} P_{x,y+e_\mu} U^*_{[x,\mu]} U^*_{[y,\mu]}) \Big] , \end{aligned} \tag{4.18}$$

where $P_{x,y} := < \chi_x \bar{\chi}_y >_U$. In analogy to the local fields we transform to momentum space

$$m^{\mu\pm}_L(q;U) = \sum_z e^{iqz} \sigma^{L'}(z)\, m^{\mu\pm}(z,0\,;U) . \tag{4.19}$$

L' is given by $L' = L$ for $\mu = 1$, $(L'_1, L'_2) = (1 - L_1, L_2)$ for $\mu = 2$. Again, after gauge field integration or in a constant background, $m^{\mu\pm}_L(q;U)$ is the (connected) correlation of the Fourier transformed covariant fields in eqs. (1.119), (1.120)

$$M^{\mu\pm}_L(q) = \sum_x e^{iqx} M^{\mu\pm}_L(x) , \tag{4.20}$$

L gives the flavour quantum number.

The 1-link correlations have the following important property: Inserting eq. (4.14) in eq. (4.18) and using eq. (4.12) we find that

$$m^{\mu\pm}(x,y;U) = -\epsilon(x-y)\, m^{\mu\mp}(x,y;U) , \tag{4.21}$$

i.e. the one link fields $M^{\mu\pm}_L(x)$ and $M^{\mu\mp}_{\bar{L}}(x)$, with $(\bar{L}_1, \bar{L}_2) = (1 - L_1, 1 - L_2)$, have the same connected correlation up to an overall minus-sign. From Table 1.2 it can be seen that this equality would correspond to a degeneracy of the correlations of isovector and isoscalar currents or to a degeneracy of the correlations of (pseudo)scalars, which should be splited up by the anomalous breaking of the $U(1)_A$-symmetry. This unwanted degeneracy is broken by the non-vanishing disconnected terms for the correlations of isoscalar current and (pseudo)scalars.

Let us finally give the form of the disconnected contributions of one-link field correlations. For a general background field U we obtain

$$\begin{aligned} & d^{\mu\pm}(x,y;U) = < M^{\mu\pm}(x) M^{\mu\pm}(y) >_U^{disconnected} \\ = & \pm \frac{1}{4} \Big[(P_{x+e_\mu,x} U_{[x,\mu]} \pm P_{x,x+e_\mu} U^*_{[x,\mu]}) \, (P_{y+e_\mu,y} U_{[y,\mu]} \pm P_{y,y+e_\mu} U^*_{[y,\mu]}) \Big] \\ = & -\rho(\mu, H_{x-y})\, \mathcal{P}^\mu_\pm(x)\, \mathcal{P}^\mu_\pm(y) , \end{aligned} \tag{4.22}$$

with $\mathcal{P}^\mu_+(x) = \Im(P_{x+e_\mu,x} U_{[x,\mu]})$, $\mathcal{P}^\mu_-(x) = \Re(P_{x+e_\mu,x} U_{[x,\mu]})$.

If we have a constant background field $U_{[x,\mu]} = c_\mu$, $\mathcal{P}^\mu_\pm(x)$ becomes a constant too. So after Fourier transformation

$$d^{\mu\pm}_L(q;t) = \sum_z e^{iqz} \sigma^{L'}(z)\, d^{\mu\pm}(z,0\,;t) \tag{4.23}$$

we obtain a non-vanishing $d^{\mu\pm}_L(q;t)$ only for $q = 0$ and $L = (0,0)$. This means the lattice bilinears corresponding to the isovector current get no disconnected contributions in the case of a constant background field. We expect this from the absence of disconnected contributions for such correlations in the continuum. For the same reason the absence of disconnected contributions for these lattice bilinears should approximately hold for an arbitrary gauge field background, if one is close enough to the continuum limit.

4.1.3 Monte Carlo results

Before we analyze the detailed properties of the MC data for the isovector current, we describe our general procedure for MC measurements of fermion bilinear correlations. Out of the minimal bilinears quoted in Table 1.2 we study the correlations for local fields and fields with one link in 1-direction. For this we took the configurations on a 6×16-lattice for $\tilde{\beta} = 10,3$, described in subsection 2.1.3.

In order to evaluate the mass spectrum contained in these correlations it is convenient to take correlations of fields with fixed momentum in space direction q_1 and with a fixed 1-component L_1 of the flavour quantum number

$$m_\sigma^\alpha(t;q_1) = < M_\sigma^\alpha(x_2;q_1) M_\sigma^\alpha(y_2;-q_1) > , \quad t = x_2 - y_2 , \tag{4.24}$$

$$M_\sigma^\alpha(x_2;q_1) = \frac{1}{\sqrt{L_1}} \sum_{x_1} e^{iq_1 x_1} \sigma^{x_1} M^\alpha(x_1,x_2) . \tag{4.25}$$

$M^\alpha(x)$ are the bilinears from eqs. (4.13), (4.17), i.e. $\alpha = 0, 1\pm$, L_1 is given by $\sigma = (-1)^{L_1}$. Up to the flavour component L_2, α and σ establish the relation to the covariant fields in Table 1.2. As already explained in the previous subsection, the possible momenta are $q_1 = 2\pi n/L_1 \in [-\pi/2, \pi/2)$. With eqs. (4.13), (4.18) we obtain

$$m_\sigma^\alpha(t;q_1) = \sum_{z_1} e^{iq_1 z_1} \sigma^{z_1} < m^\alpha((z_1,t),0;U) > . \tag{4.26}$$

For the inclusion of the disconnected contributions for 1-link fields one has to substitute $m^{\mu\pm}(x;U)$ from eq. (4.18) by $m^{\mu\pm}(x;U) + d^{\mu\pm}(x;U)$ with eq. (4.22).

Using the transfer matrix formalism for staggered fermions [50], one expects [29], [51]

$$m_\sigma^\alpha(t;q_1) = \sum_i c_i (\epsilon_i)^t \cosh\left[E_i(q_1)\left(\frac{L_2}{2} - t\right)\right] . \tag{4.27}$$

The relation to the momentum space propagators $m_L^\alpha(q)$ in eqs. (4.15), (4.19) can be established in the continuum limit. There the energies E_i depend on q_1 by $E_i^2 = q_1^2 + m_i^2$, and each mass m_i corresponds to a pole in the momentum space propagators $m_L^\alpha(q)$ by

$$m_L^\alpha(q) = \frac{c_i}{q^2 + m_i^2} . \tag{4.28}$$

The flavour quantum number L in this propagator is connected to σ, ϵ_i in eq. (4.27) by $\sigma = (-1)^{L_1}$ for these α, as above, and by $\epsilon_i = (-1)^{L_2}$. In this manner each decay energy E_i is related to a field $M_L^\alpha(x)$ and thus to unique lattice quantum numbers[1]. According to Table 1.2 these lattice quantum numbers correspond to the continuum quantum numbers of currents and (pseudo)scalars.

However, in order to disentangle the contributions to different quantities one has to rely on a fit of $m_\sigma^\alpha(t;q_1)$ in the sense of eq. (4.27). This has the disadvantage, that in this fit the quite simple structure for the lattice bilinears corresponding to continuum currents is mixed with the more complicated spectrum corresponding to the continuum situation for scalars and pseudoscalars, see below.

The lattice bilinears which correspond to the continuum isovector current can be taken from Table 1.2. Here we shall consider the fields $M^0_{(0,1)}(x)$ and $M^{1^-}_{(1,1)}(x)$. So we must evaluate $m^0_+(t;q_1)$ and $m^{1^-}_-(t;q_1)$, see eqs. (4.24), (4.25). Since the continuum isovector current correlation shows only a small constant for $q_1 = 0$ (see eq. (4.9)), we are forced to take $q_1 = \pi/3$

[1]This determination of the quantum numbers matches with the results in [29],[51], where the transformation behaviour of field operators was considered in the Hamiltonian formalism and then these operators were identified with Grassmann fields via the transfer matrix formalism.

on our 6×16-lattice. Within the fit following eq. (4.27) we expect that the energies, which correspond to $L_2 = 1$ and thus have an $(-1)^t$-factor, approximately fit the continuum result from eq. (4.9), i.e. there is only one massless intermediate state. In fact, it turned out for $\bar\beta = 10$ that the MC data are well described by

$$\begin{aligned} m_\sigma^\alpha(t;\tfrac{\pi}{3}) &= c_1^+ \cosh\left[E_1^+\left(\frac{L_2}{2} - t\right)\right] + c_2^+ \cosh\left[E_2^+\left(\frac{L_2}{2} - t\right)\right] \\ &+ c_1^- \cosh\left[E_1^-\left(\frac{L_2}{2} - t\right)\right](-1)^t , \end{aligned} \tag{4.29}$$

with $t = 0, \ldots, 8$ for $m_\sigma^\alpha = m_+^0$, $t = 1, \ldots, 8$ for $m_\sigma^\alpha = m_-^{1^-}$, with and without the inclusion of the topologically non-trivial sectors $Q_{top} \neq 0$ and with and without the disconnected contributions for the correlations of 1-link fields[2]. On the quite small lattice it was possible to calculate the propagators P_{za} for all points z, a in each configuration, i.e. we performed the matrix inversion eq. (2.3) for each starting point a[3]. We then evaluated eqs. (4.13), (4.18) depending on (x,y) for each y an averaged over y. Therefore the correlations eqs. (4.15), (4.19) were symmetric with respect to the interchange of t and $L_2 - t$ as they would be in any case, if the integral over the gauge configurations U was exact. That is why we fitted only the decreasing branch of each correlation, $t = 0(1), \ldots, 8$. The probabilities of the fits of the MC data with $\bar\beta = 10$ following eq. (4.29) were $P \geq 90\%$[4]. Combined with the small errors in the MC data this means the fits describe the data up to an absolute deviation $< 10^{-5}$. Figure 4.1 shows the fit eq. (4.29) for $m^0_+(t;\pi/3)$ and $m^{1^-}_-(t;\pi/3)$ at $\bar\beta = 10$ with disconnected contributions and including all topological sectors. Because of the factors $(-1)^t$ it makes no sense to evaluate the fit ansatz for non-integer values of t, so we drew the fit with a polygon line.

The results for E_1^-, $C_1^- = \frac{1}{2} c_1^- e^{E_1^- L_2/2}$, which are the quantities concerning to the isovector current correlation, can be found in Table 4.1. It can be seen that the influence of the topologically non-trivial sectors as well as the influence of the disconnected contributions are very small. However, if we had not generated a large number of $Q_{top} \neq 0$-contributions by a separate run of the MC algorithm (see subsection 1.2.2), these sectors would worsen the errors considerably. The results for $C_1^+, E_1^+, C_2^+, E_2^+$ are discussed in section 4.3 on scalars and pseudoscalars. The $C_i^\pm$ are defined such that

$$c_i^\pm \cosh[E_i^\pm(\frac{L_2}{2} - t)] = C_i^\pm \left(e^{-tE_i^\pm} + e^{(L_2 - t)E_i^\pm}\right) . \tag{4.30}$$

In this form the fit procedure for eq. (4.29) showed a better convergence behaviour.

In Table 4.1 also the results from the continuum with assumed scaling and the results of the lattice calculation with constant background field are presented for C_1^-, E_1^-. Note that the continuum results in eq. (4.9) do not depend on the coupling, because the isovector current does not couple to the $b(x)$-part of the gauge field. We have $E = |q_1| = \pi/3$ corresponding to a massless particle.

[2]The correlation of local fields does not have a disconnected part, as remarked already in the previous subsection.

[3]This meant no additional computational effort, because we needed all propagators for the evaluation of the disconnected contributions.

[4]If we took $t = 0, \ldots, 8$ for m^{1^-} too, the values of the fit parameters confirmed the original ones (obtained with $t = 1, \ldots, 8$) within the errors, but the probability of the fit then was $50\% - 70\%$.

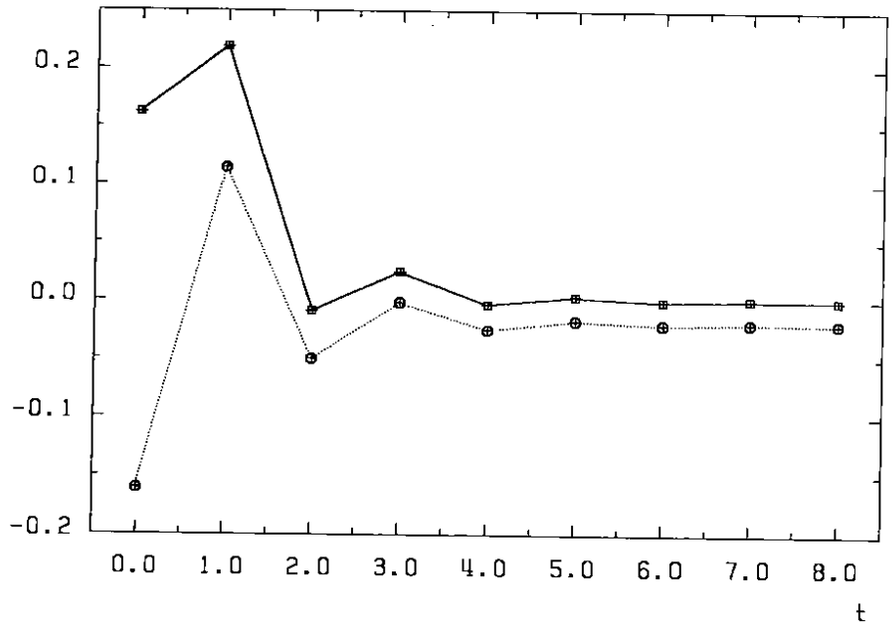

Figure 4.1: Fit of $m_+^0(t;\pi/3)$ (full line, squares) and $-m_-^{1-}(t;\pi/3)$ (dotted line, circles). Data and fit for $-m_-^{1-}(t;\pi/3)$ are shifted by -0.02 in y-direction.

		$m_+^0(t;\pi/3)$		$m_-^{1-}(t;\pi/3)$	
		E_1^-	C_1^-	E_1^-	C_1^-
scaling		1.0472	$-1/3$	1.0472	1/3
constant background		0.9492	-0.2651	0.9500	0.2611
$\bar{\beta}$	$Q_{top}=0$, (c):	0.9409(4)	$-0.2662(2)$	0.9429(5)	0.2595(4)
=	$Q_{top}=0$, (c+d):	—	—	0.9431(5)	0.2597(4)
10	$Q_{top}\in\mathbf{Z}$, (c+d):	0.9409(5)	$-0.2663(3)$	0.9429(6)	0.2596(5)
$\bar{\beta}$	$Q_{top}=0$, (c):	0.85(3)	$-0.22(2)$	0.93(2)	0.22(2)
=	$Q_{top}=0$, (c+d):	—	—	0.92(1)	0.257(7)
3	$Q_{top}\in\mathbf{Z}$, (c+d):	0.86(3)	$-0.22(2)$	0.920(7)	0.259(5)

Table 4.1: Results for the correlations of isovector current bilinears without disconnected contributions (c), and with disconnected contributions (c+d).

In the case of a constant background field on the lattice, we evaluated eq. (4.24) with the help of eq. (B.3) and eqs. (4.13), (4.18), and integrated numerically over the toron background weighted with the continuum toron partition $P(t)$ in eq. (1.46). This is justified as a real lattice result by the check of the toron partition on the lattice in subsection 1.2.3, which agrees with the continuum partition very well for $\bar{\beta}=3,10$. However, the dependence of the correlations in question on the toron background is small, as long as the torons are not near the forbidden point $t_\mu=0$. It can be seen that the MC results for $\bar{\beta}=10$ are very close to the toron results. Thus the main lattice effect in the scaling region is described by the change of the continuum fermion propagator to the lattice fermion propagator in a toron background, the coupling of the bilinears corresponding to the isovector current to the lattice field strength F_x remains negligible in a first approximation. Moreover this means that the 10% difference between the MC result for the decay energy E in both isovector correlations on the one hand and the continuum dispersion relation for massles particles $E=|q_1|$ on the other hand is no dynamical effect but due to lattice effects, which appear already in the free theory. We expect that this difference would be smaller for smaller momenta q_1, which could be taken on larger lattices.

Finally Table 4.1 shows the results for $\bar{\beta}=3$, in order to estimate the finite a effects. However, the fits were not so good in this case. For all fits of data with $\bar{\beta}=3$, except those including the disconnected contributions in $m_-^{1-}(t;q_1)$, the best we found was to restrict the fit range to $t=3,\ldots,8$ and to fit only with one decay energy for each L_2, i.e. the second term in eq. (4.29) was omitted. In this way we obtained probabilities between 20% and 30%. For the case of included disconnected contributions in $m_-^{1-}(t;q_1)$ the situation was somewhat better. We took $t=1,\ldots,8$ here and achieved a probability of about 40% with a three-energy fit as for $\bar{\beta}=10$.

At last we want to remark that the data for the lattice bilinears $m_+^0(t;q_1)$ and $m_-^{1-}(t;q_1)$ show the flavour symmetry restoration. Both correspond to the isovector current in the continuum but to different lattice irreps. In particular, the comparison of the data for $\bar{\beta}=3$ and $\bar{\beta}=10$ gives an impression of this effect as a consequence of the lattice approaching the continuum limit.

4.2 Isoscalar current correlations

In this section we treat the correlation of the isoscalar currents. In the continuum its disconnected part must be treated with the gauge invariant point-splitting procedure, leading to a massive decay of this correlation. This mechanism is related to the anomalous breaking of the $U(1)_A$-symmetry. The lattice analogue of the point-splitting procedure is the fact that the minimal lattice bilinears representing the isoscalar current are 1-link fields, which can couple to the gauge field degrees of freedom with the included link variable. The disconnected contributions to the correlations of these fields are then expected to change the massless decay of the connected correlation to a massive decay. We shall be able to show this in our Monte Carlo measurements.

The whole situation is similar to the $U(1)$-puzzle in (4-dimensional) QCD, where the mass of the η'-particle is also generated by the inclusion of disconnected contributions [2]. Attempts to show this mechanism within MC calculations were not yet successful [52]. Again the Schwinger model proves to be a useful toy model for such problems.

The first subsection shortly presents the continuum results of [AJ]. In the second subsection we will then discuss the MC results on the lattice.

4.2.1 Continuum results

For the correlation of the isoscalar current we can use the general formulas given already in subsection 4.1.1. As remarked together with eq. (4.2) the contributions from the non-trivial topological sectors $k \neq 0$ vanish for current correlations, it remains the $k = 0$-contribution of eq. (4.4). The isospin matrix is now given by $\tau^0 = \mathbf{1}_2$, so in contrast to the isovector case, the disconnected contribution I_d does not vanish because of the traces in the flavour index.

In eq. (4.4) the expression $S(x, x'; A^0)|_{x=x'}$ in I_d needs a regularization by the gauge invariant point-splitting procedure. One defines the point-splited current

$$J^0_\mu(x;\xi) = \bar\psi(x+\xi)\tau^0\gamma^\mu e^{ie\int_{x-\xi}^{x+\xi} A_\alpha(\bar x)d\bar x^\alpha}\psi(x-\xi)\,, \tag{4.31}$$

where again γ^μ acts on the spinor index, τ^0 acts on the isospin index of $\bar\psi, \psi$. For its disconnected contribution one obtains [AJ]

$$\begin{aligned} &< J^0_\mu(x;\xi)J^0_\nu(y;\xi') >^{dc} = \frac{4}{Z}\int \mathcal{D}[A^0]\, e^{-S_g[A^0]}\, e^{\frac{1}{2}\Gamma_{\mathrm{eff}}[A^0]} \\ \times\ & \mathrm{Tr}\left(\gamma^\mu S(x-\xi, x+\xi; A^0)\right)\, e^{ie\int_{x-\xi}^{x+\xi} A_\alpha(\bar x)d\bar x^\alpha} \\ \times\ & \mathrm{Tr}\left(\gamma^\nu S(y-\xi', y+\xi'; A^0)\right)\, e^{ie\int_{y-\xi'}^{y+\xi'} A_\beta(\bar y)d\bar y^\beta} \\ =\ & \frac{1}{\pi^2}\frac{\xi_\mu}{|\xi|^2}\frac{\xi_\nu}{|\xi|^2} + \frac{4e^2}{\pi^2}\epsilon_{\mu\rho}\epsilon_{\nu\sigma}\partial_\rho\partial_\sigma\, G(x-y) - \frac{1}{\pi^2 L_1 L_2}R_{\mu\nu}(\tau)\,. \end{aligned} \tag{4.32}$$

Now one omits the divergence for $\xi \to 0$, and defines

$$< j^0_\mu(x) j^0_\nu(y) >^{dc} = \lim_{\xi,\xi'\to 0}\left(< J^0_\mu(x;\xi)J^0_\nu(y;\xi') >^{dc} - \frac{1}{\pi^2}\frac{\xi_\mu}{|\xi|^2}\frac{\xi_\nu}{|\xi|^2}\right)\,. \tag{4.33}$$

This corresponds to the definition of the regularized current in the Schwinger model [7].

Together with the connected terms of the isoscalar current correlation, which are the same as for the isovector current correlation in eq. (4.8) one finally obtains

$$< j^0_\mu(x) j^0_\nu(y) > = -\frac{2}{\pi}\epsilon_{\mu\rho}\epsilon_{\nu\sigma}\partial_\rho\partial_\sigma\, G_0(x-y) + \frac{4e^2}{\pi^2}\epsilon_{\mu\rho}\epsilon_{\nu\sigma}\partial_\rho\partial_\sigma\, G(x-y)\,, \tag{4.34}$$

with $G(x)$, $G_0(x) = G_m(x)|_{m=0}$ defined in eq. (4.3). It is easy to see from this definition that

$$G_m(x-y) = G_0(x-y) - m^2\, G(x-y)\,, \tag{4.35}$$

where $m^2 = 2e^2/\pi$ is the mass which governs the gauge field dynamics, see eq. (1.45). Thus eq. (4.34) becomes

$$< j^0_\mu(x) j^0_\nu(y) > = -\frac{2}{\pi}\,\epsilon_{\mu\rho}\epsilon_{\nu\sigma}\partial_\rho\partial_\sigma\, G_m(x-y)\,. \tag{4.36}$$

As for the isovector current we form the correlations of fields with a fixed momentum q_1 in space direction and obtain (with $x = (x_1, t)$)

$$\begin{aligned} m^0_\mu(t;q_1) &:= \int dx_1\, e^{iq_1x_1} < j^0_\mu(x_1,t) j^0_\mu(0,0) > \\ &= c_\mu(q_1)\frac{\cosh\left[E(q_1)\,(L_2/2-t)\right]}{\pi\sinh\left[E(q_1)L_2/2\right]}\,, \end{aligned} \tag{4.37}$$

where $E(q_1) = \sqrt{m^2+q_1^2}$, $c_\mu(q_1) = -E(q_1)$ for $\mu = 1$, $c_\mu(q_1) = q_1^2/E(q_1)$ for $\mu = 2$.

Summing up, the isoscalar current correlation couples to the gauge field by its disconnected contributions. These make the difference to the correlation of isovector currents, they change the massless decay in that case into a massive decay with mass $m^2 = 2e^2/\pi$. As an important consequence the isoscalar vector current is expressed in terms of a free massive scalar field (compare to eq. (4.10))

$$j^{V,0}_\mu = \epsilon_{\mu\rho}\partial_\rho\,\phi^m(x)\,, \quad \text{with } \Box\phi^m(x) = m^2\phi^m(x)\,. \tag{4.38}$$

It follows that the total divergence of the axial isoscalar current does not vanish in this case

$$\partial_\mu j^{A,0}_\mu = i\,\epsilon_{\mu\nu} j^{V,0}_\nu = i\,\Box\phi^m(x) = i\,m^2\phi^m(x)\,. \tag{4.39}$$

That means the non-vanishing mass in the isoscalar current correlation is directly related to the anomalous breaking of the $U(1)_A$ symmetry.

4.2.2 Lattice results

A minimal lattice bilinear corresponding to the isoscalar current in the continuum is $M^{\mu+}_{(0,0)}(x)$, as can be read off from Table 1.2. As remarked above, the fact that we have to take a 1-link field corresponds to the gauge invariant point-splitting for a correct definition of the continuum isoscalar current. Thus in this case we have to evaluate eq. (4.26) with $m^\alpha_\sigma(t;q_1) = m^{\mu+}_+(t;q_1)$. In its decomposition following eq. (4.27) the energies, which have no $(-1)^t$-factor, belong to

$M^{\mu+}_{(0,0)}(q)$, i.e. to the isoscalar current in the continuum. They should approximately fit the continuum result from eq. (4.37), i.e. there should be only one such energy

$$E_1^+ \simeq \sqrt{m^2 + q_1^2}\ , \tag{4.40}$$

$m^2 = 2/(\pi\bar{\beta})$ in lattice units.

The connected part of the correlation $m_+^{\mu+}(t;q_1)$ is the same as for $m_-^{\mu-}(t;q_1)$ up to a factor $-(-1)^t$, see eq. (4.21). The disconnected contributions are included with the substitution of $m^{\mu+}(x;U)$ by $m^{\mu+}(x;U) + d^{\mu+}(x;U)$ in eq. (4.26), they are given by

$$d^{\mu+}(x,y;U) \ = \ -\rho(\mu, H_{x-y})\ \mathcal{P}_+^\mu(x)\ \mathcal{P}_+^\mu(y)\ , \tag{4.41}$$

with $\mathcal{P}_+^\mu(x) = \Im(P_{x+e_\mu,x}U_{[x,\mu]})$, see eq. (4.22). There is an intuitive picture of the meaning of $\mathcal{P}_+^\mu(x)$. One might consider the propagator $P_{x+e_\mu,x}$ as a sum over fermion lines from $x+e_\mu$ to x with certain weights. These fermion lines complete the link variable $U_{[x,\mu]}$ in $\mathcal{P}_\pm^\mu(x)$ to Wilson loops. For $\mathcal{P}_+^\mu(x)$ opposite directions of these loops are subtracted, which leads to a form similar to the lattice quantities Φ_x, defined in eq. (3.8). These Φ_x are related to the field strength, see eq. (3.9). This may give an idea why we can expect to obtain a part of massive decay in the correlation of $\mathcal{P}_-^\mu(x)$, with a mass $m^2 = 2/(\pi\bar{\beta})$ in lattice units in the continuum limit.

We measured $m_+^{1+}(t;q_1)$ with the $L_1 \times L_2 = 6 \times 16$ MC configurations for $\bar{\beta} = 10, 3$, described in subsection 2.1.3. As momenta in space direction we took $q_1 = 0$ and $q_1 = \pi/3$ and fitted by

$$\begin{aligned} m_+^{1+}(t;q_1) \ &= \ c_1^+ \cosh\left[E_1^+\left(\frac{L_2}{2} - t\right)\right] \ + \ c_1^- \cosh\left[E_1^-\left(\frac{L_2}{2} - t\right)\right](-1)^t \\ &+ \ c_2^- \cosh\left[E_2^-\left(\frac{L_2}{2} - t\right)\right](-1)^t\ . \end{aligned} \tag{4.42}$$

In some cases we omitted the third term with the energy E_2^-. This is called a two-energy fit. The probabilities of the fits with zero momentum $q_1 = 0$ were $P \geq 95\%$ for $\bar{\beta} = 10$ and $P = 78\%$ for $\bar{\beta} = 3$ without disconnected contributions. In these cases we fitted the data for $t = 0, \ldots, 8$ with a three-energy fit following eq. (4.42). For $\bar{\beta} = 3$ with disconnected contributions a two-energy fit in eq. (4.42) led to higher probabilities $P \simeq 60\%$. With $q_1 = \pi/3$ the situation was worse. In particular the probabilities for $\bar{\beta} = 10$ with disconnected contributions were only $P \simeq 4\%$, where we fitted the data for $t = 0, \ldots 8$ with a three-energy fit as above. As reason we guess a more complicated mass structure in the part of the correlation which oscillates with a factor $(-1)^t$ in the sense of eq. (4.42), and thus belongs to the lattice quantum numbers corresponding to the (pseudo)scalars in the continuum. This part seems not to be well-described by maximal two cosh-decay functions. We substantiate this guess in the next subsection on the (pseudo)scalar sector. The $\bar{\beta} = 3$ fits for the $q_1 = \pi/3$ correlations with disconnected contributions show better probabilities $P \simeq 75\%$. This seems to be due to the larger errors in this case. Note that the data without disconnected contributions for $m_+^{1+}(t;q_1)$ are the same as for $m_-^{1-}(t;q_1)$ up to the factor $-(-1)^t$ because of eq. (4.21). Therefore the values obtained without disconnected contributions for E_1^+ with $q_1 = \pi/3$ in Table 4.2 and E_1^- in Table 4.1 are equal. For the fit quality in these cases see subsection 4.1.3.

		$m_+^{1+}(t;0)$		$m_+^{1+}(t;\pi/3)$	
		E_1^+	C_1^+	E_1^+	C_1^+
scaling ($\bar{\beta} = 10$)		0.252	—	1.0772	—
$\bar{\beta}$	$Q_{top} = 0$, (c):	0.15(25)	−0.0007(12)	0.9429(5)	−0.2595(4)
=	$Q_{top} = 0$, (c+d):	0.267(4)	−0.095(2)	0.972(1)	−0.2662(5)
10	$Q_{top} \in \mathbf{Z}$, (c+d):	0.267(5)	−0.095(2)	0.972(1)	−0.2663(5)
scaling ($\bar{\beta} = 3$)		0.461	—	1.144	—
$\bar{\beta}$	$Q_{top} = 0$, (c):	0.45(15)	−0.029(21)	0.93(2)	−0.22(2)
=	$Q_{top} = 0$, (c+d):	0.86(17)	−0.42(16)	1.16(2)	−0.32(1)
3	$Q_{top} \in \mathbf{Z}$, (c+d):	0.80(12)	−0.37(11)	1.13(1)	−0.309(5)

Table 4.2: Results for the correlation of the isoscalar current bilinears without disconnected contributions (c), and with disconnected contributions (c+d).

The results for E_1^+, $C_1^+ = \frac{1}{2}c_1^+ e^{E_1^+ L_2/2}$, which are the quantities concerning to the isoscalar current correlation, can be found in Table 4.2, for the remaining parameters $C_1^-, E_1^-, C_2^-, E_2^-$ see subsection 4.3.2. The values for E_1^+ with $q_1 = 0$ show clearly the coupling to the gauge field due to the disconnected contributions in agreement with the continuum mechanism. This coupling leads to a massive decay with an energy very close to the mass $m = \sqrt{2/(\pi\bar{\beta})}$, which we expect for ideal scaling from the continuum result. Without disconnected contributions, we get the same result as in the isovector case, where for $q_1 = 0$ only a small constant is expected, see subsection 4.1.1. The same mechanism can be seen for $q_1 = \pi/3$. The disconnected contributions increase the energy from the value of the isovector case E_0, corresponding to a massless decay, to an energy E_1, which is approximately given by $E_1^2 = m^2 + E_0^2$. The mass extracted this way becomes $m = 0.2435(5)$, see Table 4.2. We checked that the data do not give rise to a second energy without an $(-1)^t$ factor, i.e. the massless decay of the connected contributions is canceled by the disconnected contributions as in the continuum, see eqs. (4.34)-(4.36).

Finally the $\bar{\beta} = 3$ values show that the finite size effects soon become significant. However, the interplay of connected and disconnected contributions could be extracted qualitatively also in that case. As remarked in subsection 4.2.1, the massive decay of the isoscalar current correlation is related to the anomalous breaking of the $U(1)_A$-symmetry. In this sense we found that the lattice reproduces this anomaly for $\bar{\beta} = 10$ clearly.

4.3 The scalar and pseudoscalar sector

This last section deals with the correlations of scalars and pseudoscalars. In the continuum they can be seen to obtain contributions from the topologically non-trivial sectors with the Chern index $k = \pm 1$. The correlations of scalar fermion bilinears, which are in the same irreducible representation of the $U(2)_L \otimes U(2)_R$ flavour symmetry but in different irreps of the restricted $U(1)_V \otimes SU(2)_L \otimes SU(2)_R$, become different because of these contributions. That indicates anomalous symmetry breaking. We describe these features in the first subsection.

The reproduction of the above results on a lattice with parameters close enough to the continuum limit requires a sensible treatment of the lattice remnants of the Chern sectors and related topological zero modes. The difficulties coming up in a Monte Carlo simulation are already described in subsection 1.2.2 and subsection 2.1.2. There we suggested a preliminary method to deal with these difficulties on our small 6×16-lattice. The MC results presented in subsection 4.3.2 will show that the topological sectors were treated correctly in this framework. It can also be seen that the explicit analysis of the connection between continuum and lattice symmetry from section 1.3 is important to understand how the lattice reproduces the $U(1)_A$-anomaly.

4.3.1 Continuum results

The correlations of scalars and pseudoscalars in the geometric Schwinger model show a subtle interplay of the contributions from the trivial topological sector $k = 0$ and the non-trivial topological sectors $k = \pm 1$ [AJ]. We define scalars $s^i(x) = \bar{\psi}(x)\tau^i\psi(x)$ and pseudoscalars $s_5^i(x) = \bar{\psi}(x)\gamma^5\tau^i\psi(x)$, as in eq. (1.95). With the equations already given in section 4.1.1 one gets in the trivial sector $k = 0$

$$\begin{aligned} < s^k(x)s^l(y) >^0 &= 2C\,\delta_{kl}\,\frac{|\Theta_1(\frac{z}{2}|i\tau)|^4 + |\Theta_3(\frac{z}{2}|i\tau)|^4}{|\Theta_1(z|i\tau)|}\,\exp(2\pi\,G_m(x-y))\,, \\ \text{with } C &= \eta^2(\tau)\,\frac{e^{4e^2G(0)}\,|\Theta_1'(0|i\tau)|}{\pi\,L_1^2\,|\Theta_3(0|i\tau)|^4}\,, \end{aligned} \tag{4.43}$$

$$< s_5^k(x)s_5^l(y) >^0 = - < s^k(x)s^l(y) >^0\,, \tag{4.44}$$

the notations are those of subsection 4.1.1. The contributions for the topologically non-trivial sectors $k = \pm 1$ are the same for scalars and pseudoscalars, but they take a sign depending on the isospin I, $I = 0$ for $l = 0$, $I = 1$ for $l = 1, 2, 3$, l is the index of the isospin matrices τ^l. Evaluating the traces in eq. (4.2) we obtain

$$\begin{aligned} < s_{(5)}^k(x)s_{(5)}^l(y) >^{\pm 1} &= C\,\delta_{kl}\,(-1)^I\,\frac{|\Theta_1(\frac{z}{2}|i\tau)|^4 + |\Theta_3(\frac{z}{2}|i\tau)|^4}{|\Theta_1(z|i\tau)|} \\ &\times\ \exp(\frac{-2\pi^2}{e^2L_1L_2})\,\exp(-2\pi\,G_m(x-y))\,. \end{aligned} \tag{4.45}$$

If one defines the massive Greens function including the zero mode $\overline{G}_m(x) = G_m(x) + 1/(m^2L_1L_2)$ (compare the definition of G_m in eq. (4.3)), the sum over the contributions of

the three different topological sectors becomes

$$\begin{aligned} < s_\pm^k(x)s_\pm^l(y) > &= \delta_{kl}\,(-1)^I\,2C\,\frac{|\Theta_1(\frac{z}{2}|i\tau)|^4 + |\Theta_3(\frac{z}{2}|i\tau)|^4}{|\Theta_1(z|i\tau)|}\,e^{-\frac{2\pi}{m^2L_1L_2}} \\ &\times\ \left[\exp(-2\pi\,\overline{G}_m(x-y)) \pm \exp(2\pi\,\overline{G}_m(x-y))\right]. \end{aligned} \tag{4.46}$$

We have defined $s_\pm^k(x)$ with $s_+^k(x) = s^k(x)$ for $k = 0$, $s_+^k(x) = s_5^k(x)$ for $k = 1, 2, 3$, and conversely for $s_-^k(x)$. Note that this definition corresponds to the decomposition of the scalar and pseudoscalar fields in the irreducible representation spaces of the $U(1)_V \otimes SU(2)_L \otimes SU(2)_R$ symmetry, which remains after the anomalous breaking of the $U(1)_A$ part of the flavour symmetry, see Table 1.2. Thus, in this case the anomalous $U(1)_A$ symmetry breaking is realized by the contributions from the topologically non-trivial sectors with Chern index $k = \pm 1$.

The structure of eq. (4.46) becomes more clear, if we take formally the infinite volume limit and then consider large distances $(x - y)$. Then $\overline{G}_m(x - y)$ becomes small and we can expand the functions $\exp(\pm 2\pi\overline{G}_m(x - y))$ leading to

$$< s_+^k(x)s_+^l(y) > \ \sim\ \delta_{kl}\,\frac{1}{|z|}\,, \tag{4.47}$$

$$< s_-^k(x)s_-^l(y) > \ \sim\ \delta_{kl}\,\frac{1}{|z|}\,2\pi\,\overline{G}_m(x-y)\,. \tag{4.48}$$

In leading order the decay of the s_+-correlation is determined by a massless intermediate state, while the s_--correlation is determined by the coupling to a massive state. However, in cases being compared with MC lattice calculations, the above limits are far away and we expect a strong impact of multi-particle states. Moreover, the difference between both kinds of (pseudo)scalar correlations becomes smaller, because for small $(x - y)$ $\overline{G}_m(x - y)$ is not small and the relative factor $\exp(-4\pi\overline{G}_m(x - y)$ suppresses the topologically non-trivial contributions.

For the comparison with our MC data we evaluated

$$s_\pm(t; q_1) = \pm(-1)^I \int dx_1\, e^{iq_1x_1} < s_\pm^k(x_1, t)s_\pm^k(0, 0) > \tag{4.49}$$

for the momenta $q_1 = 0, \pi/3$ and for the values corresponding to our $\bar{\beta} = 10$-simulations on the lattice: $L_1 = 6$, $L_2 = 16$, $1/e^2 = 10$. The signs are chosen so as to obtain $s_\pm(t; q_1) > 0$. The results are plotted in Figure 4.2. It can be seen, that in fact the difference between the two kinds of correlations has become small. In particular, for $q_1 = \pi/3$ we do not expect to have any chance to distinguish both curves in MC simulations. Nevertheless, we will see in the following subsection that our MC data qualitatively reproduce the splitting of the correlations $s_+(t; q_1)$, $s_-(t; q_1)$ for momentum $q_1 = 0$.

4.3.2 Lattice results

The minimal lattice bilinears corresponding to the scalar and pseudoscalar fields in the continuum are taken from Table 1.2. Here we shall consider $M_{(0,0)}^0(x)$ and $M_{(1,0)}^1(x)$, corresponding

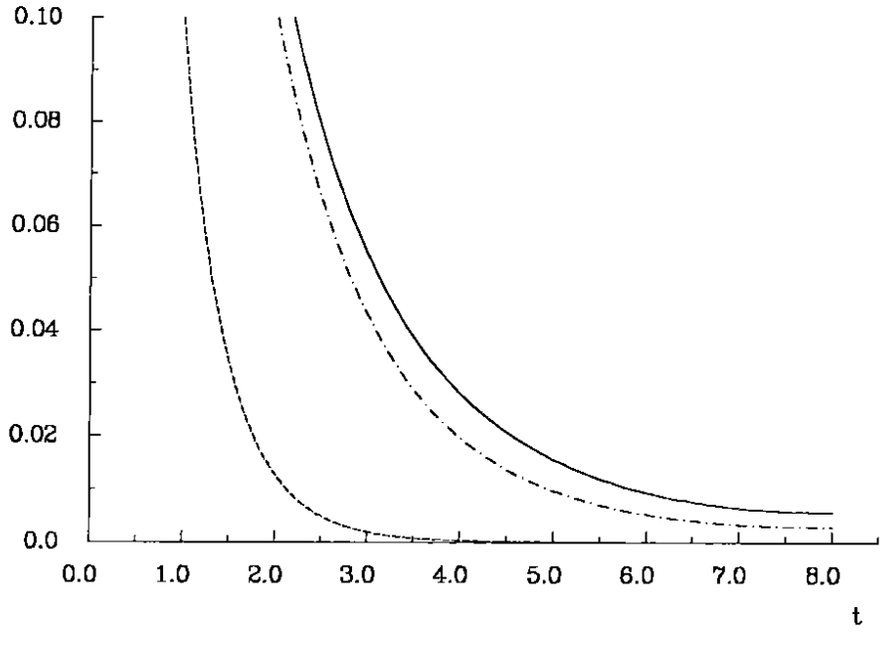

Figure 4.2: The (pseudo)scalar correlations $s_+(t;0)$ (full line) $s_-(t;0)$ (dashed-dotted line), $s_+(t;\pi/3)$ (dashed line) and $s_-(t;\pi/3)$ (dotted line). The last two can not be resolved by the present plot.

$m^0_+(t;\pi/3)$	E_1^+	C_1^+	E_2^+	C_2^+
$Q_{top}=0$, (c):	1.16(3)	0.14(4)	1.40(2)	0.28(4)
$Q_{top}\in\mathbf{Z}$, (c+d):	1.18(5)	0.17(8)	1.42(5)	0.26(8)
$m^{1-}_-(t;\pi/3)$	E_1^+	C_1^+	E_2^+	C_2^+
$Q_{top}=0$, (c):	1.2(1)	−0.07(8)	1.5(4)	−0.05(8)
$Q_{top}=0$, (c+d):	1.2(1)	−0.07(8)	1.5(4)	−0.05(8)
$Q_{top}\in\mathbf{Z}$, (c+d):	1.2(1)	−0.07(8)	1.5(4)	−0.05(8)
$m^{1+}_+(t;0)$	E_1^-	C_1^-	E_2^-	C_2^-
$Q_{top}=0$, (c):	0.51(3)	0.11(3)	0.96(6)	0.37(3)
$Q_{top}=0$, (c+d):	0.56(8)	0.14(8)	1.05(12)	0.27(8)
$Q_{top}\in\mathbf{Z}$, (c+d):	0.48(19)	0.11(16)	0.94(10)	0.35(8)
$m^{1+}_+(t;\pi/3)$	E_1^-	C_1^-	E_2^-	C_2^-
$Q_{top}=0$, (c):	1.2(1)	0.05(8)	1.5(4)	0.07(8)
$Q_{top}=0$, (c+d):	1.273(9)	0.113(2)	—	—
$Q_{top}\in\mathbf{Z}$, (c+d):	1.275(9)	0.113(2)	—	—

Table 4.3: Fit parameters for the (pseudo)scalar content in different correlations at $\bar{\beta}=10$, without disconnected contributions (c), and with disconnected contributions (c+d).

to $s^k_+(x)$ in the continuum, and $M^{1+}_{(0,1)}(x)$, corresponding to $s^k_-(x)$. For that we take the Monte Carlo data for the fixed space momentum correlations $m^0_+(t;q_1)$, $m^{1-}_-(t;q_1)$ and $m^{1+}_+(t;q_1)$ already considered in subsection 4.1.3 and subsection 4.2.2. Because of the situation in the continuum (see Figures 4.2, 4.3) we do not expect really significant data for the only non-zero space momenta $q_1=\pm\pi/3$ on our 6×16-lattice. Thus we restrict the investigation on the $q_1=0$-correlations.

We now have to focus on the part which does not take an oscillating factor $(-1)^t$ for $m^0_+(t;0)$, $m^{1-}_-(t;0)$, and which does take such a factor for $m^{1+}_+(t;0)$. This means we use the fits in eqs. (4.29), (4.42) to separate the current and the (pseudo)scalar content in the above lattice correlations. It has to be remarked that from the continuum we do not expect a behaviour of the (pseudo)scalar sector corresponding to the ansatz in those fits, which describe the correlation for this part by maximal two cosh-decay functions[5]. However, on the lattice these fits worked well in the cases we are interested in, i.e. for zero space momentum q_1. In Table 4.3 we give the fit parameters for the (pseudo)scalar sector at $\bar{\beta}=10$. This completes the parameters of the fits, on which Tables 4.1, 4.2 are based.

Despite of the somewhat unclear situation, we expect that the separation of the scalar

[5]It appeared, that a fit of $s_\pm(t;q_1)$ in eq. (4.49) at the discreet points $t=1,\ldots,8$ by a sum of up to 2 $\cosh(E_i(L_2/2-t))$-functions did not yield probabilities $P\geq 0.1\%$, if we assumed errors of 1% for the data.

and current contributions by these fits makes sense for two reasons. First, because of their principal difference by the factor $(-1)^t$ the correlation between different ansätze for both sectors is small, as can be seen by playing with the proposed fits. Secondly, the situation in the current sector is simple in the continuum and well reproduced by the lattice data using the fits in question.

Thus we proceed as follows: We take the fits quoted in subsections 4.1.3, 4.2.2 and define the (pseudo)scalar part by the subtraction of the current sector

$$S_+^{1+}(t;0) \;=\; m_+^{1+}(t;0) - c_1^+ \cosh[\,E_1^+(L_2/2-t)\,]\,, \tag{4.50}$$

see eq. (4.42). For $S_+^0(t;0)$, $S_-^{1-}(t;0)$ we only had to subtract the small contributions $c_1^-(-1)^t$, i.e. we found energies E_1^- compatible with zero, with constants $c_1^- < 1\cdot 10^{-3}$ in the current sector[6]. Furthermore, we define $S_-^{1-}(t;0)$ with an extra minus-sign

$$S_-^{1-}(t;0) \;=\; -[\,m_-^{1-}(t;0) - (-1)^t c_1^-\,]\,, \tag{4.51}$$

because it has to be compared with the zero momentum correlation of the continuum scalar $s_s^2(x)$ (see Table 1.2). This correlation is given by $-s_+(t;0)$, because a factor $(-1)^t$ is inserted in eq. (4.49) for positive functions $s_\pm(t;0)$.

Now we can compare the obtained data for the (pseudo)scalar sector directly with the scaled zero momentum correlations in the continuum. All together, $S_+^0(t;0)$, $S_-^{1-}(t;0)$ correspond to $s_+(t;0)$, $S_+^{1+}(t;0)$ corresponds to $s_-(t;0)$.

Before we do this quantitatively, let us make some remarks on the expected general structure of the lattice data. In principal we have four kinds of contributions to correlations of general lattice bilinears: connected and disconnected contributions in the topological sectors $Q_{top}=0$ and $Q_{top}=1$. The contributions from $Q_{top}=-1$ should be the same as for $Q_{top}=1$ because of the lattice charge conjugation symmetry eq. (1.105), if the gauge field average is good enough. Thus we must weight the $Q_{top}=1$ contributions with a factor $2q_1$ and the $Q_{top}=0$ contributions with a factor $1-2q_1$, where q_1 is the probability of the $Q_{top}=1$-sector, given in subsection 1.2.2. Connected and disconnected contributions in the $Q_{top}=1$-sector do not correspond to connected and disconnected contributions in the continuum, but to the product of zero-modes determining the topologically non-trivial contributions in eq. (1.42). However, on the lattice the disconnected contributions are the ones, which remove the degeneracy of the 1-link correlations (with subtracted current sector) $S_-^{1-}(t;q_1)$ and $(-1)^t\,S_+^{1+}(t;q_1)$ (see eq. (4.21)), which correspond to the s_+- and s_--correlations in the continuum respectively. We therefore expect the following behaviour for sufficiently large $\bar\beta$:

1. The disconnected contributions for $S_-^{1-}(t;q_1)$ and $S_+^{1+}(t;q_1)$ with $Q_{top}=1$ should increase strongly with increasing $\bar\beta$, setting off the suppression of the topologically non-trivial contributions by the strongly decreasing q_1. They should be equal in their absolute value but have an opposite sign, corresponding eq. (4.45).

2. The $Q_{top}=1$ connected contribution of the local correlation $S_+^0(t;q_1)$, which has no disconnected part, should increase in the same rate, since this correlation should equal $S_-^{1-}(t;q_1)$ in the continuum limit, due to symmetry restoration.

[6] The fit for $m_+^0(t;0)$ is given by eq. (4.29) with $t=1,\ldots,8$ and with a probability $P>85\%$, for $m_-^{1-}(t;0)$ we also took $t=1,\ldots,8$, yielding a probability $P>90\%$. The parameters in the current sector are approximately the same as those for $m_+^{1+}(t;q_1)$ without disconnected contributions quoted in subsection 4.2.2.

field:	Q_{top}	$t=1$	$t=2$	$t=7$	$t=8$
$s_+^0(t;0)$	0	0.2722(3)	0.1155(3)	0.0056(2)	0.0048(2)
$s_+^0(t;0)$	1	2.34(9)	1.85(8)	0.36(2)	0.32(2)
$s_-^{1-}(t;0)$ (c)	0	0.1837(2)	0.0846(3)	0.0046(2)	0.0039(2)
$s_-^{1-}(t;0)$ (c)	1	0.30(5)	0.13(4)	0.01(1)	0.01(1)
$s_-^{1-}(t;0)$ (d)	0	0.0008(1)	0.0003(1)	−0.0001(1)	−0.0001(1)
$s_-^{1-}(t;0)$ (d)	1	1.81(5)	1.5(1)	0.28(1)	0.25(3)
$s_+^{1+}(t;0)$ (d)	0	−0.0091(7)	−0.0052(7)	−0.0006(7)	−0.0005(7)
$s_+^{1+}(t;0)$ (d)	1	−1.79(9)	−1.61(4)	−0.31(2)	−0.216(8)

Table 4.4: The different parts of the correlations with momentum $q_1=0$ in the (pseudo)scalar sector at $\bar\beta=10$: connected contributions (c), disconnected contributions (d) in the topological sectors $Q_{top}=0$ and $Q_{top}=1$. The connected contributions for $S_+^{1+}(t;0)$ are the same as for $S_-^{1-}(t,0)$ up to a factor $(-1)^t$. For a simple comparison this factor is multiplied to the quoted disconnected contributions of $S_+^{1+}(t;0)$ too.

3. The $Q_{top}=1$ connected part of $S_-^{1-}(t;q_1)$ and $S_+^{1+}(t;q_1)$ should not increase essentially with increasing $\bar\beta$ and thus be suppressed by the small weight q_1, corresponding to the fact that the part which is equal for the s_+ and s_--correlations in the continuum, is coming from the topologically trivial sector $k=0$.

This principal structure required for lattice data at large $\bar\beta$ can be found for our MC data at $\bar\beta=10$, see Table 4.4. However, we did not find fits in the sense of eq. (4.27) for the pure $Q_{top}=1$ data, in order to subtract a possible current content in these contributions. It can be assumed that the main part of the correlations $m_\pm^\alpha(t;0)|_{Q_{top}=1}$ comes from the (pseudo)scalar sector, because of the situation in the continuum. It can also be seen that the fit parameters for $m_\pm^\alpha(t;0)|_{Q_{top}\in\mathbb{Z}}$ depend very little on the $Q_{top}=1$ contributions in the current sector, compared with a stronger dependence in the (pseudo)scalar sector (see Figure 4.4).

Thus, for the qualitative discussion of the structure of the lattice data, we identified the $Q_{top}=1$ contributions with their (pseudo)scalar part in Table 4.4. The increase of the disconnected part for $S_-^{1-}(t;0)$ and $S_+^{1+}(t;0)$ and the connected part of $S_+^0(t;0)$ in the topologically non-trivial sector $Q_{top}=1$ can be seen by the comparison with the $Q_{top}=0$ data. This increase is not so strong as to balance the small $q_1\simeq 0.002$ approximately. The reason is the suppression of the topologically non-trivial part of the (pseudo)scalar correlations for small distances, which also appears in the continuum, see the remarks to eqs. (4.47), (4.48) and Figure 4.2. The other features of the $Q_{top}=1$ lattice data, quoted above, can also be seen. We have not given the same data for $\bar\beta=3$. They show only weak hints for such a structure.

Finally we compare the MC data for the (pseudo)scalar sector with the results from the continuum in eq. (4.46) and eq. (4.49). We take the MC data for $\bar\beta=10$ on our 6×16-lattice, and the corresponding continuum parameters, see eq. (4.49). In Figure 4.3 the data for the local field correlation $S_+^0(t;0)$ are plotted together with the corresponding continuum

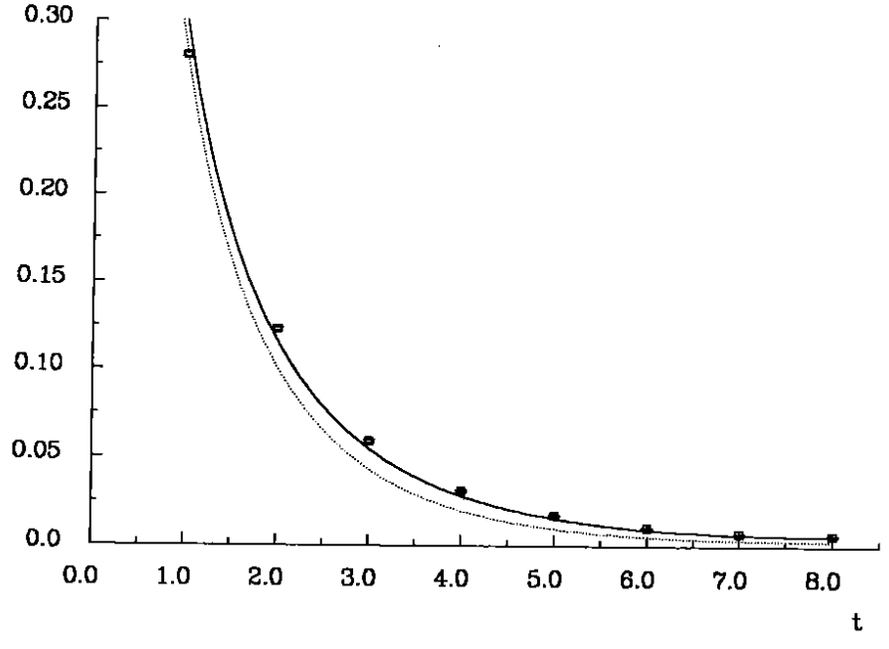

Figure 4.3: The (pseudo)scalar continuum correlations $s_+(t;0)$ (full line) and $s_-(t;0)$ (dotted line) compared with the Monte Carlo data for the local correlations $S^0_+(t;0)$ (squares).

correlation $s_+(t;0)$. For comparison we have also plotted $s_-(t;0)$. The MC data fit the continuum result quite well.

On the other hand the 1-link correlations $S^{1-}_-(t;0)$, $S^{1+}_+(t;0)$ reproduce the splitting of the continuum correlations $s_+(t;0)$, $s_-(t;0)$ well within the range of the error bars. On the lattice this splitting comes from the $Q_{top} = 1$-contributions as in the continuum. The main difference of the lattice 1-link field correlations to the continuum curves can be described by an overall factor 1/1.15 for the lattice data. It can be explained by a renormalization factor for the lattice 1-link fields, which can differ from the case of local fields. Figure 4.4 shows the comparison of the continuum correlations with the Monte Carlo data for 1-link fields scaled with a factor 1.15. Note that for a comparison with the continuum results we must omit eventual $(-1)^t$-factors in the lattice correlations, since they are due to the flavour transformation behaviour of the corresponding fields, as discussed above.

We have also quoted the values of the continuum and lattice correlations in Table 4.5 for a more detailed comparison. Here it can be seen that for $t = 1, 2$ the MC data differ more strongly from the values expected from the continuum calculation. We assume that these deviations are due to strong lattice effects at the small distance of one or two lattice spacings.

Summing up we can say with the reproduction of the continuum splitting in the scalar

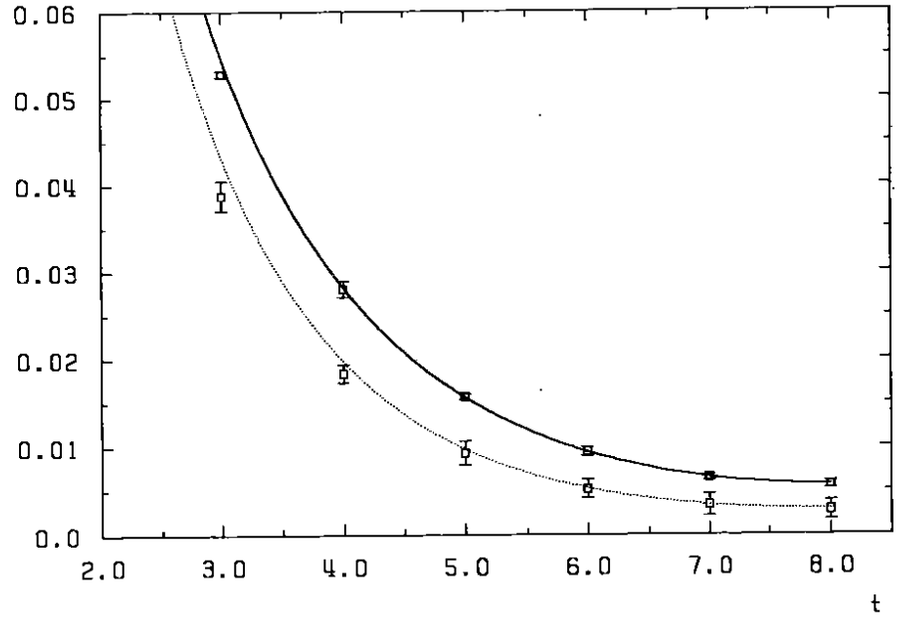

Figure 4.4: The (pseudo)scalar continuum correlations $s_+(t;0)$ (full line) and $s_-(t;0)$ (dotted line) and the MC data for the 1-link correlations $S^{1-}_-(t;0)$ (squares) and $S^{1+}_+(t;0)$ (circles). The lattice data are multiplied with a factor 1.15 and the factor $(-1)^t$, which appears in $S^{1+}_+(t;0)$, is omitted.

	continuum results		Monte Carlo data		
t:	$s_+(t;0)$	$s_-(t;0)$	$s^0_+(t;0)$	$s^{1-}_{\pm}(t;0)$	$s^{1+}_{\pm}(t;0)$
1	0.2983	0.2807	0.280(1)	0.2213(3)	0.1923(20)
2	0.1161	0.1013	0.123(1)	0.105(1)	0.0845(11)
3	0.0547	0.0432	0.0591(9)	0.0528(4)	0.0387(17)
4	0.0282	0.0198	0.0308(6)	0.0280(9)	0.0183(11)
5	0.0156	0.0097	0.0170(6)	0.0156(3)	0.0093(14)
6	0.0094	0.0053	0.0102(4)	0.0094(5)	0.0052(10)
7	0.0065	0.0034	0.0070(4)	0.0065(3)	0.0034(13)
8	0.0057	0.0029	0.0061(3)	0.0056(4)	0.0027(11)

Table 4.5: Comparison of the continuum correlations $s_+(t;0)$ and $s_-(t;0)$ with the Monte Carlo data for the lattice correlations $S^0_+(t;0)$, $S^{1-}_{\pm}(t;0)$ and $S^{1+}_{\pm}(t;0)$ for $t = 1,\ldots,8$. The data for the last two are multiplied with a factor 1.15 and the factor $(-1)^t$, which appears in $S^{1+}_{\pm}(t;0)$, is omitted.

sector we managed to verify the anomaly in the symmetry restoration mechanism outlined in subsection 1.3.3.

Conclusion

The aim of our analysis was to compare the realization of typical non-perturbative features of the geometric Schwinger model on the lattice with corresponding continuum results. It was possible to reproduce the investigated continuum properties with MC simulations at $\bar{\beta} = 10$ quite well. Moreover, we could estimate the finite a effects and the transition to strong coupling behaviour with MC measurements at $\bar{\beta} = 3.0, 1.0, 0.3$. For gauge field observables the MC measurements were complemented by an unquenched strong coupling expansion. We achieved the following results:

We measured the *toron partition*, i.e. the toron part of the effective action. With an appropriate definition of the lattice torons we found perfect agreement with the continuum result. So the finite a effects are very small in this case.

We could control the *contributions from the topologically non-trivial sectors* $Q_{top} = \pm 1$. For that it was necessary to perform separate simulations in the sectors $Q_{top} = 0$ and $Q_{top} = 1$. The probabilities of these sectors could be evaluated to a reasonable accuracy, as we modified the action in order to lift the low probabilities for $Q_{top} = 1$.

As gauge field observables we measured the correlation of (opposite oriented) lattice plaquettes and Polyakov loops. The *plaquette correlation* corresponds to the field strength correlation in the continuum. For $\bar{\beta} = 10$ the decay of this lattice correlation leads to a mass, which perfectly agrees with the gauge field mass in the continuum. In the strong coupling region the SCE of this correlation shows the correct behaviour, i.e. an exponential decay. An interpolation between the gauge field mass at strong coupling and in the scaling region is given by MC simulations at $\bar{\beta} = 0.3, 1.0, 3.0$. The agreement between SCE and MC simulations is quite good, even in the cross-over region ($\bar{\beta} = 1.0$).

A similar scenario comes out for the *heavy quark potential*, extracted from Polyakov loop correlations. In addition, we quoted the lattice and continuum results in the quenched approximation. So one can compare the screening effect of dynamical fermions with the quenched and unquenched finite volume effects. In the quenched case the influence of the non-trivial sectors is considerable.

In the analysis of fermion observables we relate lattice bilinears to currents, scalars and pseudoscalars in the continuum by the consideration of the *irreps of the continuum and lattice symmetry groups*. The effect of the anomalous broken axial $U(1)$ symmetry is included. The results in Table 1.2 set up a scheme of anomalous symmetry restoration as analogue to the anomaly in the continuum. This scheme can be seen to be realized in the correlations of fermion bilinears, measured with the MC simulation at $\bar{\beta} = 10$.

We find an approximately massless decay of lattice correlations for different fermion bilinears, corresponding to the *isovector current correlation*. They belong to different irreps of the lattice symmetry group. This is an example of symmetry restoration.

A massive decay is found in the lattice correlation, corresponding to the *isoscalar current correlation*, the appearing mass is very close to the continuum gauge field mass at $\tilde{\beta} = 10$. This results from the inclusion of the disconnected contributions, similar to the scheme of mass generation in the isoscalar current sector in the continuum. This effect is related to the axial anomaly.

Finally, the lattice correlations, corresponding to the *correlations of (pseudo)scalars* in the continuum, show the splitting, which indicates the breaking of the $U(1)_A$ symmetry. For that one must include the contributions of the topologically non-trivial sectors $Q_{top} = \pm 1$. This provides also a check of the results on the weight of the different topological sectors on the lattice.

The measurements of the mentioned fermion observables at $\tilde{\beta} = 3$ showed that the finite a effects are quite strong in this case. The comparison with the $\tilde{\beta} = 10$ data in the isovector current sector gives an impression of the symmetry restoration as a consequence of the lattice approaching the continuum limit.

Let us make some remarks on the methods we used. The unquenched SCE led to qualitatively correct results for the gauge field observables under consideration. The exponential decay of the field strength correlation and the charge screening were reproduced. The agreement with MC simulations in the strong coupling region and even in the cross-over region was good. However, this expansion is evaluated on a fix volume, so we could check the existence of the thermodynamical limit only numerically. Moreover, there is an oscillating part in the Polyakov loop correlation in the strong coupling region, which we do not understand yet. We want to remark that the evaluation of the given SCE relies on methods, which are exact only for massless staggered fermions in two dimensions. For non-vanishing fermion mass and for dimensions $d > 2$ there are approximate results [44], which might be used instead.

The HMC algorithm managed to generate the correct average of configurations, also with respect to the torons which are global quantities related to harmonic zero modes. In contrast, it did not manage to change the topological sectors. This had to be cured by separate instanton hits. They are originally designed for pure QED_2, and had to be combined with random toron shifts. In this form they work only on small lattices. A better analysis of the reasons and an improvement of the instanton hits are desirable.

Our MC simulations were performed on a quite small lattice $L_1 \times L_2 = 6 \times 16$. $L_2/2 = 8$ is the length over which the different correlations decay. This is sufficient, only if the mass content in these correlations is poor. It is not possible to suppress higher masses by sufficiently long 'decay times'. In our case this was a shortcoming in the (pseudo)scalar sector. However, there it was possible to compare continuum and lattice data directly. The small size $L_1 = 6$ imposed strong restrictions on our analysis of non-zero momentum correlations.

Summing up, we can say the reproduction of the studied non-perturbative effects on the lattice was possible. For that the comparable simple structure and the existence of exact continuum results in the geometric Schwinger model were very helpful. Even so, we hope that the given analysis could help to investigate non-perturbative effects on the lattice also in physical theories, in particular in QCD. There, an explicit study of the finite size dependence on the lattice should take the part of the exact finite size continuum results in our case. A detailed consideration of the symmetry properties including the anomalous effects showed to be very useful.

Acknowledgements

I am much indebted to my supervisor, Prof. H. Joos, for his guidance throughout this work, for interesting and encouraging discussions and for helpful suggestions.

Further, I would like to thank G. Schierholz for useful hints and for making a hybrid Monte Carlo computer program available to me. I also want to acknowledge useful discussions with M. Grabenstein on Monte Carlo simulations and instanton hits in the Schwinger model.

The financial support given by the *Deutsche Forschungs-Gesellschaft* as a part of the *Graduiertenkolleg für theoretische Elementarteilchenphysik* is gratefully acknowledged.

Appendix A

We give explicit formulas for the dimer gas expressions used in section 2.2. First we calculate the dimer gas partition functions $Z^{\epsilon_1\epsilon_2}$, where $\epsilon_\mu = \pm$ denotes the periodic or antiperiodic boundary condition in μ-direction. It was defined in eqs. (2.19), (2.20) by

$$Z^{\epsilon_1\epsilon_2} = \int \mathcal{D}[\bar\phi,\phi] e^{-S_D^{\epsilon_1\epsilon_2}} \ , \ S_D^{\epsilon_1\epsilon_2} = \sum_{x:even}\sum_{y:odd} \bar\phi_x \, Q_{xy}^{\epsilon_1\epsilon_2} \phi_y \ , \tag{A.1}$$

$$Q_{xy}^{\epsilon_1\epsilon_2} = \rho_{\mu,x}^{\epsilon_1\epsilon_2}(\delta_{x+e_\mu} - \delta_{x-e_\mu}) \ . \tag{A.2}$$

For $\epsilon_1\epsilon_2 = ++$ we diagonalize $Q^{\epsilon_1\epsilon_2}$ by the following transformations, which are essentially the modified Fourier transformation of eq. (1.106),

$$\bar\phi_a^b(p) = \frac{1}{N}\sum_{x:even} e^{-ipx} \gamma_{ab}^{H_x{}^*} \bar\phi_x \ , \ \ \phi_a^b(p) = \frac{1}{N}\sum_{x:odd} e^{ipx} \gamma_{ab}^{H_x} \phi_x \ , \tag{A.3}$$

$$\bar\phi_x = \frac{1}{N}\sum_{p,a} e^{ipx} \gamma_{a\bar a}^{H_x} \bar\phi_a^{\bar a}(p) \ , \ \ \phi_x = \frac{1}{N}\sum_{p,a} e^{-ipx} \gamma_{a\bar a}^{H_x{}^*} \phi_a^{\bar a}(p) \ . \tag{A.4}$$

where $\bar a = 1$ for $a = 2$ and vice versa. $N^2 = L_1L_2/2$ makes this a orthonormal transformation. We took off-diagonal γ^μ-matrices, i.e γ^{12} is diagonal, so the restriction of $\bar\phi_x, \phi_y$ on even x and odd y respectively leads to a restriction of $\bar\phi_a^b(p)$ to $a = b$ and $\phi_a^b(p)$ to $a \neq b$. The momenta p in the sums of eq. (A.4) run over the Brillouin zone of the coarse lattice, i.e

$$p^\mu = \frac{2\pi}{L_\mu} n_\mu \ , \ n_\mu \in [-L/4, L/4) \cap \mathbf{Z} \ . \tag{A.5}$$

With these definitions the dimer action can be written as

$$S_D^{++} = -2i \sum_{p,a} \bar\phi_a^a(p) \ \gamma_{a\bar a}^\mu \ \sin p^\mu \ \phi_{\bar a}^a(p) = \sum_{p,a}\sum_{p',a'} \bar\phi_a^a(p) \tilde Q_{a\,p}^{\ a'p'} \phi_a^{\bar a}(p) \ , \tag{A.6}$$

$$\text{so} \qquad \tilde Q_{a\,p}^{\ a'p'} = \gamma_{a\bar a}^\mu \ \sin p^\mu \ \delta_{pp'} \, \delta_{\bar a a'} \ . \tag{A.7}$$

It can be seen easily that for antiperiodic boundary conditions in μ-direction ($\epsilon_\mu = -$) the sum over momenta in eq. (A.6) given by eq. (A.5) must be shifted to

$$p^\mu = \frac{2\pi}{L_\mu}(n_\mu + \frac{1}{2}) \ , \ n_\mu \in [-L/4, L/4) \cap \mathbf{Z} \ . \tag{A.8}$$

Using the usual Grassmann integration formula we obtain for the partition functions

$$Z^{\epsilon_1\epsilon_2} = \det(\tilde Q^{\epsilon_1\epsilon_2}) = \prod_{\{p\}^{\epsilon_1\epsilon_2}} [4\det(i\gamma^\mu \sin p^\mu)] = \prod_{\{p\}^{\epsilon_1\epsilon_2}} [4\sum_\mu \sin^2 p^\mu] \ , \tag{A.9}$$

where $\{p\}^{\epsilon_1\epsilon_2}$ is the set of all momenta p, given by

$$p_\mu = \frac{2\pi}{L_\mu}(n_\mu + \alpha_{\epsilon_\mu}) \ , \ n_\mu \in [-\frac{L_\mu}{4}, \frac{L_\mu}{4}) \cap \mathbf{Z} \ , \ \alpha_+ = 0 \ , \ \alpha_- = \frac{1}{2} \ . \tag{A.10}$$

Next we turn to the dimer n-point functions. Let us first exclude the periodic case $\epsilon_1\epsilon_2 = ++$, which leads to zero modes in $\tilde Q$. For simplicity of notation we write

$$\frac{1}{Z^{\epsilon_1\epsilon_2}} \int \mathcal{D}[\bar\phi,\phi] \, e^{-S_D^{\epsilon_1\epsilon_2}} \Omega[\bar\phi,\phi] = \langle \, \Omega[\bar\phi,\phi] \, \rangle_D^{\epsilon_1\epsilon_2} \ . \tag{A.11}$$

So we must calculate (compare with eq. (2.19))

$$y_\Omega^{\epsilon_1\epsilon_2} = \langle \prod_{i=1}^n (\bar\phi_{x_i}\phi_{x_i'}) \, \rangle_D^{\epsilon_1\epsilon_2} = \sum_\pi \mathrm{sign}(\pi) \prod_{i=1}^n \langle \, \bar\phi_{x_i}\phi_{x'_{\pi(i)}} \, \rangle_D^{\epsilon_1\epsilon_2} \ . \tag{A.12}$$

Here the x_i (x_i') are the even (odd) points on the lines of the graph of the observable Ω. It is not necessary to care about the order of the Grassmann variables in eq. (A.12) leading to a sign factor, because we need only the absolute value of $y_\Omega^{\epsilon_1\epsilon_2}$. Again the two-point functions can be calculated with the modified Fourier transformation of $\bar\phi, \phi$ in eqs. (A.3), (A.4). We write

$$\langle \, \bar\phi_{x_i}\phi_{x'_{\pi(i)}} \, \rangle_D^{\epsilon_1\epsilon_2} = \tau^{\epsilon_1\epsilon_2}(x'_{\pi(i)} - x_i) \tag{A.13}$$

and define

$$S^{\epsilon_1\epsilon_2}(z) = \frac{1}{L_1L_2} \sum_{\{p\}^{\epsilon_1\epsilon_2}} \frac{\cos(pz)}{\sum_\nu \sin^2 p^\nu} \ . \tag{A.14}$$

Then we obtain

$$\tau^{\epsilon_1\epsilon_2}(z) = \begin{cases} \rho_{\mu,x}[S^{\epsilon_1\epsilon_2}(z+e_\mu) - S^{\epsilon_1\epsilon_2}(z-e_\mu)] & \text{for } H_z = \mu \\ 0 & \text{else} \end{cases} \ . \tag{A.15}$$

With $y_\Omega^{\epsilon_1\epsilon_2}$ we can calculate the $Y_\Omega^{\epsilon_1\epsilon_2}$ in eq. (2.19) by $Y_\Omega^{\epsilon_1\epsilon_2} = Z^{\epsilon_1\epsilon_2}|y_\Omega^{\epsilon_1\epsilon_2}|$.

For the treatment of the case $\epsilon_1\epsilon_2 = ++$ we can not proceed as above, because $Z^{++} = 0$ but in general $Y_\Omega^{++} \neq 0$. We write

$$\begin{aligned} Y_\Omega^{++} &= \int \mathcal{D}[\bar\phi,\phi] \, e^{-S_D^{++}} \prod_{i=1}^n (\bar\phi_{x_i}\phi_{x_i'}) \ = \ \lim_{\epsilon\to 0} Y_\Omega^\epsilon \ , \\ Y_\Omega^\epsilon &= \int \mathcal{D}[\bar\phi,\phi] \, e^{-\bar\phi Q^\epsilon \phi} \prod_{i=1}^n (\bar\phi_{x_i}\phi_{x_i'}) \ , \end{aligned} \tag{A.16}$$

where we define $Q_{xx'}^\epsilon$ so that its representation in the basis given in eq. (A.3) is

$$(\tilde Q^\epsilon)_{a\,p}^{\ a'p'} = \begin{cases} \tilde Q_{a\,p}^{\ a'p'} & \text{for } p,p' \neq 0 \\ -2i\,\epsilon\,\gamma_{\bar a a'}^1 \delta_{pp'} & \text{for } p = p' = 0 \end{cases} \ . \tag{A.17}$$

The matrix $\tilde{Q}_{a\,p}^{\;a'p'}$ is that of eq. (A.7). Now Y_Ω^ϵ can be calculated with the above methods. We get (a prime indicates omitted zero modes in eq. (A.10))

$$Y_\Omega^\epsilon = Z^\epsilon \left| \sum_\pi \mathrm{sign}(\pi) \prod_{i=1}^{n} \tau^\epsilon(x'_{\pi(i)} - x_i) \right| , \tag{A.18}$$

with

$$Z^\epsilon = 4\epsilon^2 \, (Z^{++})' \; , \; (Z^{++})' = \prod_{\{p\}^{++}}{}' \; [4 \sum_\mu \sin^2 p^\mu] \, , \tag{A.19}$$

and

$$\tau^\epsilon(z) = (\tau^{++})'(z) - \frac{1}{\epsilon} \, \frac{2i}{L_1 L_2} \, \delta_{H_s,1} \; . \tag{A.20}$$

From the definition of Y_Ω^{++} as number of dimer configurations it is clear that Y_Ω^ϵ remains finite in the limit $\epsilon \to 0$. So for Y_Ω^{++} we must only consider the order $\mathcal{O}(\epsilon^0)$ in eq. (A.18). We obtain

$$\begin{aligned} Y_\Omega^{++} &= \frac{16\,(Z^{++})'}{(L_1 L_2)^2} \sum_\pi \mathrm{sign}(\pi) \sum_{n_1 < n_2} \delta_{H(x'_{\pi(n_1)}),\, H(x_{n_1})\triangle 1} \; \delta_{H(x'_{\pi(n_2)}),\, H(x_{n_2})\triangle 1} \\ &\times \prod_{i \neq n_1, n_2} (\tau^{++})'(x'_{\pi(i)} - x_i) \; . \end{aligned} \tag{A.21}$$

For the SC expansion of Polyakov loop correlations we must calculate the partition functions (see eq. (2.45)) and n-point functions (see eq. (2.49)) under Polyakov loop boundary conditions in subsection 2.2.3. So we must diagonalize the matrix Q_{xy}^{+-} from eq. (A.2) on a $R \times L_2$-lattice with the restriction that $Q_{xy} = 0$ for $x_1 = 0\,(R)$ or $x_2 = 0\,(R)$. The idea is to change to a basis with a sort of half sinus waves, i.e. to double the lattice in 1-direction and then to take the antisymmetric modes with respect to a space reflection. It turns out that we need the geometric space reflections Π from eq. (1.102)

$$\Pi \phi_{(x_1,x_2)} = (-1)^{x_1} \phi_{(-x_1,x_2)} \; , \tag{A.22}$$

which is a symmetry of the staggered fermion action. We write

$$\begin{aligned} S[\bar{\phi},\phi] &= \sum_{x_1=1}^{R-1} \sum_{x_2,\, x:even} \sum_\mu \rho_{\mu,x} \bar{\phi}(x) [\phi(x+e_\mu) - \phi(x-e_\mu)] & \text{(A.23)} \\ &= \frac{1}{2} \sum_{x_1=-R}^{R-1} \sum_{x_2,\, x:even} \sum_\mu \rho_{\mu,x} \bar{\psi}(x) [\psi(x+e_\mu) - \psi(x-e_\mu)] \; , & \text{(A.24)} \end{aligned}$$

where ψ depends on ϕ by $\psi_x = \phi_x$ for $1 \leq x_1 \leq R$, $\psi_x = -\Pi\phi_x$ for $-R+1 \leq x_1 \leq -1$, $\psi_x = 0$ for $x_1 = -R, 0$. The reason for this rewriting is that we can consider the ψ_x as general fields on a $2R \times L_2$-lattice which underly the restriction

$$\Pi \psi_x = -\psi_x \; . \tag{A.25}$$

Note that this restriction already requires $\psi_x = 0$ for $x_1 = -R, 0$, if we take in 1-direction periodic boundary conditions for R even and antiperiodic boundary conditions for R odd. As

mentioned in subsection 2.2.3 we must take antiperiodic boundary conditions in 2-direction. It is now possible to diagonalize the action with a basis $\psi_a^b(p)$ derived as in eq. (A.3)[1]. According to eq. (A.25) we take only combinations antisymmetric with respect to Π. As in eq. (A.9) we come then to the partition function under Polyakov loop boundary conditions

$$Z_{PL}(R) = \begin{cases} \prod_{p_1,p_2} (4 \sum_{\mu=1,2} \sin^2 p_\mu) & \text{for } R \text{ odd} \\ \prod_{p_2} |2 \sin p_2| \prod_{p_1} (4 \sum_{\mu=1,2} \sin^2 p_\mu) & \text{for } R \text{ even} \end{cases} , \tag{A.26}$$

where p_1, p_2 take the values

$$p_1 = \begin{cases} \frac{\pi}{2R}, \frac{3\pi}{2R}, \ldots, \frac{(R-2)\pi}{2R} & \text{for } R \text{ odd} \\ \frac{\pi}{R}, \frac{2\pi}{R}, \ldots, \frac{(R/2-1)\pi}{R} & \text{for } R \text{ even} \end{cases} , \tag{A.27}$$

$$p_2 = \frac{2\pi(n_2 + 1/2)}{L_2} \; , \; n_2 \in [-L_2/4, L_2/4) \cap \mathbf{Z} \; . \tag{A.28}$$

The procedure to calculate the n-point functions under Polyakov loop boundary conditions $x_{PL(R)}(\bar{G})$ from eq. (2.49) is similar to the calculation of the $y_\Omega^{\epsilon_1\epsilon_2}$ in eq. (A.11) – (A.13). But here we have another diagonalization of the action, which leads to different 2-point functions

$$\langle \, \bar{\phi}_x \phi_{x'} \, \rangle_D^{PL(R)} = \begin{cases} \rho_{\mu,x} \, [f^\mu(x - x') - (-1)^{x_1} f^\mu(\Pi x - x')] & \text{for } H_{x-x'} = \mu \\ 0 & \text{else} \end{cases} . \tag{A.29}$$

The functions $f^\mu(z)$ are defined with the momenta to sum over from eq. (A.28), and $\bar{\mu} = 2$ for $\mu = 1$ and vice versa as

$$f^\mu(z) = \frac{4}{L_1 L_2} \sum_p \frac{\sin(p_\mu z_\mu) \cos(p_{\bar{\mu}} z_{\bar{\mu}}) \sin p_\mu}{\sum_\nu \sin^2 p^\nu} \tag{A.30}$$

for R odd. For R even we have

$$f^\mu(z) = \frac{4}{L_1 L_2} \sum_p \frac{\sin(p_\mu z_\mu) \cos(p_{\bar{\mu}} z_{\bar{\mu}}) \sin p_\mu}{\sum_\nu \sin^2 p^\nu} + \delta_{\mu,2} \, \frac{2}{L_1 L_2} \sum_{p_2} \frac{\sin(p_2 z_2)}{\sin p_2} \; . \tag{A.31}$$

This completes the formulas necessary for the evaluation of Polyakov loop correlations in the strong coupling expansion. It is easy to check the formulas for partition functions and n-point functions under the various boundary conditions ($\epsilon^\mu = \pm$ and Polyakov loop b.c.) by explicit counting of dimer configurations on small lattices. We did this for lattices up to 6×6, 12×4.

[1] It is important to be careful with the normalization of this basis transformation, since the above restrictions diminish the number of degrees of freedom.

Appendix B

Since the isovector current correlation in the continuum is determined by the fermion propagator $S_t(x)$ in a constant background field t, we calculate the correlation of the corresponding lattice bilinears with constant background too. In this toron case we have link variables $U_{[x,\mu]} = e^{it_\mu}$, thus the fermion action becomes

$$\begin{aligned} S_f &= \frac{1}{2}\sum_{x,\mu}\rho_{\mu,x}\left[\bar{\chi}_x\, e^{it_\mu}\chi_{x+e_\mu} - \bar{\chi}_{x+e_\mu}\, e^{-it_\mu}\chi_x\right] \\ &= \sum_{p,\bar{a},a,b}\bar{\psi}^b_{\bar{a}}(p)\left[-i\sum_\mu \gamma^\mu_{\bar{a}a}\sin(p_\mu - t_\mu)\right]\psi^b_a(p)\,, \end{aligned} \tag{B.1}$$

where $\psi^b_{\bar{a}}(p)$, $\bar{\psi}^b_a(p)$ are given by the modified Fourier transformation in eq. (1.106), the momenta p are defined in the Brillouin zone of the coarse lattice, i.e $p_\mu = 2\pi n_\mu/L_\mu \in [-\pi/2, \pi/2)$. The 2-point function of these fields is

$$< \psi^b_a(p)\,\bar{\psi}^{\bar{b}}_{\bar{a}}(\bar{p}) >_t = \delta_{p\bar{p}}\,\delta_{b\bar{b}}\,\frac{i\gamma^\mu_{a\bar{a}}\sin(p_\mu - t_\mu)}{\sum_\nu \sin^2(p_\nu - t_\nu)}\,. \tag{B.2}$$

If we transform back to x-space with eq. (1.107) we get

$$< \chi_x\bar{\chi}_y >_t = \rho(H_z, H_x)\frac{1}{N^2}\sum_{p,a,\bar{a}} e^{-ipz}\gamma^{H_t}_{a\bar{a}}\,\frac{i\gamma^\mu_{\bar{a}a}\sin(p_\mu - t_\mu)}{\sum_\nu \sin^2(p_\nu - t_\nu)}\,, \tag{B.3}$$

with $z = x - y$, $N^2 = L_1L_2/2$. Because of the sign factor $\rho(H_z, H_x)$ this propagator is not invariant under shifts of one unit on the fine lattice, but under the restricted flavour transformations in eq. (1.103), as it should be. It can be seen that eq. (B.3) is the lattice version of the continuum propagator $S_t(x)$, if one inserts the relation of the continuum Dirac basis to the DK basis eq. (1.14). The latter corresponds to the χ-fields on the lattice, see eq. (1.56).

If we evaluate correlations of bilinears, i.e. products of fermion propagators, we come to a modified folding formula in momentum space, related to the modified Fourier transformation in eq. (1.106). We give these formulas for local bilinears and one-link fields (bilinears including one link). For the Fourier transformed correlations of local fields in eq. (4.15) we use eqs. (B.3), (4.13) leading to

$$\begin{aligned} m^0_L(q;t) &= \frac{1}{N^4}\sum_z e^{iqz}\sigma^L(z)\sum_{p,p',a,a',b,b'} e^{-ipz}\gamma^{H_z}_{aa'}\, e^{ip'z}\gamma^{H_*}_{bb'} \\ &\times \frac{\gamma^\mu_{a'a}\sin(p_\mu - t_\mu)}{\sum\sin^2(p_{\mu'} - t_{\mu'})}\,\frac{\gamma^{\nu^*}_{b'b}\sin(p_\nu - t_\nu)}{\sum\sin^2(p_{\nu'} - t_{\nu'})}\,. \end{aligned} \tag{B.4}$$

With the momentum representation of the δ-function on the coarse lattice and with the relations of orthogonality and completeness of the γ-matrix elements eqs. (1.16), (1.16) we obtain

$$m^0_L(q) = -\frac{2}{N^2}\sum_p F^L(q,p;t)\,, \tag{B.5}$$

$$F^L(q,p;t) = \frac{\sum_\mu \sin(p-t)_\mu \sin(q-p+t)_\mu\,\sigma^L(\mu)}{\left(\sum_\nu \sin^2(p-t)_\nu\right)\left(\sum_{\nu'}\sin^2(q-p+t)_{\nu'}\right)}\,. \tag{B.6}$$

In the same way we get for the one-link correlations in eq. (4.19)

$$m^{\mu\,\epsilon}_L(q;t) = -\frac{1}{N^2}\sum_p[1 + \epsilon\sigma^{L'}(\mu)\cos(q - 2p + 2t)_\mu]\,F^{L''}(q,p;t)\,, \tag{B.7}$$

L' is given by $L' = L$ for $\mu = 1$, $(L'_1, L'_2) = (1 - L_1, L_2)$ for $\mu = 2$ (see eq. (4.19)), L'' is given by $(L''_1, L''_2) = (L_1, 1 - L_2)$ for $\mu = 1$, $(L''_1, L''_2) = (1 - L_1, L_2)$ for $\mu = 2$.

A comparison of eqs. (B.5), (B.7) shows that in the continuum limit $a \to 0$, the connected contributions to the correlations of $M^0_L(q)$ and $M^{\mu-}_{L''}(q)(M^{\mu-}_{\overline{L}''}(q))$ degenerate up to an overall normalization factor. Whether we take L'' or $\overline{L}''$, depends on which leads to a non-vanishing correlation in eq. (B.7) in the continuum limit, i.e. we must have $\sigma^{L'}(\mu) = \epsilon$ in eq. (B.7). In Table 1.2 we find that the local and one-link fields corresponding to the continuum isovector current form such pairs. Since for $a \to 0$ we also expect that the correlations of isovector currents depend only on the toron part of the gauge field and have no disconnected contributions[1], the above degeneration is a necessary consequence of the symmetry restoration mechanism, sketched in subsection 1.3.3.

The mass content of the propagators in momentum space in eqs. (B.5), (B.7) is evaluated in subsection 4.1.3 in terms of the decay of correlations between fields with fixed space momentum for increasing distance in time direction. This will be done for a fluctuating toron field weighted with the continuum toron partition $P(t)$ from eq. (1.46).

[1] In the toron case the correlations of lattice bilinears corresponding to the isovector current have no connected contributions on the lattice too. .

Bibliography

[AJ] S.I. Azakov and H. Joos, 'The Schwinger Model on the Torus II', in preparation.

[1] H. Joos and I. Montvay, Nucl. Phys. B 225 (1983) 565;
M. Campostrini et al., Phys. Lett. B 193 (1987) 78;
M. Fukugita et al., Phys. Lett. B 191 (1987) 164;
K.D. Born et al., Phys. Rev. D 40 (1990) 1653;
R. Gupta et al., Phys. Rev. D 44 (1991) 3272;
The MT_c Collaboration, K.D. Born et al., 'The Interquark Potential: A QCD Lattice Analysis', in preparation.

[2] E. Witten, Nucl. Phys. B 156 (1979) 269;
G. Veneziano, Nucl. Phys. B 159 (1979) 213.

[3] S.L. Adler and W.A. Bardeen, Phys. Rev. 182 (1969) 1517.
J.S. Bell and R. Jackiw, Nuovo Cim. 51 (1969) 47.

[4] L.H. Karsten and J. Smit, Nucl. Phys. B 183 (1981) 103.

[5] H.B. Nielsen and M. Ninomiya, Phys. Lett. B 105 (1981) 219.

[6] J. Schwinger, Phys. Rev. 128 (1962) 2425.

[7] J. Lowenstein and A. Swieca, Ann. of Phys. 68 (1971) 172.

[8] E. Kähler, Rend. Mat. Ser. V, 21 (1962) 425.

[9] S. Duane et al., Phys. Lett. B 195 (1987) 216.

[10] J. Kogut and L. Susskind, Phys. Rev. D 31 (1975) 395;
L. Susskind, Phys. Rev. D 16 (1976) 3031.

[11] P. Becher and H. Joos, Z. Phys. C 15 (1982) 343.

[12] P. Rossi and U. Wolff, Nucl. Phys. B 284 (1984) 105.

[13] M. Karowski, R. Schrader and H.J. Thun, Comm. Math. Phys. 97 (1985) 5.

[14] H. Dilger, Phys. Lett. B 294 (1992) 263.

[15] H. Joos, Helv. Phys. Acta 63 (1990) 670; Nucl. Phys. B (Proc. Suppl.) 17 (1990) 704.

[16] P.B. Gilkey: 'Invariance Theory, the Heat Equation and the Atiyah-Singer Index Theorem', Publish or Perish Inc. 1984.

[17] For an overview of topological concepts in gauge theories see e.g. M. Göckeler and T. Schücker: 'Differential Geometry, Gauge Theories and Gravity', Cambridge University Press 1987.

[18] A. Belavin et al., Phys. Lett. B 59 (1975) 85.

[19] W. Magnus, F. Oberhettinger and R.P. Soni, 'Special Functions of Mathematical Physics', Berlin 1966.

[20] C. Jayewardena, Helv. Phys. Acta 61 (1988) 636.

[21] I.M. Singer and J.A. Thorpe: 'Lecture Notes on Elementary Topology and Geometry', Springer, New York 1967.

[22] O. Napoly, Phys. Lett. B 132 (1983) 145.

[23] J. Smit and J.C. Vink, Nucl. Phys. B 286 (1987) 485.

[24] J. Smit and J.C. Vink, Nucl. Phys. B 303 (1988) 36.

[25] M. Lüscher, Comm. Math. Phys. 85 (1982) 39;
A. Phillips and D. Stone, Comm. Math. Phys. 103 (1986) 599.

[26] S. Gupta, Phys. Lett. B 278 (1992) 317.

[27] H. Joos and M. Schäfer, Z. Phys. C 34 (1987) 456.

[28] W. Neudenberger, Diplomarbeit, Hamburg 1987.

[29] M.F.L. Golterman and J. Smit, Nucl. Phys. B 245 (1984) 61;
M.F.L. Golterman, Nucl. Phys. B 273 (1986) 663.

[30] G.W. Kilcup and S.R. Sharpe Nucl. Phys. B 283 (1987) 493.

[31] S.I. Azakov and H. Joos, private communication.

[32] G.W. Mackey: 'The Theory of Group Representations' (Chicago mimeographed Lecture Notes); Acta Math. 99 (1958) 365.

[33] M. Göckeler and H. Joos, 'Progress in Gauge Field Theory' (Cargese 1983), p.247, G. t'Hooft et al. (eds.), New York, Plenum Press 1984.

[34] I. Polonyi, H.W. Wyld and J.B. Kogut, Phys. Rev. Lett. 53 (1984) 644;
O. Martin and S.W. Otto, Phys. Rev. D 31 (1985) 435.

[35] G.G. Batrouni et al., Phys. Rev. D 32 (1985) 2736.

[36] R. Gupta, G.W. Kilcup and S.R. Sharpe, Phys. Rev. D 38 (1988) 1278.

[37] F. Fucito and S. Solomon, Phys. Lett. B 314 (1984) 230.

[38] See e. g. J.H. Wilkinson, C. Reinsch: Lineare Algebra, Springer 1971.

[39] R. Ben-Av et al., Phys. Lett. B 253 (1991) 185; Bonn preprint BONN-HE-90-15.

[40] M. Grabenstein, private communication.

[41] E. Seiler: 'Gauge Theories as a Problem of Constructive Quantum Field Theory and Statistical Mechanics', Springer Lecture Notes in Physics 159, Springer, Berlin 1982.

[42] A. Burkitt, K.H. Mütter and P. Überholz, Nucl. Phys. (Proc. Suppl.) 4 (1988) 215.

[43] I. Montvay, Desy preprint DESY-89-051; Cargese School 1989, 87.

[44] S. Samuel, J. Math. Phys. 21 (1980) 2806; ib. 2815; ib. 2820.

[45] I. Montvay, Rev. Mod. Phys. 59 (1987) 263 and lit. quoted therein; H. Gausterer, C.B. Lang and M. Salmhofer, Nucl. Phys. B 388 (1992) 275 and lit. quoted therein.

[46] J.M. Drouffe and J.B. Zuber, J. Phys. Rep. 102 (1987) 1.

[47] B.M. McCoy and T.T. Wu, 'The two-dimensional Ising Model', Cambridge 1973, pp. 61 – 67.

[48] I.S. Gradshteyn and I.M. Ryzhik, 'Table of Integrals, Series and Products', San Diego 1965.

[49] M. Lüscher and P. Weisz, Nucl. Phys. B 290 (1987) 25.

[50] H.S. Sharatchandra, H.J. Thun and P. Weisz, Nucl. Phys. B 192 (1981) 205.

[51] R. Altmeyer et al., Nucl. Phys. B 389 (1993) 445.

[52] G. Schierholz, private communication.